Gesellschaft für Anlagen- und Reaktorsicherheit (GRS) mbH

Spent Fuel Performance Assessment (SPA) for a Hypothetical Repository in Crystalline Formations in Germany

GRS - 154

Gesellschaft für Anlagen- und Reaktorsicherheit (GRS) mbH

Spent Fuel Performance Assessment (SPA) for a Hypothetical Repository in Crystalline Formations in Germany

Ludger Lührmann
Ulrich Noseck
Richard Storck

Juli 2000

Acknowledgement:

The underlying work of this report was supported by the Federal Ministery for Economy and Technology (BMWi) under the indentification number 02 E 8855.

The work was carried out under the auspices of GRS - Gesellschaft für Anlagen- und Reaktorsicherheit mbH.

Responsibility for the contents of this publication lies solely with the authors.

GRS - 154
ISBN 3-931995-16-X

Deskriptoren:
Berechnung, Endlagerung, F+E, Forschung, Gestein, Langzeitsicherheit, Modell, Publikation, Rechenverfahren

Vorwort

Die Bewertung der Langzeitsicherheit von Endlagern erfordert ein leistungsfähiges und erprobtes Instrumentarium. Dafür werden Rechenprogramme und Daten eingesetzt, mit denen die relevanten physikalischen und chemischen Prozesse bei Freisetzung von Schadstoffen, deren Ausbreitung im Deckgebirge und Exposition in der Biosphäre beschrieben werden. Ziel des Vorhabens “Wissenschaftliche Grundlagen zum Nachweis der Langzeitsicherheit von Endlagern”, FKZ 02 E 8855, war die Verfolgung nationaler und internationaler Entwicklungen sowie die Auswertung wissenschaftlicher Ergebnisse. Dabei standen experimentelle und theoretische FuE-Vorhaben im Vordergurnd, die wichtige Beiträge zu Modellvorstellungen und Modelldaten für Langzeitsicherheitsanalysen lieferten. Eine weitere relevante Aufgabe stellte die Entwicklung von Instrumentarien für die Langzeitsicherheitsanalyse von Endlagern in Hartgesteinsformationen dar.

Dieses sonderfinanzierte Vorhaben des Bundesministeriums für Wirtschaft und Technologie wurde in der Zeit vom 01.04.1996 bis 31.01.2000 durchgeführt. Zu den schwerpunktmäßig während des Projektes bearbeiteten Themen wurden die folgenden sechs wissenschaftlichen Einzelberichte angefertigt.

GRS-Bericht 129	Erzeugung und Verbleib von Gasen in einem Endlager für radioaktive Abfälle
GRS-Bericht 148	Ableitung von Permeabilitäts-Porositätsbeziehungen für Salzgrus
GRS-Bericht 151	Permeabilität von aufgelockertem Steinsalz. Ableitung einer Relation zur Modellierung von Auflockerungszonen innerhalb von Langzeitsicherheitsanalysen
GRS-Bericht 154	Spent Fuel Performance Assessment (SPA) for a hypothetical repository in crystalline formations in Germany
GRS-Bericht 155	Zusammenstellung und Auswertung geochemischer Untersuchungen zum Radionuklidverhalten aus ausgewählten Studien über Natürliche Analoga

GRS-Bericht 156 Grundlegende Ausbreitungsrechnungen mit dem Transportprogramm CHETLIN

In einem zusammenfassenden Abschlußbericht wurden außerdem alle während der Laufzeit des Projekts durchgeführten Arbeiten in Kurzbeiträgen zusammengefaßt:

GRS-Bericht 153 Wissenschaftliche Grundlagen zum Nachweis der Langzeitsicherheit von Endlagern. Abschlußbericht

Abstract

Im Rahmen dieses Vorhabens wurde eine erste Langzeitsicherheitsanalyse für ein generisches deutsches Endlager für abgebrannte Kernbrennstoffe in einer Granitformation durchgeführt. Eine Kofinanzierung der Arbeiten erfolgte im Rahmen des von der Europäischen Kommission geförderten Projekts “Spent Fuel Performance Assessment (SPA), Contract FI4W-CT96-0018”. An dem SPA-Projekt waren fünf weitere Länder mit Langzeitsicherheitsanalysen zu Endlagern in Granit-, Ton- und Salzformationen beteiligt.

In der Vergangenheit wurden kristalline Wirtsformationen im Rahmen des deutschen Endlagerprogrammes nicht berücksichtigt, da eine Endlagerung im Granit bisher nicht vorgesehen war. Durch deutsche Beteiligung in ausländischen Untertagelabors wurde diese Option aber auf internationaler Ebene verfolgt. Die Bundesanstalt für Geowissenschaften und Rohstoffe (BGR) hat eine Studie zu alternativen Endlagerstandorten in Deutschland durchgeführt. Die Ergebnisse dieser Arbeit sind in das nationale Projekt “Gegenüberstellung von Endlagerkonzepten in Salz und Hartgestein” (GEISHA) eingeflossen. Im Rahmen des GEISHA-Projekts wurden Endlager für radioaktive Abfälle in Salz und Hartgesteinsformationen gegenübergestellt und ein Konzept für ein Endlager in einer Hartgesteinsformation vorgeschlagen. Dieses bildet die Basis für die hier durchgeführte Sicherheitsanalyse.

Es wird von einer Abfallmenge von 25 000 t Schwermetall ausgegangen. Die Brennstäbe sind in Edelstahlbehältern verpackt. Einzelne Behälter werden jeweils in vertikale Bohrlöcher eingebracht, die mit einer Schicht aus kompaktierten Bentonit ausgekleidet sind. Die geologische Struktur im Granit wurde ähnlich zu der in der Kristallin-I-Studie der NAGRA angenommen, da erste Untersuchungen an deutschen Granitformationen darauf hindeuten, daß hydrogeologische und hydrogeochemische Eigenschaften ähnlich denen in der Schweiz sind.

In einem ersten Schritt wurden konzeptionelle Modelle entwickelt und anschließend in numerische Rechencodes umgesetzt. Die Modelle beschreiben die relevanten Prozesse im Nahbereich und Fernfeld des Endlagersystems. Für die Nuklidmobilisierung und den diffusiven Transport durch den Bentonit-Buffer wurde der Code GRAPOS, für den Nuklidtransport im Fernfeld durch Kluftsysteme im Granit der Code CHETMAD entwickelt.

CHETMAD berücksichtigt advektiven und diffusiven/dispersiven Transport in Klüften sowie Diffusion von Radionukliden in Matrixbereiche mit immobilem Porenwasser. Sorption an der Matrixoberfläche wird über das K_d-Konzept beschrieben. Beide Rechenprogramme wurden verifiziert und für die Rechnungen eingesetzt. Zur Ermittlung der Strahlenexposition in der Biosphäre wurde das Rechenprogramm EXCON verwendet.

Als Referenz-Szenario wurde die instantane Aufsättigung des Bentonits nach der Betriebsphase, der Ausfall aller Behälter nach 1000 Jahren, Diffusion durch den Bentonit und Transport entlang von Klüften, die einen schnellen Transportweg in der geringleitenden Granitformation darstellen, angenommen. Die Mobilisierung der Radionuklide wurde entsprechend einem von allen Teilnehmern des SPA-Projekts gemeinsam entwickelten Quellterm beschrieben. Es wird angenommen, daß 25% der Behälter mit dem schnellen Transportweg im Granit verbunden sind. Die Nuklide werden bis in oberflächennahe Sedimentschichten transportiert. Das kontaminierte Wasser wird aus einem Brunnen entnommen und als Trinkwasser, sowie für die Bewässerung von Feldern, für Viehtränken und für die Fischzucht verwendet.

Neben dem Referenzszenario wurden Rechnungen für weitere drei Szenarien durchgeführt:

- Tiefer Brunnen: Die Verdünnung in der Biosphäre ist geringer als im Referenz-Szenario. Als Expositionspfad wird nur Trinkwasser berücksichtigt.

- Transport in EDZs (excavation disturbed zones) der Strecken und Schächte: Der Transport durch das Fernfeld führt durch eine poröse Zone mit einer Länge von 500 m und einer hydraulischen Leitfähigkeit von $1{,}75 \cdot 10^{-3}$ m/a.

- Sedimentabdeckung: Die Granitformation ist von einer Sedimentschicht überlagert. Der Radionuklidtransport findet zusätzlich entlang eines 200 m langen Weges durch ein poröses Medium statt.

Die Ergebnisse des Referenzfalls zeigen daß die maximale Strahlenexposition durch die Beiträge der Aktivierungsprodukte ^{14}C, ^{36}Cl und die Spaltprodukte ^{129}I, ^{79}Se, and ^{135}C bestimmt wird. Die maximalen Freisetzungsraten sowie die Transportzeiten der schwach

sorbierenden Radionuklide ^{14}C, ^{36}Cl, ^{41}Ca, ^{79}Se, ^{107}Pd, ^{129}I und ^{135}Cs werden durch die Geosphäre nur wenig beeinflußt. Dagegen stellt die Geosphäre eine starke Barriere für den Transport der stark sorbierenden Actinoide dar. Aus diesem Grund sowie aufgrund ihrer geringen Löslichkeiten liegen die durch die Actinoiden bewirkten jährlichen Strahlenexpositionen einige Größenordnungen niedriger als die der Spalt- und Aktivierungsprodukte.

Die Ergebnisse von Parametervariationen zeigen, daß sowohl der Wasserfluß durch die EDZ als auch die Zahl der Behälter, die mit den schnellen Transportwegen verbunden sind, einen großen Einfluß auf die jährlichen Strahlenexpositionen haben. Demnach sind die Endlagerauslegung sowie die Lage des Endlagers sind wichtige Einfußgrößen. Die Transportwege im Granit stellen unter den angenommenen Bedingungen für schwach sorbierende Nuklide kaum eine Barriere dar. Allerdings können weniger konservative Annahmen hinsichtlich der hydrogeologischen Parameter, wie Eindringtiefe in die Matrix, oder Klufthäufigkeit, zu einer erheblichen Reduktion der Strahlenexposition durch das wichtigste Nuklid ^{14}C führen.

Die in den anderen drei Szenarien berechneten maximalen jährlichen Strahlenexpositionen weichen nicht signifikant von der des Referenz-Szenarios ab. Im Falle des “Transports in den EDZs” stellt die Geosphäre überhaupt keine Barriere für langlebige schwach sorbierende Radionuklide wie ^{14}C, ^{129}I and ^{135}Cs dar. Daraus ergibt sich eine geringe Erhöhung der maximalen jährlichen Strahlenexposition um einen Faktor 2,7 gegenüber dem Referenz-Szenario. Die durch die Actinoiden bewirkten Strahlenexpositionen sind etwa um einen Faktor 10 höher als im Referenz-Szenario, da die Actinoiden weniger stark retardiert werden. Im Szenario “Sedimentabdeckung” bewirkt der zusätzliche Transportweg durch eine 200 m lange Sedimentschicht insbesondere eine weitere Retardation von ^{14}C, wodurch die maximale jährliche Strahlenexposition um 25% reduziert wird. Im Szenario “Tiefer Brunnen” führt die geringere Verdünnung als im Referenzszenario zu erhöhten Strahlenexpositionen für Nuklide, bei denen der Trinkwasserpfad eine wichtige Rolle spielt. Dies ist der Fall für ^{129}I, und viele Actinoide. Für ^{14}C ist die jährliche Strahlenexposition gegenüber dem Referenzszenario herabgesetzt, da für dieses Nuklid der Trinkwasserpfad nur zu einem Anteil von weniger als 1% an den Expositionspfaden in der Biosphäre beiträgt.

Abstract

Within the framework of this project a first long-term safety assessment study for a generic German repository with spent nuclear fuel in granite host formations has been performed. This work has been co-financed by the European Community within the project Spent Fuel Performance Assessment (SPA) under the contract FI4W-CT96-0018. In this European project participants from five other countries performed long-term safety assessments for repositories in granite, clay and rock salt formations.

In the past, crystalline formations were not considered in the German waste management programme since disposal in granite was not foreseen in Germany. However, this option has been followed by German participation in underground laboratories in other countries. The German institution Bundesanstalt für Geowissenschaften und Rohstoffe (BGR) has investigated potential alternative disposal sites in hard rock. The results of this study have been part of the national project “Gegenüberstellung von Endlagerkonzepten in Salz und Hartgestein” (GEISHA). Within this study concepts for repositories in rock salt and hard rock formations have been compared in detail.

The design of the repository for hard rock proposed in the GEISHA project in combination with a total spent fuel inventory of 25 000 t_{hm} packed in stainless steel containers were the basis for the study presented here. Single containers are emplaced in vertical boreholes. Compacted bentonite is used as buffer material. Because first investigations of the German granite formation indicate that hydrogeological and hydrogeochemical properties are comparable to those in Switzerland, a geological structure similar to that described in the NAGRA-study “Kristallin-I” has been considered.

Conceptual models have been developed and implemented into the numerical codes. These models describe the relevant processes in the near and far field of the repository. For the nuclide mobilisation and the diffusion-controlled transport through the bentonite barrier the computer code GRAPOS for far-field transport the code CHETMAD has been developed. Transport in the far field has been assumed to take place in a fracture network. As retardation mechanism matrix diffusion accompanied by linear equilibrium sorption on

the rock matrix is considered. Both codes have been tested by intercomparison with codes of other countries. The dose rates have been calculated by the code EXCON considering the transport pathways into the biosphere.

A reference scenario has been defined. It considers instantaneous saturation of the bentonite immediately after the operational phase of the repository, failure of all containers after 1000 years, diffusion through the bentonite, transport through fractured dykes, which represent a fast transport pathway in the low permeability region of the granite. The nuclide mobilization has been calculated according to a common source term which has been developed by all participants of the SPA project. It is assumed that 25% of the containers are connected to the considered transport pathway in the far field. The nuclides are transported to layers close to the surface. The contaminated water is pumped from a surface well and used for drinking, irrigation, cattle feed and fish ponds.

Additionally to the reference case, parameter variations and calculations for three alternative scenarios have been performed. The alternative scenarios are

- Deep well: The dilution of the water in the biosphere is lower than in the reference case and for the exposition pathway only drinking water is considered.

- Transport through EDZs (excavation disturbed zones) of tunnels and shafts: The pathway through the far field is represented by a porous zone characterized by a length of 500 m and a hydraulic conductivity of $1.75 \cdot 10^{3}$ m/y.

- Sedimentary cover: The granite site is covered by a sedimentary layer. After transport through the fractured dykes in the low permeable region of the granite the nuclides migrate through a porous, 200 m long pathway.

The main results for the reference case can be summarized as follows: The maxima of the total annual doses are determined by the contributions of the activation products ^{14}C, ^{36}Cl and the fission products ^{129}I, ^{79}Se, and ^{135}Cs. For the non-sorbed or weakly-sorbed nuclides ^{14}C, ^{36}Cl, ^{41}Ca, ^{79}Se, ^{107}Pd, ^{129}I, ^{135}Cs the maximum release rates and times of occurence are only slightly influenced by the geosphere. But near field and geosphere

are important transport barriers for the strongly-sorbed actinides. Due to that and to the relatively low solubilities, the maximum dose rates resulting from the actinides are several orders of magnitude lower than those from the relevant activation and fission products.

The results of the parameter variations indicate that repository layout and/or location of the repository are important features, since the water flow through the excavation disturbed zone as well as the number of containers coupled to the transport pathways strongly affect the dose rates. Under the assumed conditions the transport pathways in the granite formation represents almost no barrier for weakly-sorbed nuclides. However, less conservative assumptions for hydrogeological parameters of the granite, like penetration depth into the matrix or total width of open channels, could reduce the dose of the most important radionuclide ^{14}C significantly.

The maximum radiation exposures obtained for the three alternative scenarios do not significantly differ from the reference case. Looking at the scenario ”Transport through EDZs” the geosphere represents no barrier for long-lived nuclides or weakly-sorbed nuclides, like ^{14}C, ^{129}I and ^{135}Cs. Thus the maximum total dose rate is 2.7 times larger than that in the reference case and occurs earlier. The dose rates of the actinides are reduced during the transport along the migration pathway, but in comparison to the reference case they occur much earlier with more than one order of magnitude higher maxima. The scenario ”sedimentary cover” takes into account an additional barrier in the geosphere. Due to this barrier the arrival of the ^{14}C peak is delayed and, hence, after radioactive decay its maximum dose rate is reduced by about 25%. The dose rates of the long-lived nuclides as ^{135}Cs and ^{129}I are not affected. Compared to the reference case, the differences of the total dose rates for the ”deep well scenario” arise from the reduced dilution and from the fact that drinking of water is the only exposure pathway to men. The dose rate from ^{14}C is reduced, since the contribution of the drinking water pathway to the biosphere exposition pathway is smaller than 1%. In the reference case the drinking water pathway is important for ^{129}I. Thus the maximum of the dose rate is increased by one order of magnitude leading to higher total dose rates in the period of time from 10^4 to 10^6 years. The same effect causes the higher dose rates for nuclides from the decay chains.

Contents

1 Introduction

Within the European Community Project “Spent Fuel Performance Assessment” (SPA) long-term safety assessments for repositories with directly disposed spent fuel elements have been carried out. The Gesellschaft für Anlagen- und Reaktorsicherheit (GRS) mbH participated in this project, performing safety analyses for repositories in two formations, in salt rock and in crystalline rock. This report presents the safety assessment for a hypothetical repository system in crystalline rock.

At present, in Germany, no option for a repository in granitic formations exists and no site has been selected for a potential repository. However, within the GEISHA-Project general concepts for a repository in crystalline formations have been developed. The spent fuel policies, the waste packaging, the description of potential sites and repository design, mainly extracted from this study, are summarized in chapters 2 and 3.

The development and treatment of the scenarios on which the safety assessment is based are described in chapter 4. Some informations about the groundwater flow and the engineered barrier system relevant for the integrated performance assessment (IPA) are given in chapters 5 and 6.

One objective of the project has been to enhance the tools suitable for long-term safety calculations in salt formations and adapt them for the performance assessment of a hypothetical German repository system in granite. This includes the elaboration of conceptual models for all relevant processes as well as their implementation into computer codes and the derivation of model data for the repository system. Within this project two computer codes have been developed: the near-field code GRAPOS and the far-field code CHETMAD. The near-field model and data are described in chapter 7. The model and data for the far-field are given in chapter 8. A detailed description of the biosphere model and data can be found in chapter 9.

The performance assessment calculations are done with the near-field code GRAPOS, the far-field code CHETMAD, and the biosphere code EXMAS. The near-field code GRAPOS has been compared with the transport programme RIP, and the far-field code CHET-

MAD has been compared with the migration code FTRANS. The codes RIP and FTRANS have been used within the SPA-Project by ENRESA (Spain) and VTT Energy (Finland), respectively. The results of these code intercomparisons are presented in the appendix.

In chapter 10, the results of deterministic calculations with best estimate values are discussed. In a next step a sensitivity study concerning different features, effects and processes like canister failure, diffusion in bentonite, sorption, repository design or hydrodynamic properties of the geosphere is performed. Their influence on long-term safety is considered.

The impact of alternative model assumptions and alternative scenarios on the maximum radiation exposure is investigated in chapter 11.

In chapter 12 the results of the Integrated Performance Assessment are discussed and compared with those safety analyses which have been performed by other countries for repositories in granite. On the basis of these results conclusions are drawn concerning the feasibility of the evaluated spent fuel disposal concepts and the performance of alternative canister and repository designs.

2 Spent fuel policies and waste packaging

2.1 Review of national waste management policy

2.1.1 National waste management programme

In Germany, 19 nuclear power plants are on the net today. No other reactor is planned to start up within the next few years. All of the German nuclear power plants are light water reactors (LWR), either boiling water reactors (BWR) or pressurized water reactors (PWR). Within this project direct disposal of spent fuel elements is investigated, reprocessing is not considered. This means that only UO_2 spent fuel from light water reactors is regarded as waste. The amount of spent fuel, its type and characteristics, the activity inventory and the waste packaging are described in the next chapters.

2.1.2 Amount of spent fuel to be disposed of

The 19 German nuclear power plants produced in 1996 a net electric power of 21.1 GW_e [22]. The installed maximum net power is 23 GW_e altogether. In Table 2.1 relevant data and the type of each German reactor are listed.

Table 2.1: Nuclear power plants in Germany [22]

power plant	reactor type	net power [MW]	date of commissioning	total electricity generation [GWd]
Isar 1	BWR	870	1977	$4.4 \cdot 10^3$
Krümmel	BWR	1260	1984	$4.5 \cdot 10^3$
Brunsbüttel	BWR	771	1977	$2.8 \cdot 10^3$
Grundremmingen B Grundremmingen C	BWR BWR	1284	1984	$4.4 \cdot 10^3$ $4.1 \cdot 10^3$
Phillipsburg 1	BWR	890	1979	$3.9 \cdot 10^3$

Table 2.1: Nuclear power plants in Germany [22]

power plant	reactor type	net power [MW]	date of commissioning	total electricity generation [GWd]
Biblis A Biblis B	PWR PWR	1167 1240	1974 1976	$6.0 \cdot 10^3$ $5.9 \cdot 10^3$
Brokdorf	PWR	1370	1986	$4.1 \cdot 10^3$
Emsland	PWR	1290	1988	$3.7 \cdot 10^3$
Gräfenrheinfeld	PWR	1275	1981	$5.7 \cdot 10^3$
Grohnde	PWR	1360	1984	$5.2 \cdot 10^3$
Isar 2	PWR	1365	1988	$3.8 \cdot 10^3$
Mühlheim Kärlich [a]	PWR	1219	1987 - 1988	$4.2 \cdot 10^2$
Neckar 1 Neckar 2	PWR PWR	785 1269	1976 1988	$4.6 \cdot 10^3$ $3.3 \cdot 10^3$
Obrigheim	PWR	340	1968	$2.7 \cdot 10^3$
Phillipsburg 2	PWR	1385	1984	$4.9 \cdot 10^3$
Stade	PWR	630	1972	$4.7 \cdot 10^3$
Unterweser	PWR	1300	1978	$6.6 \cdot 10^3$
Sum		21 070		$8.6 \cdot 10^4$

a. The reactor Mühlheim Kärlich had been taken off the net in 1988.

A power plant with an electric power of 1000 MW and 40 GWd/t_{hm} burn-up produces about 25 t of heavy metal in spent fuel within a year [23]. Assuming a mean burn-up of 45 GWd/t_{hm} and 21.5 tons of heavy metal produced by a power plant with a net power of 1000 MW, about 495 t of heavy metal will be produced by all power plants in Germany over the period of one year.

In good agreement with these facts, 500 t_{hm} of spent fuel per year has been assumed in the GEISHA project [28] for a potential German repository and is taken as the basis for the SPA project. The operational period of the repository lasts about 50 years, i. e. the total amount of waste accumulates to 25 000 t_{hm}. The initial enrichment of the fuel is assumed to be 3.6% and the average burn-up is 45 GWd/t_{hm}. The cooling time required for disposal in a salt repository is 40 years while that for disposal in granite-formations is 60 years. All policy data are summarized in Table 2.2.

Table 2.2: Basic policy data

type of spent fuel	LWR-UO_2
initial enrichment	3.6% U-235
burn-up	45 GWd/t_{hm}
waste amount	500 t_{hm}/a
total amount	25 000 t_{hm}
cooling time	40 years for disposal in salt 60 years for disposal in granite
operational period of the repository	50 years

2.1.3 Type and characteristics of spent fuel

The LWR spent fuel element consists of UO_2 spent fuel, zircaloy cladding and structural parts. In Germany the reactors are more or less standardized. The fuel elements of different reactor types differ slightly in geometry, dimensions and weight. To all intents and purposes a PWR spent fuel element from the power plant Biblis is taken as a reference element [10]. Table 2.3 shows the geometrical data of this reference element and Table 2.4 gives the composition of the entire element and the materials used.

Table 2.3: Geometrical data and weight of the reference spent fuel element [10]

length of an element	4 925 mm
cross section of an element	230 mm x 230 mm
number of fuel rods in one element	236
data for one fuel rod length active length outer cross section of the tube wall thickness of tube material	 4 407 mm 3 900 mm 10.75 mm 0.65 mm
total weight of the element	0.84 t
weight of uranium	0.534 t

Table 2.4: Components, materials and mass fractions of a spent fuel element related to one t_{hm}

components	material	mass [kg/t_{hm}]	mass [%]
cladding tubes	Zry-4	293	20.6
support tubes, sheaths, etc.	steel 1.4541	95.8	6.7
plenum springs	steel 1.4568	9.2	0.65
spacer	Inc. 718	16.4	1.16
other metal parts	Inc. x 750	8.1	0.6
fuel	U	1000	70.3

2.2 Waste form and activity inventory

2.2.1 Inventory calculation

The radionuclide inventory is determined by burn-up calculations performed by FZK [42]. The burn-up of the spent fuel is assumed to be 45 GWd/t_{hm}. The assumptions regarding the initial inventory are summarized in the following tables. The initial inventory of all elements in the metal and fuel is the basis for the burn-up calculations. For all nuclides of these elements the activation by neutron radiation within the reactor is calculated.

The initial composition of all metal parts is listed in Table 2.5. The metal parts are divided into two sections. The middle section of the fuel element consists of the cladding tubes, sheaths and spacers. The top and bottom section of the fuel element consist of the head and tail pieces, plenum springs and other metal parts. It has been assumed that the neutron flux in the top and bottom area of the fuel elements is reduced compared with the middle section of the fuel element.

Table 2.5: Initial element inventory of the metal parts [37], [42]

element	mass [g/t_{hm}]		element	mass [g/t_{hm}]	
	middle parts	top/bottom		middle parts	top/bottom
B	$4.92 \cdot 10^{-1}$	-	Mn	$9.52 \cdot 10^{+2}$	$1.20 \cdot 10^{+3}$
C	$6.69 \cdot 10^{+1}$	$2.95 \cdot 10^{+1}$	Fe	$3.75 \cdot 10^{+4}$	$3.83 \cdot 10^{+4}$
N	$2.79 \cdot 10^{+1}$	$1.91 \cdot 10^{+1}$	Co	$9.66 \cdot 10^{+1}$	$1.92 \cdot 10^{+2}$
O	$3.80 \cdot 10^{+1}$	-	Ni	$1.35 \cdot 10^{+4}$	$1.17 \cdot 10^{+4}$
Al	$1.74 \cdot 10^{+2}$	-	Cu	$4.92 \cdot 10^{+0}$	-
Si	$5.53 \cdot 10^{+2}$	$5.98 \cdot 10^{+2}$	Zr	$2.88 \cdot 10^{+5}$	-
P	$2.26 \cdot 10^{+1}$	$2.23 \cdot 10^{+1}$	Nb	$8.21 \cdot 10^{+2}$	$8.11 \cdot 10^{+1}$
S	$1.73 \cdot 10^{+1}$	$1.75 \cdot 10^{+1}$	Mo	$5.91 \cdot 10^{+2}$	$1.28 \cdot 10^{+2}$
Ti	$2.48 \cdot 10^{+2}$	$3.42 \cdot 10^{+2}$	Sn	$4.39 \cdot 10^{+3}$	-
Cr	$1.23 \cdot 10^{+4}$	$1.13 \cdot 10^{+4}$	Ta	$1.64 \cdot 10^{+1}$	-

Table 2.6: Initial impurities of the fuel [37], [42]

element	mass [g/t_{hm}]	element	mass [g/t_{hm}]	element	mass [g/t_{hm}]
Li	$9.98 \cdot 10^{-01}$	Cl	$5.00 \cdot 10^{+00}$	Fe	$1.40 \cdot 10^{+01}$
B	$2.00 \cdot 10^{-01}$	Si	$1.60 \cdot 10^{+01}$	Co	$1.00 \cdot 10^{+01}$
C	$6.00 \cdot 10^{+00}$	P	$2.00 \cdot 10^{+00}$	Ni	$2.00 \cdot 10^{+00}$
N	$5.00 \cdot 10^{+00}$	K	$1.00 \cdot 10^{+01}$	Cu	$5.01 \cdot 10^{-01}$
O	$1.34 \cdot 10^{+05}$	Ca	$1.00 \cdot 10^{+01}$	Zn	$1.00 \cdot 10^{+01}$
F	$3.00 \cdot 10^{+00}$	Ti	$1.00 \cdot 10^{+01}$	Mo	$1.00 \cdot 10^{+00}$
Na	$1.00 \cdot 10^{+01}$	V	$1.10 \cdot 10^{+01}$	Sn	$9.92 \cdot 10^{-02}$
Mg	$2.00 \cdot 10^{+01}$	Cr	$3.00 \cdot 10^{+00}$	W	$2.00 \cdot 10^{+00}$
Al	$2.10 \cdot 10^{+01}$	Mn	$1.00 \cdot 10^{+00}$		

The LWR fuel itself is enriched to 3.6% of U-235 resulting in a composition of 0.275 kg U-234, 36 kg U-235 and 964 kg U-238 per t_{hm}. The fuel exists as UO_2 and contains small amounts of impurities. The initial inventory of the fuel impurities is shown in Table 2.6. These mass fractions are used as input values for the burn-up calculations.

2.2.2 Radionuclide selection criteria

For a safety assessment it is necessary to identify those radionuclides that might have some potential to give rise to significant radiation doses in the biosphere. For long-term safety those radionuclides have to be regarded, whose inventories are radiologically relevant and whose lifetimes are long in comparison to their transport times to the biosphere, e.g. the long-lived fission products and actinides. Additionally, parent nuclides which build long-lived daughters by radioactive decay can be of relevance. Those nuclides which only produce temperature effects and gas, have not to be regarded since no temperature effects and gas production processes are modelled in this study. A radionuclide selection based on the above-mentioned aspects and their toxicity potential has been made for a repository in salt. Fission and activation products and nuclides from the decay chains have been considered separately. The whole procedure is described in detail in [37]. Only the main aspects of this procedure are mentioned here.

2.2.2.1 Fission products

For the fission and activation products three criteria were applied in the selection process.

- Radiologically weighted activity of the nuclide after 1000 years. 1000 years are assumed as a minimum transport time for nuclides from the repository to the biosphere after closure of the repository.

- Radiologically weighted activity in a selected time frame. The time frame was chosen to be from the end of the operational phase of the repository until 10^7 years later. Activities after 10^7 years are assumed to be no longer safety relevant.

- Radiologically and temporally weighted activity in a selected time frame assuming that an early contamination of the biosphere is less probable than a later one.

These three criteria have been considered as equivalent, because it is not known at what time the biosphere contamination will occur. They have been applied to the data obtained from Korigen calculations [42] for spent fuel. The nuclides chosen by this procedure are C-14, Cl-36, Ni-59, Ni-63, Se-79, Rb-87, Sr-90, Mo-93, Nb-94, Tc-99, Pd-107, Sn-126, I-129, Cs-135, Cs-137, Sm-147 and Sm-151.

2.2.2.2 Nuclides from decay chains

For the nuclides from the decay chains a different procedure has to be applied because some of those nuclides do not exist immediately after discharge from the spent fuel but are built up by the radioactive decay of parent nuclides during transport through the repository system into the biosphere. For this reason all off the nuclides are considered and criteria were found for the purpose of neglecting some of them in the near- and far-field calculations. The following three categories have been regarded for the neglect of nuclides in decay chains.

- The first (parent) nuclides of a decay chain are to be neglected if they have shorter half-lives and masses that are a factor of 100 less than that of their respective daughters, i. e. their maximum activities are less than 1% of that of the daughter nuclides.

- Nuclides in the middle of decay chains are to be neglected if their half-lives are shorter than one year. Processes within time frames of one year are assumed to have no relevance in relation to the time frame for transport and release processes in the long-term safety assessment.

- Nuclides at the end of a decay chain are to be neglected if their half-lives are shorter than 25 years.

For the nuclides selected by this procedure:

- Cm-248, Pu-244, Cm-244, Pu-240, U-236, Th-232, U-232
- Cm-245, Pu-241, Am-241, Np-237, U-233, Th-229

- Cm-246, Pu-242, AM-242, Pu-238, U-238, U-234, Th-230, Ra-226
- Cm-247, Am-243, Pu-239, U-235, Pa-231,

release and transport will be calculated. The neglect of the other nuclides does not lead to an underestimation of radiation exposure in the biosphere because the inventories of nuclides from the first category are added at the beginning of the calculation to the inventory of their daughter nuclides. The nuclides from the second and third categories can be taken into account for the dose calculation assuming that parent and daughter nuclide are in radioactive equilibrium.

All nuclides identified by these selection procedures are in accordance with those taken into account in other safety assessment studies for repositories in granite-formations e.g. [27], [33].

2.2.3 Reference radionuclide inventory for performance assessment

The results of the burn-up calculations are summarized in Tables 2.7 and 2.8. For all radionuclides considered the calculated total inventory of the LWR-spent fuel with a burn-up of 45 GWd/t_{hm} is given as the inventory immediately after discharge. For the safety calculations a cooling time of 40 years for the repository in salt and 60 years in the case of a granite-repository has to be considered (s. Chapter 3.2).

Table 2.7: Inventory of spent fuel and metal parts (Bq·t_{hm}^{-1}) immediately after discharge: activation and fission products

element	half-life [y]	inventory		
		spent fuel	metal parts	total
C-14	$5.733 \cdot 10^{03}$	$1.28 \cdot 10^{10}$	$3.32 \cdot 10^{10}$	$4.60 \cdot 10^{10}$
Cl-36	$3.00 \cdot 10^{05}$	$6.10 \cdot 10^{08}$	$5.25 \cdot 10^{04}$	$6.10 \cdot 10^{08}$
Ca-41	$1.03 \cdot 10^{05}$	$3.01 \cdot 10^{07}$		$3.01 \cdot 10^{07}$
Co-60	$5.30 \cdot 10^{00}$	$8.16 \cdot 10^{13}$	$9.36 \cdot 10^{14}$	$1.02 \cdot 10^{15}$
Ni-59	$8.00 \cdot 10^{04}$	$6.97 \cdot 10^{07}$	$5.08 \cdot 10^{11}$	$5.08 \cdot 10^{11}$
Ni-63	$9.20 \cdot 10^{01}$	$1.09 \cdot 10^{10}$	$7.21 \cdot 10^{13}$	$7.21 \cdot 10^{13}$
Se-79	$6.50 \cdot 10^{04}$	$1.86 \cdot 10^{10}$		$1.86 \cdot 10^{10}$
Rb-87	$4.699 \cdot 10^{10}$	$1.05 \cdot 10^{06}$		$1.05 \cdot 10^{06}$
Sr-90	$2.914 \cdot 10^{01}$	$3.74 \cdot 10^{15}$	$1.37 \cdot 10^{08}$	$3.74 \cdot 10^{15}$
Zr-93	$1.531 \cdot 10^{06}$	$8.95 \cdot 10^{10}$	$9.24 \cdot 10^{09}$	$9.87 \cdot 10^{10}$
Nb-94	$2.031 \cdot 10^{04}$	$8.24 \cdot 10^{06}$	$8.49 \cdot 10^{10}$	$8.49 \cdot 10^{10}$
Mo-93	$3.501 \cdot 10^{03}$	$7.16 \cdot 10^{06}$	$4.29 \cdot 10^{09}$	$4.34 \cdot 10^{9}$
Tc-99	$2.132 \cdot 10^{05}$	$6.45 \cdot 10^{11}$	$6.87 \cdot 10^{08}$	$6.46 \cdot 10^{11}$
Pd-107	$6.50 \cdot 10^{06}$	$5.20 \cdot 10^{09}$		$5.20 \cdot 10^{09}$
Sn-126	$1.001 \cdot 10^{05}$	$2.79 \cdot 10^{10}$		$2.79 \cdot 10^{10}$
I-129	$1.571 \cdot 10^{07}$	$1.52 \cdot 10^{09}$		$1.52 \cdot 10^{09}$
Cs-135	$2.301 \cdot 10^{06}$	$1.59 \cdot 10^{10}$		$1.59 \cdot 10^{10}$
Cs-137	$3.002 \cdot 10^{01}$	$5.37 \cdot 10^{15}$		$5.37 \cdot 10^{15}$
Sm-147	$1.071 \cdot 10^{11}$	$6.70 \cdot 10^{04}$		$6.70 \cdot 10^{04}$
Sm-151	$9.006 \cdot 10^{01}$	$1.25 \cdot 10^{13}$		$1.25 \cdot 10^{13}$

The nuclides from the decay chains are not contained in metal parts but only in spent fuel.

Table 2.8: Inventory of spent fuel per t_{hm} immediately after discharge: nuclides from decay chains

nuclide	half-life [y]	invent. [Bq]	nuclide	half life [y]	invent. [Bq]
Thorium series			Uranium series		
Cm-248	$3.393 \cdot 10^{05}$	$2.91 \cdot 10^{05}$	Cm-246	$4.734 \cdot 10^{03}$	$4.25 \cdot 10^{10}$
Pu-244	$8.267 \cdot 10^{07}$	$4.34 \cdot 10^{04}$	Pu-242	$3.872 \cdot 10^{05}$	$1.15 \cdot 10^{11}$
Cm-244	$1.812 \cdot 10^{01}$	$2.16 \cdot 10^{14}$	Am-242m	$1.521 \cdot 10^{02}$	$1.91 \cdot 10^{11}$
Pu-240	$6.542 \cdot 10^{03}$	$2.39 \cdot 10^{13}$	U-238	$4.471 \cdot 10^{09}$	$1.16 \cdot 10^{10}$
U-236	$2.343 \cdot 10^{07}$	$1.19 \cdot 10^{10}$	Pu-238	$8.780 \cdot 10^{01}$	$1.63 \cdot 10^{14}$
Th-232	$1.406 \cdot 10^{10}$	$1.31 \cdot 10^{00}$	U-234	$2.447 \cdot 10^{05}$	$3.10 \cdot 10^{10}$
U-232	$7.204 \cdot 10^{01}$	$7.72 \cdot 10^{08}$	Th-230	$7.705 \cdot 10^{04}$	$6.00 \cdot 10^{05}$
			Ra-226	$1.601 \cdot 10^{03}$	$7.90 \cdot 10^{02}$
Neptunium series			Americium series		
Cm-245	$8.505 \cdot 10^{03}$	$1.70 \cdot 10^{10}$	Cm-247	$1.561 \cdot 10^{07}$	$9.34 \cdot 10^{04}$
Pu-241	$1.441 \cdot 10^{01}$	$5.79 \cdot 10^{15}$	Am-243	$7.385 \cdot 10^{03}$	$1.33 \cdot 10^{12}$
Am-241	$4.325 \cdot 10^{02}$	$6.43 \cdot 10^{12}$	Pu-239	$2.408 \cdot 10^{04}$	$1.31 \cdot 10^{13}$
Np-237	$2.141 \cdot 10^{06}$	$1.64 \cdot 10^{10}$	U-235	$7.043 \cdot 10^{08}$	$4.85 \cdot 10^{08}$
U-233	$1.586 \cdot 10^{05}$	$2.57 \cdot 10^{06}$	Pa-231	$3.279 \cdot 10^{04}$	$1.24 \cdot 10^{06}$
Th-229	$7.344 \cdot 10^{03}$	$7.95 \cdot 10^{03}$			

2.3 Waste packaging

2.3.1 Reference containers for disposal

For the disposal in granite smaller containers are used compared with the Pollux casks for disposal in salt. They are shown in Figure 2.1. This new container type was introduced in the German project GEISHA [28] as suitable for borehole disposal in granite. The container consists of a thin-walled metal tube with a wall thickness of 0.1 m and a

welded bottom. It is closed by a shielding cover, containing a neutron moderator, and a gastight welding cover. The container can hold fuel pins from three fuel elements. Its total mass is 7.95 t.

The metal parts of the container consist of fine grain steel 15MnNi6.3. Preliminary calculations show a pressure stability up to 20 MPa with a safety factor of 2.7, even if the wall thickness is reduced to about one half by corrosion-processes. The lifetime of the container is estimated to be 1000 years.

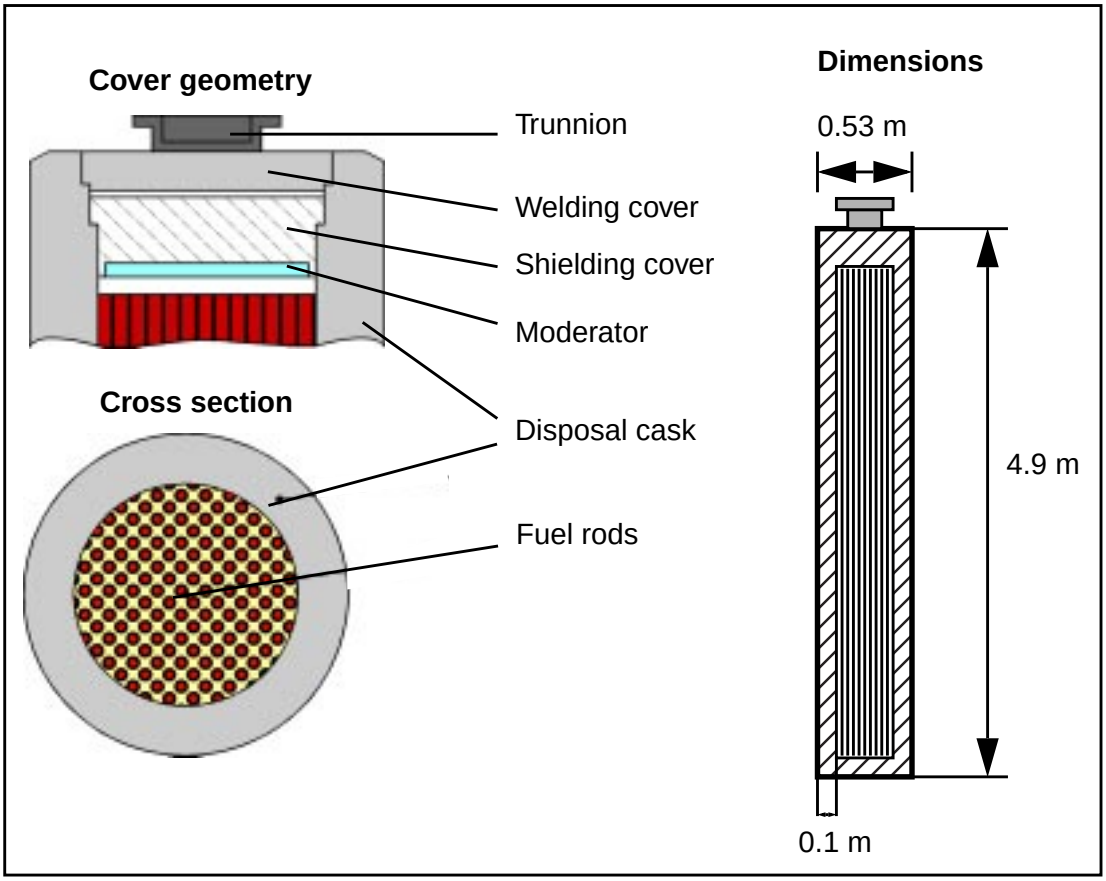

Fig. 2.1: Schematic view of a waste container for borehole disposal in granitic formations. In reality the pins are packed as compact as possible.

3 Site description and repository design in granite-formations

3.1 Site description

In Germany, the preferred host formation for the disposal of high level waste is rock salt. Therefore, no detailed investigations of granite-formations with regard to radioactive waste disposal have been performed so far. Within the national project GEISHA [28] possible German granitic sites have been compiled and roughly characterized. As shown in Figure 3.1 main granite formations are located in the southern and eastern parts of Germany, e.g. in the regions of the Black Forest, Fichtelgebirge, Erzgebirge, Lausitz and Thüringer Wald.

Most of these crystalline formations are of varistic type of age about $3 \cdot 10^8$ years. They are much younger than the Scandinavian granites. The German formations are situated in a more geologically active region and may be more intensively faulted or disturbed than the Scandinavian ones. Differences in petrography are not significant. The granitic waters in deeper layers are less mineralized than Scandinavian waters and are comparable in geochemical properties to the waters of northern Switzerland [28]. There is a direct connection between the granite formation in the Black Forest and the crystalline basement of northern Switzerland. Within this safety assessment study the properties of the German granite formation are based on the data used in the Swiss study Kristallin-I.

The potential German repository will be situated in the granite basement at 900 m depth. The thickness of the granite is assumed to be about 600 m. Some of the German formations are covered by sedimentary layers up to a thickness of 200 m. This will be regarded in parameter variations.

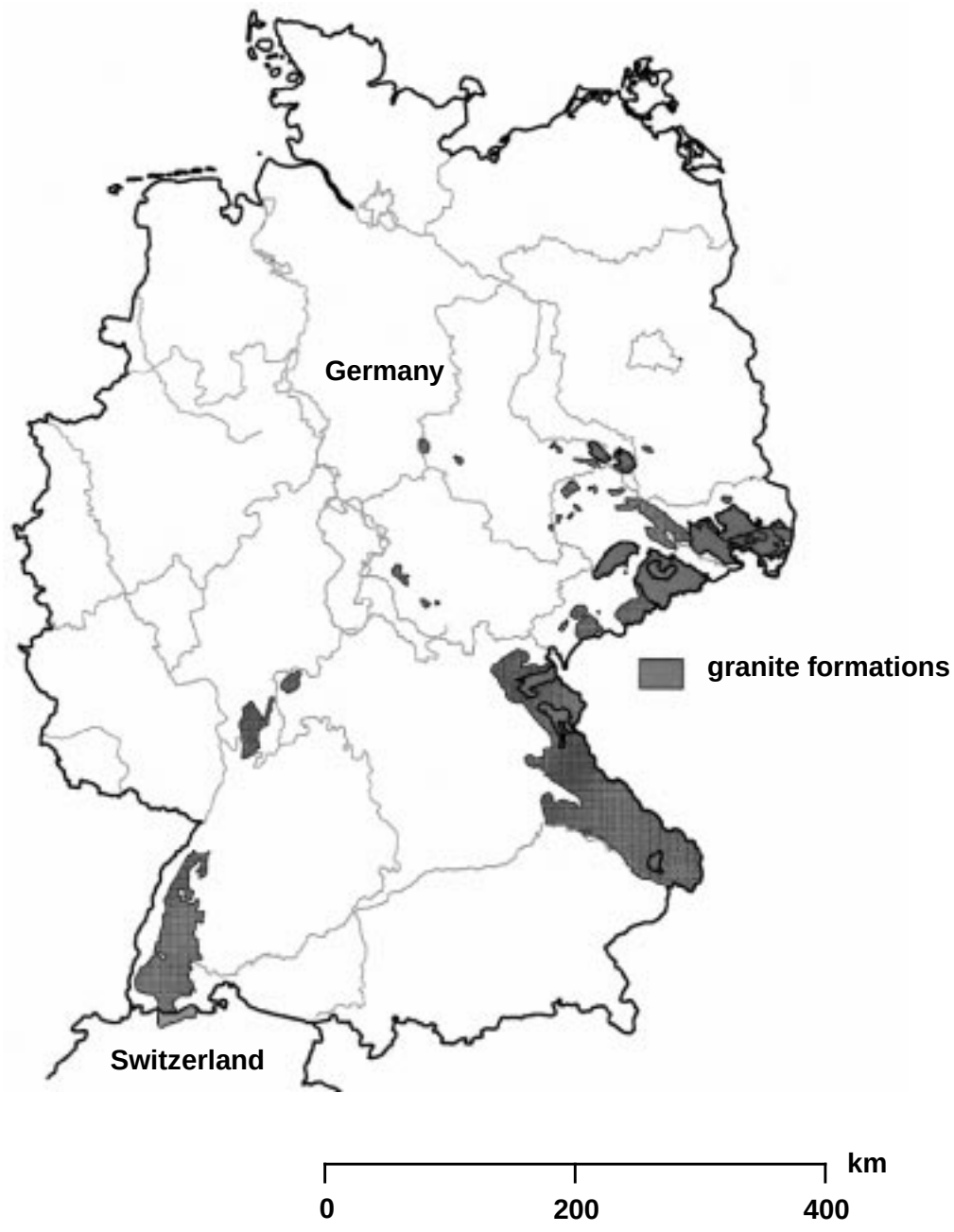

Fig. 3.1: Granite-formations in Germany and Northern Switzerland (see [8])

3.2 Repository design

3.2.1 Layout of the repository

A concept of a potential repository in a granite formation in Germany is proposed in the GEISHA project report [28] and considered as reference concept in the present study. The site of the repository is assumed to be at a depth of 900 m. A suitable place for hosting a safe repository is characterized by a large block of low-permeable crystalline rock. Generally, the geological situation is preferred, where the repository can be placed under a rock mountain (see Fig. 3.2). In this situation the repository can be customized by an access drift. If the surface of the potential site of the repository corresponds to a planar area as shown in Fig. 3.4 the repository can be customized by access tunnels.

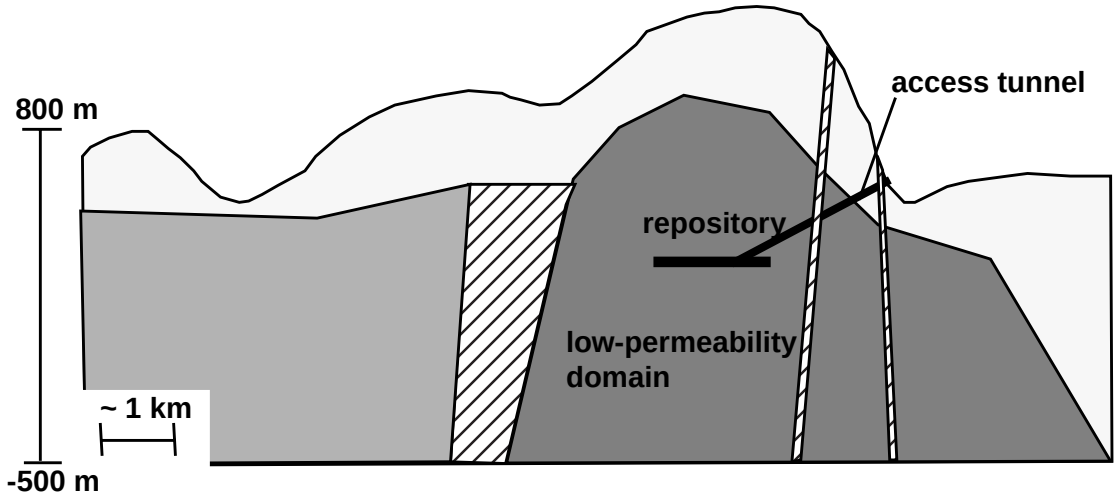

Fig. 3.2: Conceptual geological structure of a repository placed under granitic mountains. For access a tunnel is used.

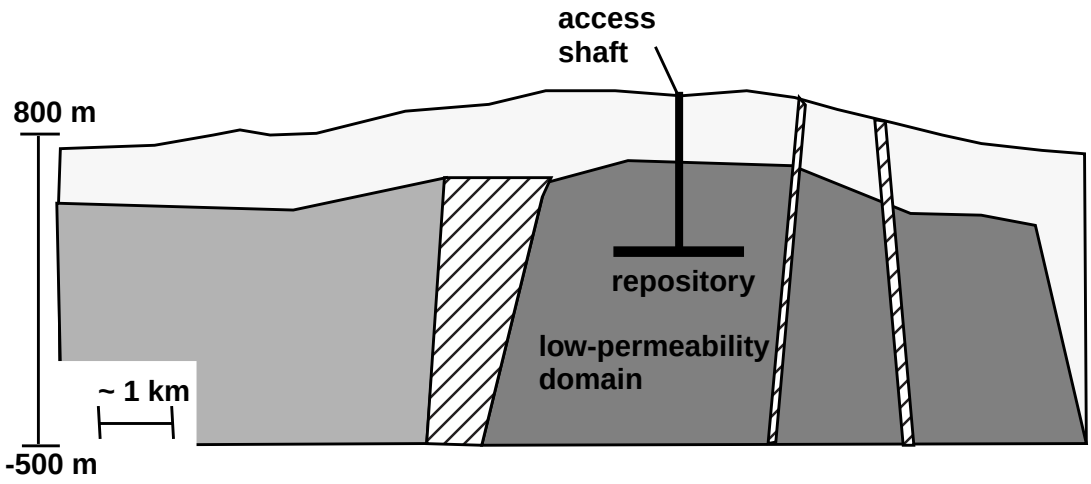

Fig. 3.3: Conceptual geological structure of a repository sited in regions with planar surface area. Shafts are used for access.

The repository is designed as a system of horizontal storage tunnels at one level schematically shown in Figure 3.4.

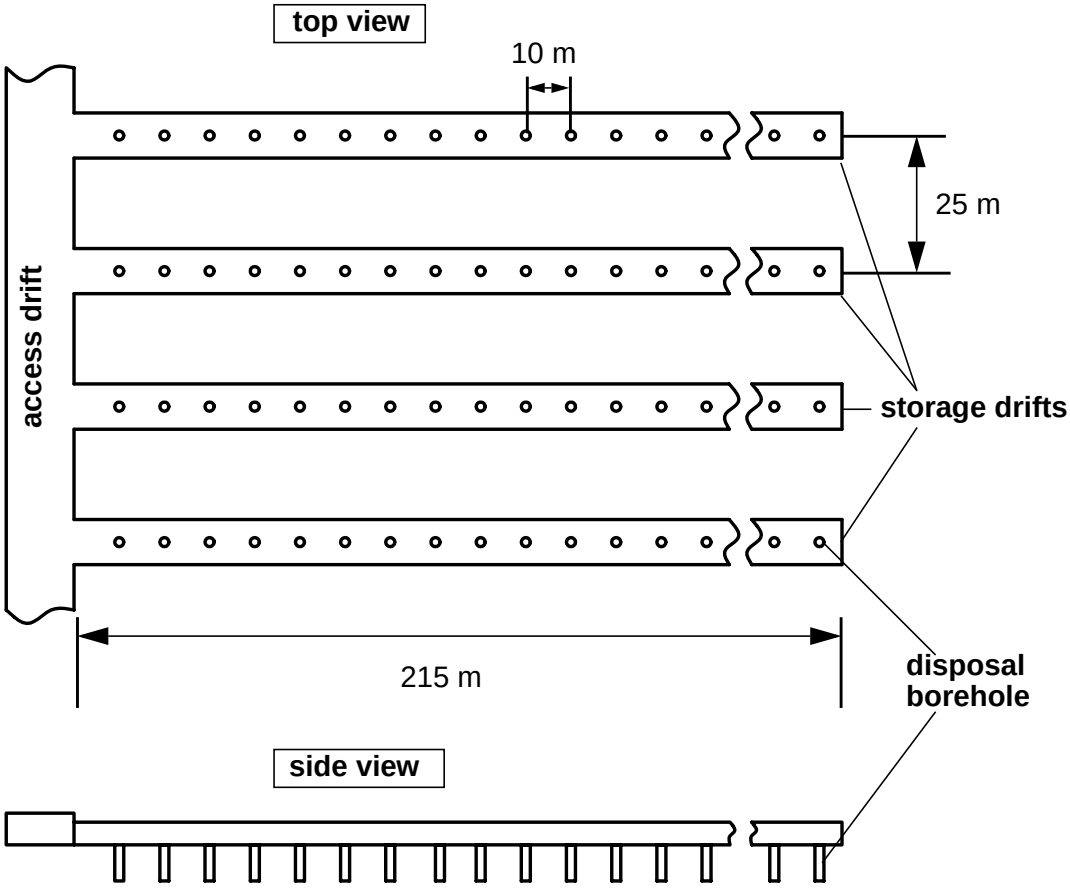

Fig. 3.4: Schematic view of the hypothetical repository for spent fuel in a granite formation

The containers are disposed of in 8.3 m deep vertical holes drilled into the floor of the drifts. The containers are surrounded by a buffer of compacted bentonite. As shown in Figure 3.5, only one container is deposed of in one borehole. A minimum spacing of 10 metres between the boreholes is necessary to keep the maximum temperature of the bentonite below 100^{o}C, since at such a temperature it is guaranteed that the bentonite will be stable and keep its barrier function [27]. The distance between the storage drifts is 25 metres.

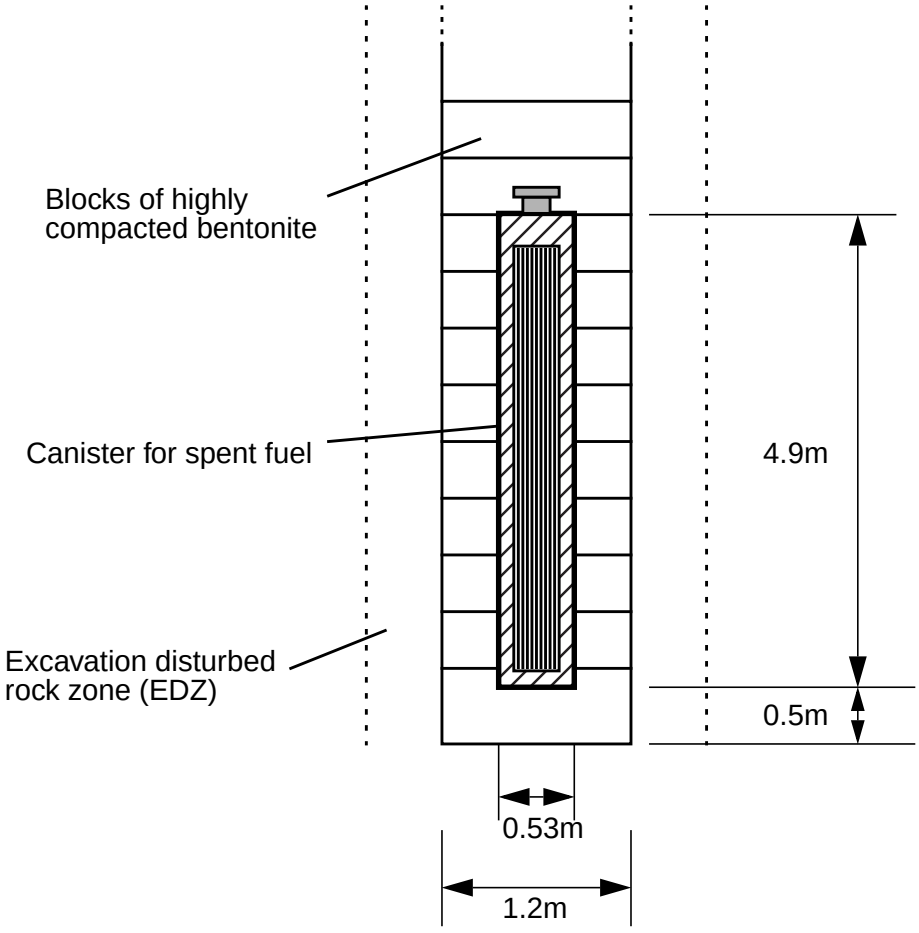

Fig. 3.5: Disposal borehole with canister, buffer and excavation-disturbed rock zone

3.2.2 Emplacement techniques

The planned transport and emplacement within the emplacement area is schematically shown in Figure 3.6. The containers are transported through the shaft to the emplacement area by a special carriage with a shielding overpack. This carriage stops at the top of the borehole and then the container is tipped into a vertical position by an implemented facility. After that it is lifted down into the borehole. This emplacement technique allows one to limit the cross section of the storage tunnel to 20 m^2.

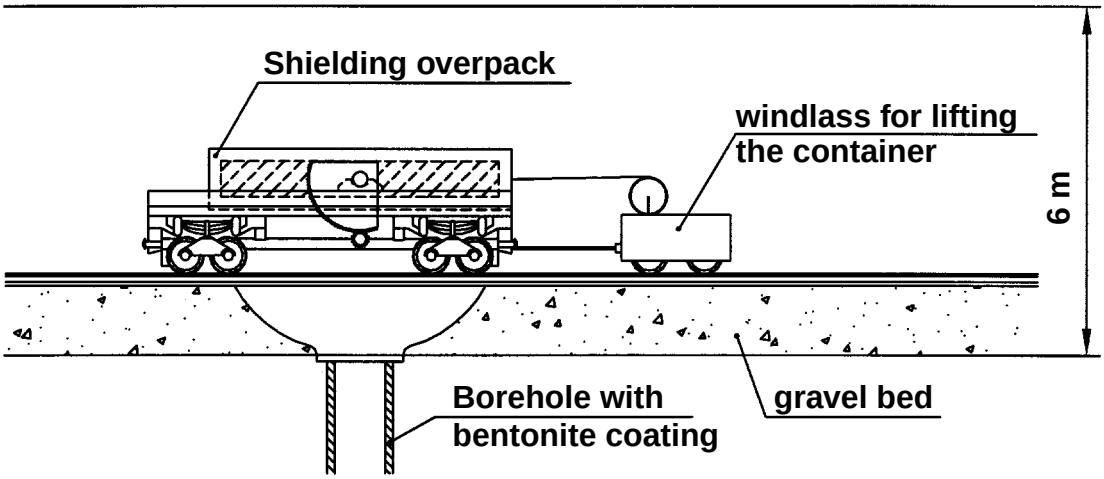

a) Transport to the borehole

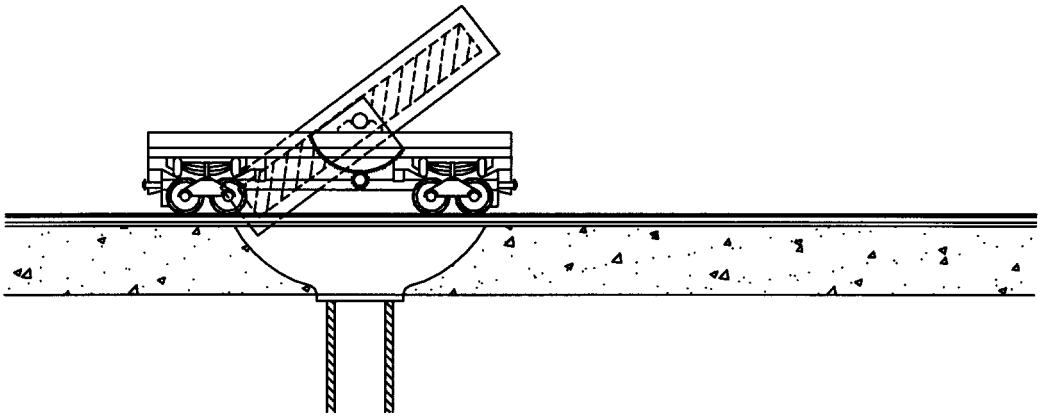

b) Tipping the container into the vertical position

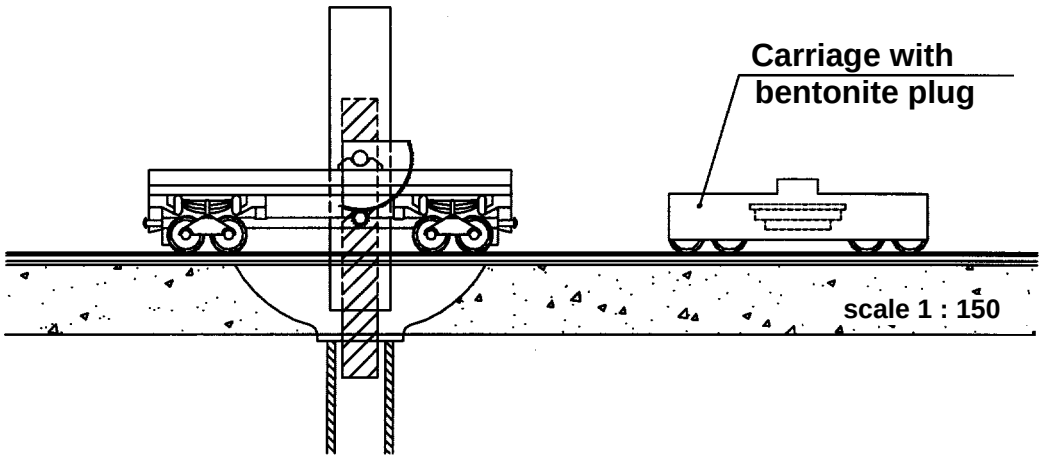

c) Lowering the container into the borehole

Fig. 3.6: Schematic representation of the emplacement procedure

3.2.3 Backfilling and sealing

The backfill concept for boreholes and emplacement drifts is similar to the Swedish study KBS-3. Before the emplacement of waste containers, bentonite powder is put into the open boreholes. The walls of the borehole will be coated with rings of compacted bentonite. The residual volume between bentonite blocks and rock will be filled with bentonite powder. After emplacement of the container into the prepared borehole the residual volume will be sealed with bentonite and the borehole will be closed with a bentonite plug. When all of the boreholes of a storage tunnel are filled with containers, the whole tunnel will be backfilled with a bentonite-sand mixture.

Since one container holds 1.602 t_{hm}, a total of 15 605 containers are required to package all of the waste. If all containers are disposed of at one level, the repository area will cover about $4.0 \cdot 10^6$ m^2.

4 Scenario development and treatment

4.1 Scenario selection methodology

The scenario selection procedure for a long-term safety assessment of a potential German repository in crystalline formations is based on a catalogue of potential features, events and processes (FEPs). Because the present study is the first German project dealing with the performance assessment of a repository in granite, the auditing of FEPs is essentially confined to the FEPs which were identified in the Swiss safety assessments PROJEKT GEWÄHR [25] and KRISTALLIN-I [27]. The following main relevant features are considered:

- waste form
- canister
- bentonite
- bentonite-host rock interface (excavation disturbed zone EDZ)
- low-permeability domain (LPD) of the granite
- sedimentary cover
- biosphere.

Starting with the FEP list the applied methodology for the scenario selection consists of the following steps:

- In a first step, the initial FEP list is screened against the potential German site and disposal concept which was proposed in the national GEISHA project [28]. The FEPs which are physically impossible or irrelevant for the specific disposal concept are excluded.
- In a second step, the remaining list is screened by using qualitative and quantitative arguments, estimation of impact and consideration of probability of the FEPs, and comparison to available assessment models. The FEPs which are excluded by this procedure can be categorised as
  - unimportant FEPs which have no significant impact on safety or have very low probability

  - reserve FEPs which could be beneficial to safety but are not included in the current assessment models
  - open questions which are potentially detrimental to safety and are identified as a subject for further investigation.
- The third step consists of the classification of those FEPs that correspond to a normal evolution scenario (reference scenario) which includes alternative model assumptions as well as altered evolution scenarios (alternative scenarios).

4.2 FEPs of the reference scenario

For the reference scenario FEPs related to engineered barriers, geological barriers and the biosphere are considered. A schematic representation of a repository system in crystalline formations is shown in figure 4.1.

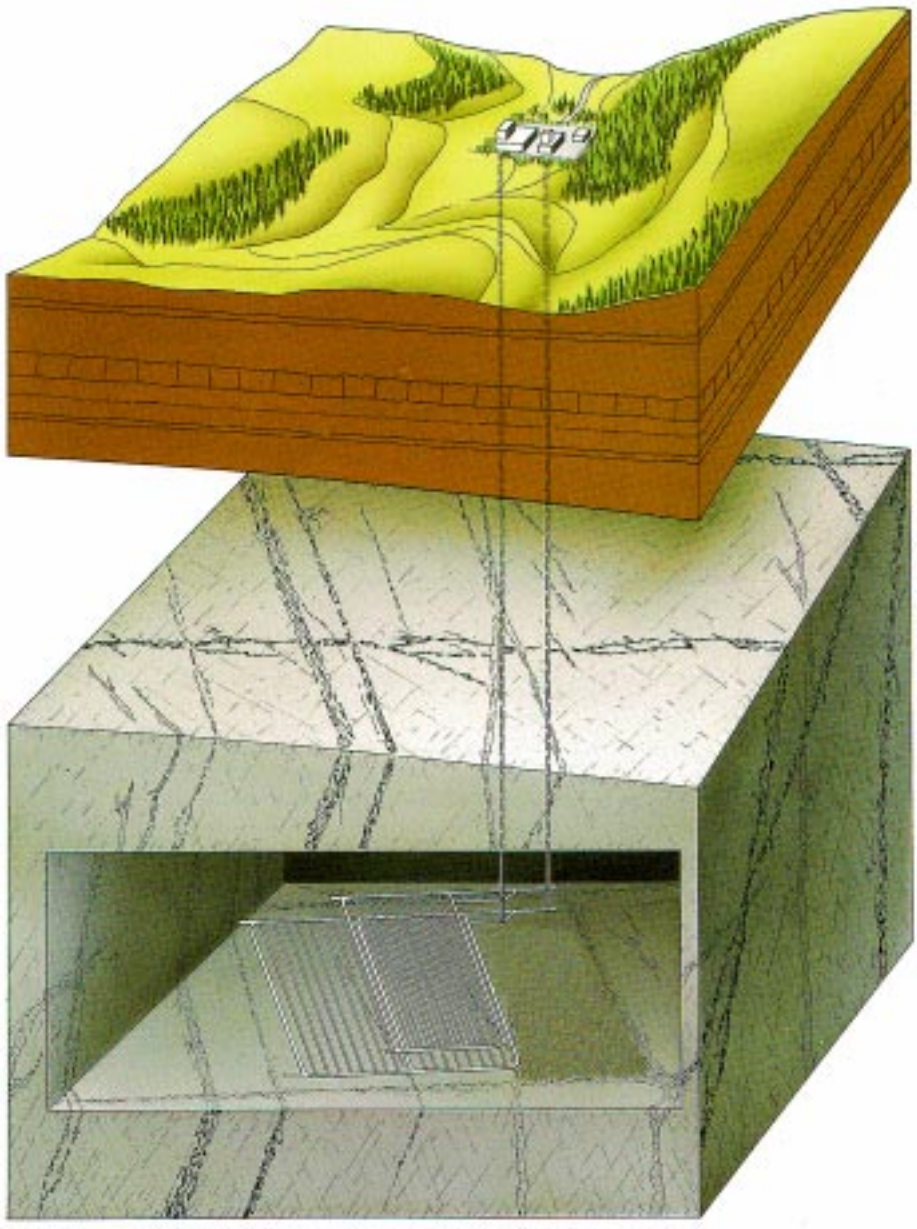

Fig. 4.1: Schematic view of a repository system (cf. [25])

4.2.1 FEPs related to the engineered barriers

When the backfill is emplaced in the repository, the highly compacted bentonite is only partly saturated. After the operational period the bentonite is slowly saturated by infiltrating water due to the difference in hydraulic potential between the surrounding rock and the bentonite. The time required for the saturation of the bentonite can be of signifi-

cance, since it delays the container corrosion and waste leaching. Calculations for Swiss repository conditions [27] using a two-phase flow model show that the time required for complete saturation of the bentonite ranges over several hundred (but less than a thousand) years. As a reference case we assume re-saturation of the bentonite immediately after repository closure, which should be a conservative assumption.

The container failure could be caused by the following processes:

- mis-sealed or unsealed container
- cracked container
- corrosion of the steel container.

In the reference scenario only corrosion of the massive steel containers is considered. The containers are assumed to fail simultaneously 1000 years after repository closure. The assumption that all containers fail at the same time is unlikely but tends to be conservative since peak releases from all containers occur simultaneously and are summed up. Estimated corrosion rates imply much longer lifetimes than 1000 years. Therefore, the assumption of container-failure at 1000 years is also conservative. The importance of the container-lifetime will be investigated by parameter variation. The influence of a non simultaneous failure of the containers can be examined by an alternative approach which considers different container-lifetimes.

During the time period from emplacement to container-failure only radionuclide decay and ingrowth are taken into account. It is assumed that, after failure, the container will offer no further physical resistance to water ingression or radionuclide release. The radionuclides are mobilized into the water which fills the void volume in the surrounding of the waste. This volume is assumed to correspond to the void volume inside the container. It is called volume of dissolution.

The chemical composition of the porewater in contact with the buffer and the waste is assumed to be dominated by the equilibrium of groundwater with bentonite and container corrosion products. In contact with bentonite the groundwater pH-values of about 7 shift into the alkaline range of 8 - 9. The redox potential, initially in the Eh range of -60 mV to 230 mV, becomes more negative because of the high amount of iron container-

material and reducing components in the bentonite. The chemical conditions will have been established in the bentonite porewater at the time of container-failure and are assumed to be stable over the whole time considered in long-term safety calculations.

The concentration of the radionuclides in the solution adjacent to the waste will be limited by element-specific solubilities. The solubility limits are estimated for reducing conditions of the bentonite porewater. The solubility limits are only applied to radionuclides in the volume of dissolution, but not within the bentonite. This may lead to an overestimation of the radionuclide release in the case of nuclides from decay chains.

Radionuclide migration through the bentonite occurs exclusively by diffusion in the aqueous phase. The advective transport can be neglected because of the very low bulk permeability of the saturated bentonite.

Colloids may be produced within the failed container. Radionuclides sorbed on colloids will not be transported away from the waste due to filtration of colloids by the microporous structure of the bentonite. Therefore, a neglect of sorption processes of radionuclides on colloids is a conservative assumption.

The diffusive transport of radionuclides is retarded by sorption on the bulk matrix of the bentonite. Sorption processes are assumed to be element-specific, instantaneous, concentration-independent and reversible.

Due to the construction of the drifts and shafts an excavation-disturbed zone (EDZ) is expected in an axial zone surrounding the drifts and shafts. The EDZ is assumed to act both as a uniform boundary condition for diffusion through the bentonite and as a connection for the radionuclide advective transport from the outer boundary of the bentonite to the water-conducting features of the host rock.

If the drift and shaft seals are not effective, two alternative transport pathways are to be cited the radionuclide transport along backfilled drifts and shafts, and the transport along continuous excavation-disturbed zones. In the safety analysis, only the transport along EDZs surrounding drifts and shafts is considered.

4.2.2 FEPs related to the geological barriers

Radionuclides released from the engineered barriers are transported by groundwater in discrete water-conducting features in the granite-formation. The present-day conditions regarding the geological, hydrological and geochemical conditions form the basis for the treatment of the geosphere. They are assumed to be unchanged during the time period under consideration. The radionuclides are transported through the geosphere by groundwater flow only. Transport by the gas phase or release to the biosphere by human activities are neglected.

Since the first investigations of the German granite-formations indicate hydrogeological and hydrogeochemical properties that are similar to those of the granite-formations in Switzerland, a geological structure similar to that described in KRISTALLIN-I is supposed:

- The geological and hydrogeological features are characterized on the largest scale (~1 km) by a low-permeability domain overlaid by a high-permeability sedimentary cover. The low-permeability domain is intersected by major water-conducting zones which extend up to the sedimentary cover.

- On an intermediate scale (~100 m) groundwater flow and radionuclide transport through the low-permeability granitic rock occurs in a network of discrete, water conducting features. They are classified as:
  - cataclastic zones
  - jointed zones
  - fractured aplite/pegmatite dykes and aplitic gneises.

The repository panels are assumed to be located in the low-permeability domain and at least 100 m away from any major water-conducting zone or sedimentary layer. Herewith, the following groundwater pathway is identified for transport of radionuclides from the repository to the biosphere:

- transport through the water-conducting features of the low-permeability domain to a major water-conducting fault, and hence through the sedimentary cover to the biosphere.

- In the reference case the radionuclides reaching the major water-conducting zones are assumed to be transported instantaneously to the biosphere.

Radionuclide advection is assumed to occur along open channels within the water-conducting features. These channels are simplified by a single type of water-conducting feature with constant characteristics in time and space. The advective transport within the rock matrix can be neglected because of the several-orders-of-magnitude lower permeabilities compared to the water-conducting features.

The interconnections between water-conducting features and their internal variability lead to a spreading of the advectivly transported concentration front. This effect of mechanical dispersion is modelled as a Fickian diffusion process in the advective flow direction. Transversal dispersion is conservatively neglected.

Molecular diffusion of radionuclides in the water-bearing zones can usually be regarded as negligible compared to the mechanical dispersion. Its significance lies in providing a mechanism for nuclide transport into accessible areas of stagnant water.

The process of matrix diffusion accompanied with sorption of the nuclides within the matrix is assumed to be the only retardation process of the nuclides relative to the velocity of the groundwater flow in the advective zones. Even neglecting the nuclide sorption in the matrix, matrix diffusion leads to a considerable retardation of the radionuclides. The sorption within the matrix is assumed to be rapid and completely reversible. The fraction of element concentration sorbed on the pore surfaces is determined by linear sorption isotherms. It is assumed that the matrix diffusion occurs only in a spatially limited region of altered rock adjacent to the fracture (“limited matrix diffusion”).

4.2.3 FEPs related to the biosphere

After far-field transport through the granite-formation the nuclides may reach the overlying sediments. From there the nuclides are transported to near-surface aquifers and the concentrations will be diluted due to mixing with the larger flux of uncontaminated groundwater. In the safety analysis the climate and natural environmental characteristics of the region of ex-filtration are assumed to be those of the present day and remain constant throughout the time period considered in the performance assessment.

In the biosphere different radionuclide pathways to humans exist:

- The contaminated groundwater is used for drinking water.
- Fish in rivers and surface lakes accumulate radionuclides from water and will be eaten by humans.
- The contaminated groundwater is used for the watering and irrigation of grass, vegetables and corn.
- The contaminated groundwater is used as drinking water and the contaminated grass and corn is used in the diet of cows and pigs.
- The inhabitants receive doses due to external irradiation from radionuclides in the soil.

It is assumed that human inhabitants of the region obtain all their dietary requirements from these local sources.

4.3 Selected scenarios for IPA

In summary, for the reference scenario the following assumptions hold:

- immediate re-saturation of the bentonite following repository closure
- canister failure not earlier than 1000 years after repository closure, at which time stable chemical and thermal conditions will have been established
- diffusion of radionuclides through the bentonite with sorption onto the bentonite pore surfaces

- advection of radionuclides away from the bentonite-host rock interface (EDZ) through the water-conducting features of the low-permeability domain taking into account dispersion, matrix diffusion, and sorption on matrix pore surfaces
- access of the radionuclides into the near-surface aquifers and exposure of man by various exposition-pathways.

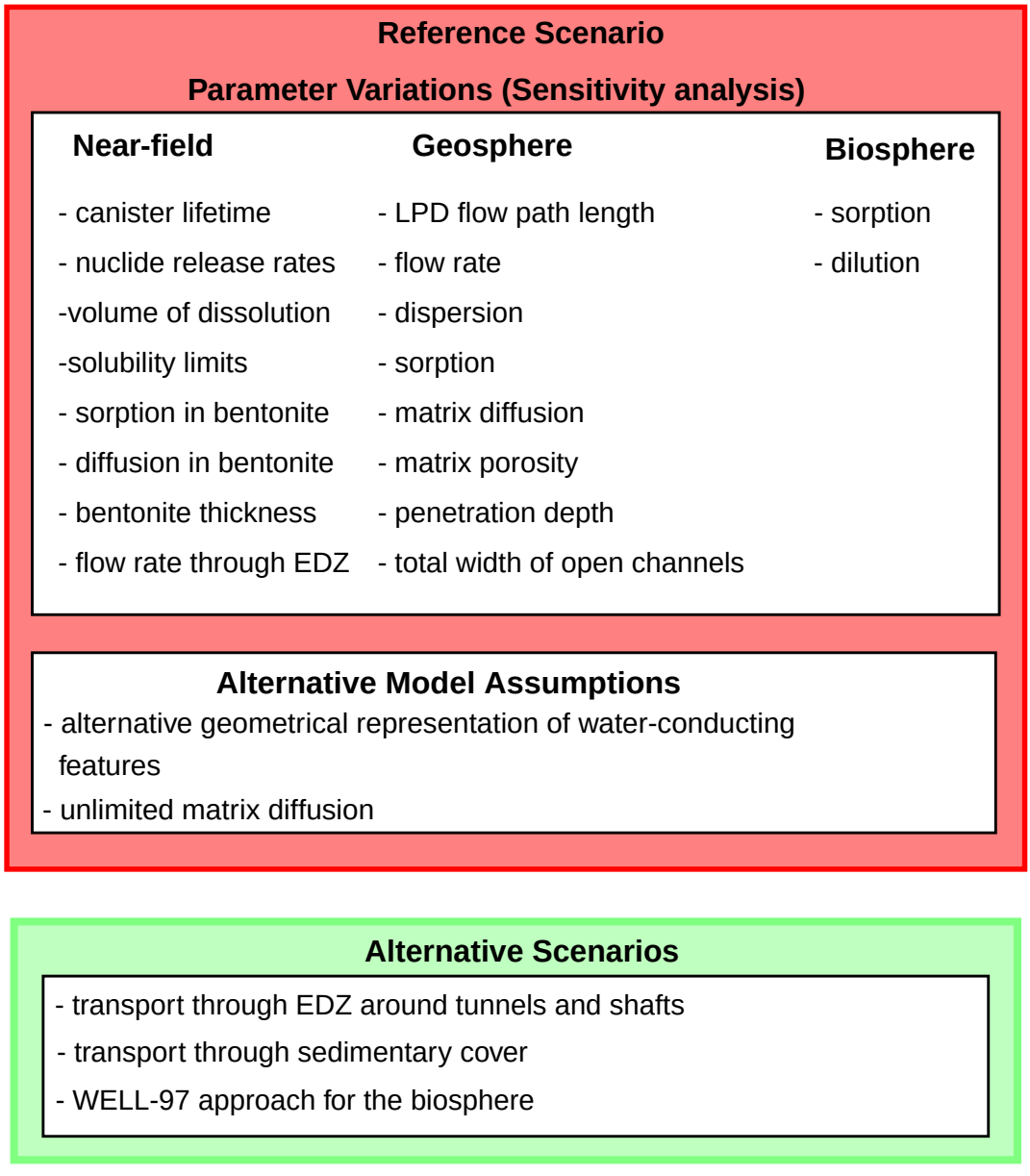

Fig. 4.2: Structure of calculations performed within the SPA-project

Within the SPA-project three alternative/extended scenarios are considered:

- In the AS-TTS scenario, the transport of radionuclides through the far-field is considered to occur through continuously connected excavation disturbed zones surrounding tunnels and shafts.
- In the extended scenario AS-TSC the barrier effect of the sedimentary cover is also taken into account.
- In the deep groundwater well scenario AS-DGW, the exposition-pathway is modelled according to the WELL-97 approach.

The safety analysis is performed deterministically, where conservative assumptions and data are used in the reference scenario. The impact of the respective features and processes are investigated via sensitivity analysis. A list of the parameters which are varied is shown in fig. 4.2. Additionally, alternative model assumptions with regard to the geosphere are considered in the sensitivity analysis.

5 Groundwater flow

5.1 Hydrogeology

As noted in chapter 3.2.1 a geological situation where the repository can be placed under a rock mountain is preferred. Under these prerequisites a generic site has been regarded, which is typical for areas found in the Erzgebirge Mountains or Black Forrest region in Germany. The repository is sited in a granite rock with a distance of at least 100 m from major water-conducting zones. A schematic representation of the site with values for the hydraulic conductivities K of each layer is given in fig. 5.1. The lower granite represents a low permeable medium. The upper part of the granite is characterized by a significantly higher hydraulic conductivity which is in the order of that from the major water conducting zones. The granite formation is covered by highly weathered granite, or a sedimentary cover, respectively.

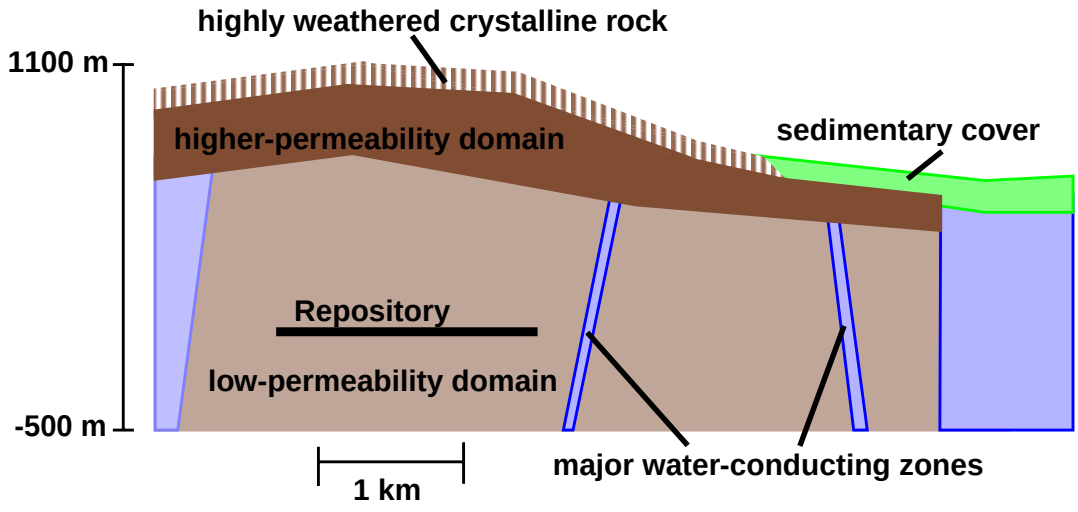

- **low-permeability domain of crystalline basement $K = 5.6 \cdot 10^{-11}$ [m/s]**
- **higher-permeability domain of crystalline basement $K = 2.8 \cdot 10^{-7}$ [m/s]**
- **highly weathered crystalline rock $K = 1.0 \cdot 10^{-5}$ [m/s]**
- **sedimentary cover $K = 1.0 \cdot 10^{-5}$ [m/s]**
- **major water-conducting zone $K = 3.2 \cdot 10^{-7}$ [m/s]**

Fig. 5.1: Schematic description of the generic German site with hydraulic conductivities assumed for distinct areas

5.2 Goundwater flow calculations

2D-groundwater flow calculations have been performed for a model area defined on the basis of the schematic description of the site in chapter 5.1. The assumed hydraulic conductivities of the distinct layers have been chosen according to the legend in figure 5.1. The values of the hydraulic heads are shown in fig. 5.2.

The calculated amount of the Darcy velocities are also shown fig. 5.2. Under the assumed conditions the Darcy velocity in the low permeability domain amounts to 10^{-5} - 10^{-4} m/y. In the major water conducting zones the Darcy velocity is in the range of 10^{-2} - 10^{-1} m/y, in the higher permeability domain 10^{-1} - 1 m/y and in the highly weathered granite and sedimentary cover at about 10 m/y.

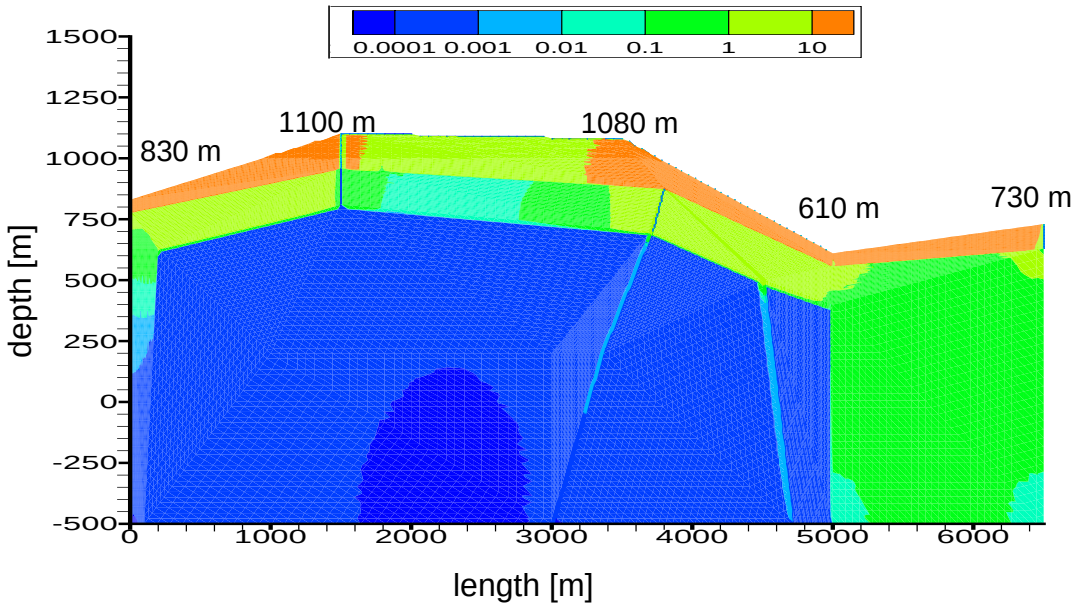

Fig. 5.2: Calculated amount of the Darcy velocities in [m/y]

5.3 Dilution

The groundwater which contains radionuclides released from the repository is diluted on its way to the ex-filtration zone. This dilution is caused by the great quantities of water circulating in higher-permeability rocks, in aquifers and near-surface water. The dilution results in an effective reduction of radionuclide concentrations in the water entering the biosphere. In the present analysis two interfaces at which dilution occurs are considered:

- interface between the low-permeability domain and major water-conducting zone
- interface between the major water-conducting zone and near-surface layers such as the sedimentary cover or strongly altered granite.

The parameters which determine the magnitude of dilution are shown in figure 5.3.
The dilution can be estimated:

$$\begin{aligned} \text{Dilution} &= \frac{Q_S}{Q_M}\frac{Q_M}{Q_L} \\ &= \frac{q_S}{q_M}\frac{b_S W_L}{b_M W_L}\frac{q_M}{q_L}\frac{b_M W_L}{b_L W_L} \\ &= \frac{q_S}{q_M}\frac{b_S}{b_L}, \end{aligned} \qquad (1)$$

with

$Q_L,\ Q_M,\ Q_S$ volumetric flows in low-permeability domain, second order major water-conducting zone and surface layer

$q_L,\ q_M,\ q_S$ Darcy-flux of the different regions

$b_L,\ b_M,\ b_S$ thicknesses of the control volumes.

W_L width of the repository in the low permeability zone

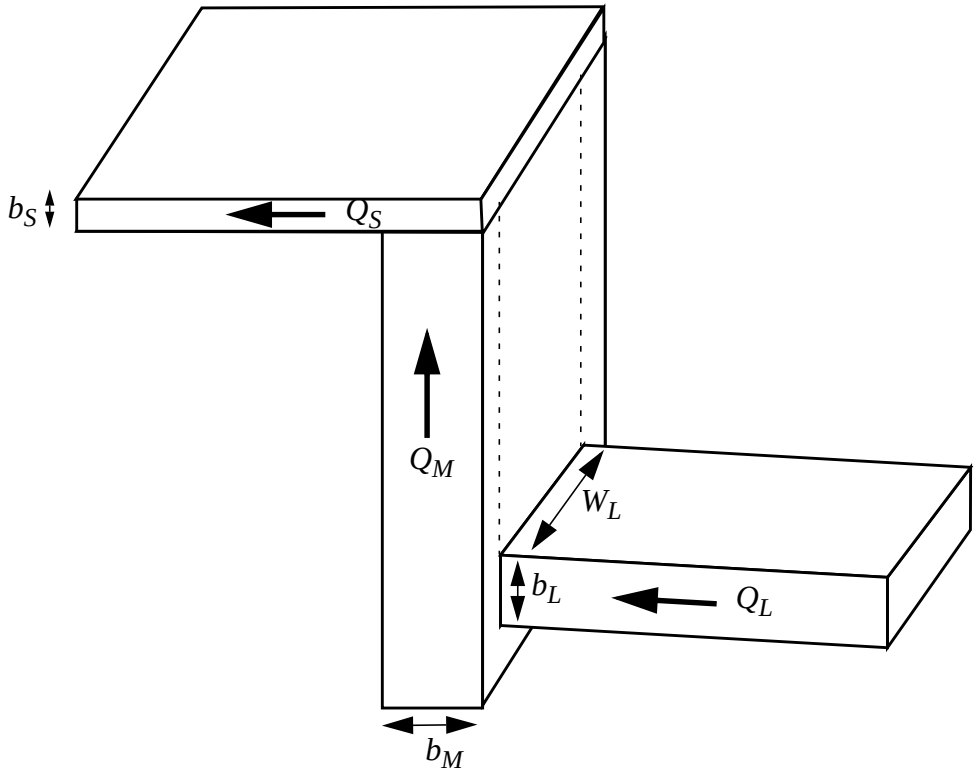

Fig. 5.3: Sketch of control volumes used for the estimation of dilution from low-permeability domain to near-surface layers; modified figure after [26].

In the NAGRA study KRISTALLIN-I an average volumetric flow through the biosphere of $5.5 \cdot 10^6$ m^3/y and an average volumetric flow through the repository site in the low-permeability domain of 30 m^3/y was assumed which corresponds to an effective dilution of about $1.8 \cdot 10^5$. The dilution between the low-permeability domain and major water-conducting zone of second order was estimated to be a factor of 400.

In our safety analysis, the dilution is estimated in the following way. Based on the groundwater calculations in chapter 5.2 the Darcy-velocity in the low-permeability domain and in the near-surface layer is estimated to be $3.5 \cdot 10^{-5}$ m/y and 10 m/y, respectively. The surface layers are supposed to have a thickness of 40 m and the thickness b_L is assumed to be 200 m. This results in a dilution of $5.7 \cdot 10^4$. Under the assumption of an average volume flow of 140 m^3/y through the repository, the dilution factor corresponds to a volumetric flow through the layers near the biosphere of $8 \cdot 10^6$ m^3/y.

6 Engineered barrier system

6.1 Canister

The design of the container for borehole disposal in granite has already been described in chapter 2.3.1. The container consists of a thick-walled steel metal tube of thickness 0.1 m and a welded bottom. It is closed by a shielding cover containing a neutron moderator, and a gastight welding cover. The metal parts of the container consist of fine grain steel 15MnNi6.3.

Preliminary calculations show that the container will guarantee the following criteria

- a pressure stability up to 20 MPa (a safety factor of 2.7 and a reduction of the wall thickness by about 50 % due to corrosion are assumed) and
- a minimum lifetime of 1000 years. The 15MnNi6.3 steel provides high resistance against corrosion by the surrounding brine or water.

For the calculations, it is assumed in the reference case that all containers will fail after 1000 years. This is conservative, since the estimated corrosion rates imply lifetimes ≥ 1000 years. In parameter variations it will be assumed that some containers are defective and fail earlier, and that the remaining containers will fail e.g. between 1000 and 2000 years.

6.2 Bentonite buffer

6.2.1 Temperatures and mechanical stability

The stability of the fine grain steel 15MnNi6.3 in different brines has been investigated by the German Institut für Nukleare Entsorgungstechnik (INE, FZK). The results of the corrosion experiments show that even in aggressive salt brines not more than 50 mm of the steel will corrode in 1000 years at temperatures of 100^{o}C. No local corrosion has been

observed. The groundwater in German granite-formations is expected to be less aggressive than salt brines, i.e. the container wall thickness of 100 mm will be sufficient to guarantee a container lifetime of at least 1000 years.

If in Germany a decision for a site within a granite formation for disposal of radioactive waste is made, more detailed corrosion experiments with waters from such sites will have to be performed in order to verify container performance criteria.

6.3 Engineered barrier performance

6.3.1 Performance constraints and criteria

The containers are disposed of in 8.3 m deep vertical holes drilled into the floor of the tunnels as described in chapter 3.2. The containers are surrounded by a buffer of compacted bentonite. The main criteria is to keep the maximum temperature of the bentonite below 100^{o}C, since at such temperatures it is guaranteed that the bentonite will be stable and retain its barrier function [27]. For that reason temperature calculations based on geometrical data of the potential German repository design have been performed [28].

The calculated temperature at the interface between container and bentonite is plotted in fig. 6.1 for the three different cases described in table 6.1. A burn-up of 45 GWd/t_{hm} and a distance of 25 m between the storage tunnels are assumed. Under these conditions only case A fulfils the 100^{o}C criterion. If the burn-up of the elements is increased a longer cooling time is needed to keep the temperature below 100^{o}C, i.e. 70 years for 50 GWd/t_{hm} and 90 years for 60 GWd/t_{hm}.

Table 6.1: Description of cases A, B and C considered in temperature calculations

case A	3 fuel elements	cooling time: 60 y	1.090 W	borehole distance: 10 m
case B	3 fuel elements	cooling time: 30 y	1.795 W	borehole distance: 8 m
case C	5 fuel elements	cooling time: 60 y	1.817 W	borehole distance: 8 m

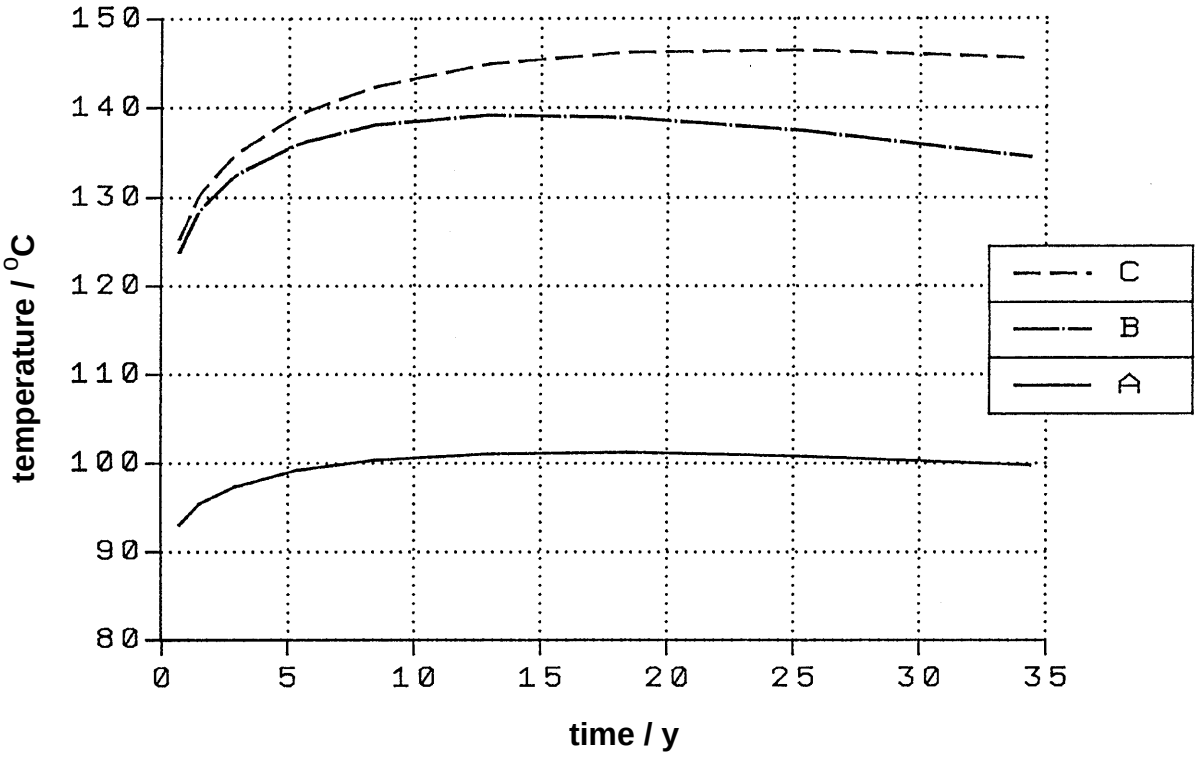

Fig. 6.1: Temperature at the container/bentonite interface for three different cases [28]

6.3.2 Re-saturation of bentonite

After the emplacement of the waste and the closure of the repository, groundwater flow regimes begin to establish themselves in the repository area. With time, the bentonite, proposed as a backfill material around the spent fuel waste becomes re-saturated due to the influx of groundwater from the crystalline basement. The bentonite is expected to swell and seal gaps between blocks, at the bentonite-host rock interface, and at the bentonite-canister interface, so that a homogeneous mass is formed.

The time required for saturation of the bentonite is important concerning the corrosion rate of the canister, the leaching of the waste matrix, and the radionuclide transport through the bentonite backfill. This time depends on the hydraulic properties of the bentonite as well as on the hydraulic conductivity of the crystalline rock.

6.3.2.1 Re-saturation model

The infiltration of water in the bentonite backfill can be physically described as a two-phase flow problem consisting of a water phase and a gas phase. A common approach for the flow in unsaturated zones, assuming the gas to be static and focusing on the movement of the water phase, leads to the so-called Richard's equation [12]:

$$M(\theta)\frac{\partial \psi}{\partial t} = \operatorname{div}(K(\theta)\operatorname{grad}\psi) + \frac{\partial}{\partial z}K(\theta), \qquad (2)$$

with

$K(\theta)$ hydraulic conductivity

$M(\theta)$ specific moisture capacity = $d\theta \,/\, d\psi$

θ moisture content = (volume of water) / (total volume of bentonite)

$\psi(\theta)$ pressure head = $p \,/\, (\rho g)$

g acceleration of gravity

p pressure.

Equation (2) is based on the assumptions of a constant water density ρ and the incompressibility of the porous medium. For horizontal flow the gravity term can be neglected and the moisture-content based formulation of equation (2) is given by

$$\frac{\partial \theta}{\partial t} = \operatorname{div}(D\operatorname{grad}\theta), \qquad (3)$$

with the water diffusivity or moisture diffusivity $D(\theta) = K(\theta) \,/\, M(\theta)$. In terms of the saturation S equation (3) results in

$$\frac{\partial S}{\partial t} = \operatorname{div}(D\operatorname{grad}S), \qquad (4)$$

with

S water saturation = θ / n

n porosity.

For the estimation of the saturation of the bentonite barrier the diffusion through the bentonite is considered radial, and the diffusion equation (4) becomes

$$\frac{\partial S}{\partial t} = \frac{\partial}{\partial r}\left(r D \frac{\partial S}{\partial r} \right). \qquad (5)$$

The boundary at the inner radius r_{in} of the bentonite is assumed to be closed for diffusive flux:

$$D \frac{\partial S}{\partial r}\bigg|_{r = r_{\text{in}}} = 0. \qquad (6)$$

As the boundary condition at the outer boundary of the bentonite buffer with radius r_{out} an influx boundary condition is used:

$$n D \frac{\partial S}{\partial r}\bigg|_{r = r_{\text{out}}} = F_{\text{in}}. \qquad (7)$$

The influx F_{in} is determined as the maximum between the water flux through the excavation-disturbed zone Q and the diffusive influx into the bentonite buffer assuming water saturation on the outer bentonite boundary. For a sufficiently large water flux through the disturbed zones compared with the water flux into the bentonite, the condition (7) corresponds to the Dirichlet boundary condition

$$S|_{r = r_{\text{out}}} = 1. \qquad (8)$$

6.3.2.2 Estimation of the re-saturation time

The calculations for the estimation of the re-saturation time are based on the diffusive-type equation (7). For the assessment of the impact of water flux through the disturbed zones surrounding the bentonite, simulations with varying water fluxes are performed. A constant water diffusivity of $3 \cdot 10^{-10}$ m^2/s is assumed in accord with the results of the experiment on bentonite saturation reported in [2, 21]. The residual water saturation of the bentonite is estimated to be 0.25 %. The bentonite buffer is assumed to be 6.4 m in height with an inner radius of 0.265 m and an outer radius of 0.6 m. For the porosity of the bentonite a value of 0.38 has been used [27].

The results of the calculations are shown in figure 6.2. Hereby, the bentonite has been considered to be in a saturated state, i.e. at 95 % saturation. For a water flux per canister in the range of 1 - 100 l/y the saturation time of bentonite is limited by the water flux through the disturbed zones. The saturation times range approximately from 100 to 1000 years. For values of water flux higher than 100 l/y the saturation time is limited by the diffusion time of the water into the bentonite. As can be seen in figure 6.2, this time is independent of the water flux surrounding the bentonite buffer.

For a water flux per canister of 10 l/y , the bentonite is estimated to be saturated after 150 years. Compared with the saturation times assessed for the bentonite buffers used in the Swiss disposal concept [27], the obtained saturation times are shorter. This is due to the fact that the bentonite thickness is about a factor of four smaller than the thickness of the bentonite buffer proposed in the Swiss disposal concept.

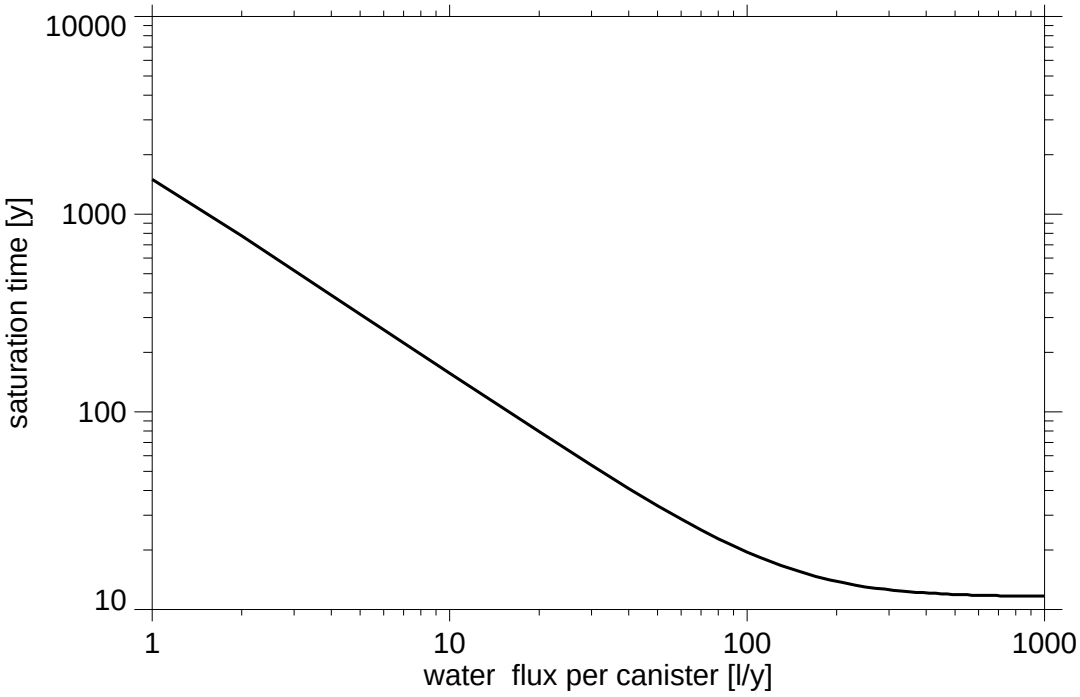

Fig. 6.2: Saturation time of the bentonite buffer versus water flux per canister

7 Near-field model and data

7.1 Near-field model

The near-field model describes the release of radionuclides and their transport through the engineered barriers of the near field to the water-conducting zones of the geosphere. A schematic representation of the near-field is given in Figure 7.1.

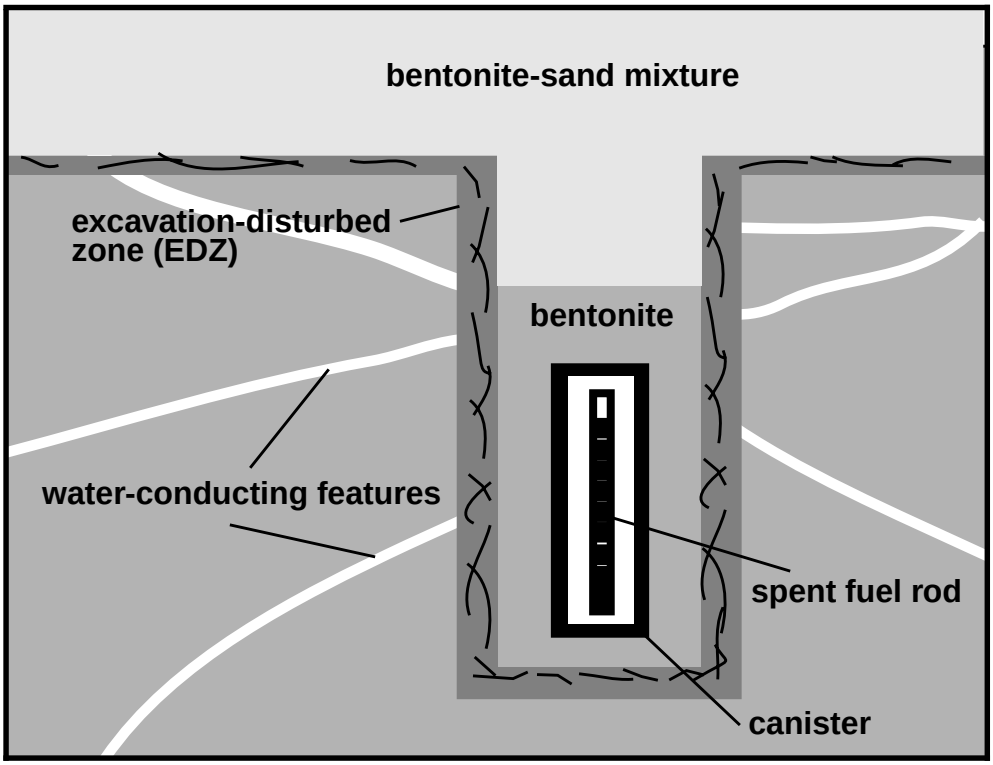

Fig. 7.1: Schematic representation of the near field with canister, borehole, excavation-disturbed rock zone and emplacement drift

The following principal components of the engineered barriers have been taken into account in the conceptual near-field model:

- the spent fuel matrix
- the massive steel container
- the highly compacted bentonite buffer.

If the spent-fuel matrix is dissolved the radionuclides may be mobilised in the water phase or immobilised in other phases caused by processes such as precipitation/dissolution and sorption. The radionuclides may diffuse through the bentonite barrier and reach water-conducting zones of the far-field.

A schematic representation of the transport mechanisms considered in the near field is given in Figure 7.2.

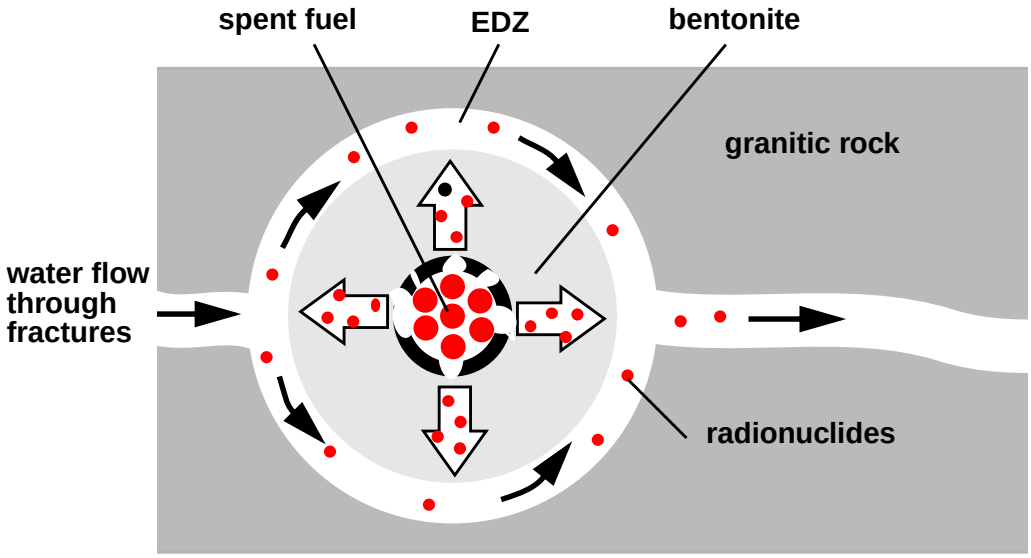

Fig. 7.2: Schematic representation of the mechanisms modelled in the near-field transport code GRAPOS

7.1.1 Mobilisation of radionuclides from spent fuel

Before the container failure, the activities of radionuclides will change due to radioactive decay and ingrowth only. For the *i*th radionuclide with decay constant λ^i the change of inventory A^i is given by the following differential equation:

$$\frac{\partial}{\partial t}A^i(t) = -\lambda^i\left(A^i(t) - \sum_k A^k(t)\right), \qquad (9)$$

where the index k denotes the parent radionuclides of the *i*th radionuclide.

In calculating the release of radionuclides from the waste matrix a potential barrier effect of the container or cladding is neglected. Therefore, the radionuclide release into the volume of dissolution starts immediately after failure of the first container. The mobilisation process is modelled according to the common source term model developed by all SPA participants [4]. The source term model distinguishes between the inventory in the gap, the metallic parts and the fuel matrix. The metallic parts include the cladding and the structural parts of the fuel element. For the gap inventory, an instantaneous release whereas for the metallic part and the fuel matrix a constant degradation rate is assumed (s. chapter 7.2.2).

The release $S^i(t)$ of nuclide *i* is described by

$$S^i(t) \;=\; n_c(t) \sum_x \alpha_{x,\ e(i)}\, r_x A^i(t)\ , \qquad (10)$$

where r_x is the constant release rate in the respective regions *x* (gap, metal parts, matrix), $a_{x,\ e(i)}$ the element-specific fraction of the so called “hypothetical inventory” $A^i(t)$ of the *i*th nuclide in region *x*, and $n_c(t)$ is the number of failed containers at the time *t*. The “hypothetical inventory” $A^i(t)$ corresponds to the initial inventory changed only by radioactive decay and ingrowth.

7.1.2 Solubility limits and the waste-bentonite interface

After container failure the interior of the container becomes water-saturated and then the radionuclides are mobilized. In the model a hypothetical “volume of dissolution” V_{dis} is assumed, in which radionuclides are released. The change in the inventory M^i in this volume is given by the differential equation

$$\begin{aligned} \frac{\partial}{\partial t} M^i(t) \;=\; & -\lambda^i \left[M^i(t) - \sum_k M^k(t) \right] + S^i(t) \\ & -2\pi r_{\mathrm{in}} h \varepsilon_b D_b \frac{\partial}{\partial r} C^i(t) \Big|_{r \,=\, r_{\mathrm{in}}}, \end{aligned} \qquad (11)$$

where r is the radial distance, r_{in} the initial radius and h the axial length of a waste container. The terms on the right-hand side represent radioactive decay and ingrowth, release from spent fuel, and diffusion into the bentonite, respectively. The release from spent fuel $S^i(t)$ is given in chapter 7.1.1.

The boundary condition at the inner interface of the bentonite is defined by the radionuclide concentration in the hypothetical volume of dissolution V_{dis}. Including the solubility limits $L^{e(i)}$ [mol/m^3], the concentration C^i [Bq/m^3] of the ith radionuclide at the inner interface of the bentonite is determined by

$$C^i\Big|_{r\,=\,r_{\mathrm{in}}} \;=\; \min\left(\frac{M^i}{V_{\mathrm{dis}}},\; \frac{M^i}{M_{\mathrm{el}}^{e(i)}} L^{e(i)}\right) , \qquad (12)$$

where $M_{\mathrm{el}}^{e(i)}$ is the number of moles of element e of which the radionuclide i is an isotope.

7.1.3 Diffusion through the bentonite

The radionuclides are assumed to be transported through the bentonite only by diffusion. For the calculation of this diffusive transport the geometry is simplified in such a way that only one-dimensional radial diffusion is considered. Then the governing equation for the transport through the bentonite is given by

$$R^i \frac{\partial C^i}{\partial t} \;=\; D_b \left[\frac{1}{r}\frac{\partial}{\partial r}\left(r\frac{\partial C^i}{\partial r}\right)\right] - \lambda^i \left[R^i C^i - \sum_k R^k C^k\right] . \qquad (13)$$

The index k denotes the parent radionuclides of the ith radionuclide. Assuming linear sorption yields the following retardation factor R^i:

$$R^i \;=\; 1 + \frac{1-\varepsilon_b}{\varepsilon_b}\rho_b K_d^{e(i)} \qquad (14)$$

with the density of bentonite ρ_b [kg/m^3], the bentonite porosity ε_b, and the element-specific distribution coefficient for bentonite $K_d^{e(i)}$ [m^3/kg]. No solubility limits are applied during the transport through the bentonite. This means that the dissolved amount of daughter nuclides formed during the diffusion process by decay of their parents may exceed the solubility limits.

7.1.4 Release to the host rock

At the interface between the bentonite and the excavation-disturbed zone (EDZ) which is intersected by water-conducting features of the granitic rock, the so called “mixing tank” boundary condition is used. In that case, the diffusive flux across the bentonite-host rock interface is determined in such a way that the diffusive flux is equal to the mass flux by advection in the excavation-disturbed zone:

$$2\pi r_{\text{out}} h \varepsilon_b D_b \frac{\partial C^i}{\partial r}\bigg|_{r = r_{\text{out}}} = Q_{\text{EDZ}} C^i . \qquad (15)$$

The groundwater flow Q_{EDZ} [m^3/y] through an excavation-disturbed zone of a deposition hole is controlled by the total water flow Q through the repository area by $Q = F_{\text{nc}} \sum_n Q_{\text{EDZ}}$. The fraction of the water flow around a deposition hole entering the excavation-disturbed zone is determined by the parameter F_{nc}. For the reference case a total flow rate around a deposition hole of 9 l/y and a flow rate through the EDZ of 1 l/y is assumed.

7.2 Near-field data

7.2.1 Available data and backing assumptions

The radionuclide migration data are based on results from different countries which are planning repositories for high level radioactive waste in granite-formations. Most of the data, especially geochemical parameters, are taken from the NAGRA study Kristallin-I [27] because geochemical conditions in the near-field are expected to be similar to conditions assumed for the near-field of Swiss repositories in granite-formations.

7.2.2 Source term

All data for the mobilisation process are chosen according to the common approach developed within the SPA project [4]:

- degradation of fuel matrix at a constant rate within 10^6 years

- instant release fractions of spent fuel
  - 5% of Cs, I, Rb, Zr, Cl
  - 2% of Tc, Pd, Sn, C
  - 1% of Se, Sm, Sr, Ca
  - 0.5% of Ni, Mo, Nb, Ra, actinides

- release of activation products within the cladding material and other metal parts using a constant degradation rate of 10^{-3} y^{-1}.

For the activation products the following (element-specific) fractions with respect to the total inventory are assumed to be within metal parts: C (72.2%), Ni (99.5%), Rb (95%), Zr (9.4%), Mo (99.5%), Nb (99.5%), Tc (0.1%).

7.2.3 Sorption values

The distribution coefficients are taken from the Kristallin-I study. The Swiss data collection procedure is transferable because similar bentonite barriers are assumed in the Swiss and the German studies. It is likely that the intruding water will equilibrate with bentonite before it comes into contact with the waste. Under these assumptions geochemical calculations have been performed in [11] and sorption values have been estimated in [36]. In Table 7.1, sorption values are given for all relevant nuclides. Distribution coefficients for those elements which have not been considered in Kristallin-I were derived from studies mentioned in foot-notes. If oxidising conditions occur in the near field, it is assumed that Se, Mo and Tc do not sorb onto the bentonite. For U and Np, values of $5 \cdot 10^{-3}$ m^3/kg from the Finnish study TVO-96 [40] are used, in agreement with distribution coefficients between $5 \cdot 10^{-3}$ and 0.6 m^3/kg documented for uranium in the NEA data base ISIRS [3], [31].

Table 7.1: Distribution coefficients in bentonite in [m^3/kg] [27] and [36]; r denotes the same data as used in the reference case.

element	reference	conserv.	
	reducing		oxidizing
C [a]	$1.0 \cdot 10^{-2}$	0	r
Cl [a]	0	r	r
Ca [a]	$2.0 \cdot 10^{-1}$	$2.0 \cdot 10^{-2}$	r
Ni	$1.0 \cdot 10^{0}$	$1.0 \cdot 10^{-1}$	0
Se	$5.0 \cdot 10^{-3}$	$1.0 \cdot 10^{-3}$	0
Sr	$1.0 \cdot 10^{-2}$	$1.0 \cdot 10^{-3}$	r
Zr	$1.0 \cdot 10^{0}$	$1.0 \cdot 10^{-1}$	r
Nb	$1.0 \cdot 10^{0}$	$1.0 \cdot 10^{-1}$	r
Mo[b]	$5.0 \cdot 10^{-3}$	$1.0 \cdot 10^{-3}$	r
Tc	$1.0 \cdot 10^{-1}$	$5.0 \cdot 10^{-2}$	0
Pd	$1.0 \cdot 10^{0}$	$1.0 \cdot 10^{-1}$	r
Sn	$1.0 \cdot 10^{0}$	$1.0 \cdot 10^{-1}$	r
I [a]	$5.0 \cdot 10^{-3}$	$1.0 \cdot 10^{-3}$	r
Cs, Rb[c]	$1.0 \cdot 10^{-2}$	$1.0 \cdot 10^{-3}$	r

Table 7.1: Distribution coefficients in bentonite in [m^3/kg] [27] and [36]; r denotes the same data as used in the reference case.

element	reference reducing	conserv. oxidizing
Sm [d]	$5.0 \cdot 10^{0}$	$5.0 \cdot 10^{-1}$	r
Ra	$1.0 \cdot 10^{-2}$	$1.0 \cdot 10^{-3}$	r
U	$5.0 \cdot 10^{0}$	$5.0 \cdot 10^{-1}$	$5.0 \cdot 10^{-3}$
Am	$5.0 \cdot 10^{0}$	$5.0 \cdot 10^{-1}$	r
Cm	$5.0 \cdot 10^{0}$	$5.0 \cdot 10^{-1}$	r
Pu	$5.0 \cdot 10^{0}$	$5.0 \cdot 10^{-1}$	r
Np	$5.0 \cdot 10^{0}$	$5.0 \cdot 10^{-1}$	$5.0 \cdot 10^{-3}$
Th	$5.0 \cdot 10^{0}$	$5.0 \cdot 10^{-1}$	r
Pa	$1.0 \cdot 10^{0}$	$1.0 \cdot 10^{-1}$	r

a. data from SKI [33]
b. Mo is assumed to exist as MoO_4^{2-} or polyanion. Sorption values of Se are used
c. Data of Cs are used for Rb
d. Data of the tetravalent actinides are used

7.2.4 Solubility limit values

For the repository in granite, reducing conditions are assumed because of the high Fe content of the containers and reducing species in bentonite and groundwater. An alkaline pH value (8-9) after equilibration of the groundwater with the bentonite is assumed, based on calculations of Curti [11]. As mentioned above, typical waters in deep granitic formations in Germany are more like those observed in Swiss studies than for example in the Scandinavian or Canadian formations [28]. The Swiss data collection procedure is transferable because a similar bentonite barrier is assumed and the water will equilibrate with bentonite before it makes contact with the waste. Consequently, all data except that for Rb, Sr, Mo and Ra are taken from the Swiss study Kristallin-I [27]. Rb, Sr and Mo have not been considered in the crystalline study and the values for Ra are not transferable to the conditions for the repository with disposed spent fuel elements. Best estimate values and upper limits (as conservative values) have been taken from the studies SAM

and PACOMA determined for areas with alkaline conditions [9]. No probabilistic calculations are performed, hence, only best estimate and conservative values are given in Table 7.2.

Table 7.2: Solubility limits in the near field for reducing conditions; r denotes the same data as used in the reference case.

element	$L^{e(i)}$ [mol/l]		
	best est. reducing	conserv. reducing	oxidizing
C, Cl, I, Cs, Rb, Ni	high	high	r
Ca [a]	$1.0 \cdot 10^{-2}$	high	r
Se	$1.0 \cdot 10^{-8}$	$6.0 \cdot 10^{-7}$	high
Sr	$1.0 \cdot 10^{-5}$	$1.0 \cdot 10^{-4}$	r
Zr	$5.0 \cdot 10^{-9}$	$5.0 \cdot 10^{-7}$	r
Nb	$1.0 \cdot 10^{-3}$	$1.0 \cdot 10^{-3}$	r
Mo	$1.0 \cdot 10^{-4}$	$1.0 \cdot 10^{-1}$	r
Tc	$1.0 \cdot 10^{-7}$	high	high
Pd	$1.0 \cdot 10^{-11}$	$1.0 \cdot 10^{-6}$	r
Sn	$1.0 \cdot 10^{-5}$	$1.0 \cdot 10^{-5}$	r
Sm	$1.0 \cdot 10^{-5}$	$1.0 \cdot 10^{-5}$	r
Ra	$1.0 \cdot 10^{-6}$	$1.0 \cdot 10^{-4}$	r
U	$1.0 \cdot 10^{-7}$	$7.0 \cdot 10^{-5}$	high
Am	$1.0 \cdot 10^{-5}$	$1.0 \cdot 10^{-5}$	r
Cm	$1.0 \cdot 10^{-5}$	$1.0 \cdot 10^{-5}$	r
Pu	$1.0 \cdot 10^{-8}$	$1.0 \cdot 10^{-6}$	r
Np	$1.0 \cdot 10^{-10}$	$1.0 \cdot 10^{-8}$	$1.0 \cdot 10^{-9}$
Th	$5.0 \cdot 10^{-9}$	$1.0 \cdot 10^{-7}$	r
Pa	$1.0 \cdot 10^{-10}$	$1.0 \cdot 10^{-7}$	r

a. from Projekt Gewähr [25]

7.2.5 Diffusion values

The diffusion of radionuclides in compacted bentonite is described by an element-specific apparent diffusion coefficient D_a which is defined as the quotient of pore diffusion and retention according to

$$D_a = \frac{D_b}{1 + (1 - \varepsilon_b)\rho_b K_d / \varepsilon_b}, \qquad (16)$$

where ρ_b is the bentonite solid density (2760 kg/m^3) and K_d is the distribution coefficient for the bentonite. The pore diffusion constant takes into account retardation effects due to the tortuosity of the pore space and exclusion effects of ions. The values of the pore diffusion coefficient and the diffusion porosity are given in Table 7.3.

Table 7.3: Pore diffusion coefficient and diffusion porosity in the bentonite buffer

pore diffusion coefficient D_b: $5.0 \cdot 10^{-10}$ m^2/s
diffusion porosity ε_b: 0.38

7.2.6 List of near-field data for IPA

Canister and borehole design have been proposed within the German study GEISHA [28]. These data as well as the basic policy data have been described in detail in SPA Topical Report I and are summarised in table 7.4. All other data are based on investigations from performance assessment studies from other countries for repositories in granite and information from the German institution BGR.

Table 7.4: Data of the near-field transport model

Canister • fuel: 1.602 t_{hm}/canister • water volume: 300 l • number of canisters: 3 900 (25 % of the total number of disposed canisters) • life time: 1000 y
Bentonite • height of bentonite: 6.3 m • bentonite inner radius: 0.265 m • bentonite outer radius: 0.6 m • bentonite porosity: 0.38 • bentonite dry density: 2760 kg/m^3
Excavation-disturbed zone (EDZ): • flow rate around deposition hole: 9 l • flow rate through EDZ of deposition hole: 1 l
sorption distribution coefficients: see table 7.1
solubility limits: see table 7.2
diffusion coefficients: see table 7.3

7.3 The near-field code GRAPOS

The solution of the mathematical model is performed by the computer code GRAPOS. The domain considered by the code consists of three regions:

- the waste form including the spent fuel and cladding as well as the container with its contents and degraded walls
- the bentonite barrier through which the radionuclides can be transported by diffusion and
- an excavation-disturbed zone (EDZ) which is intersected by water-conducting zones.

The code GRAPOS considers one-dimensional transport and radial symmetry. The mobilisation of radionuclides from the spent fuel has been incorporated into a source term. The equations of the diffusive transport are solved by the Finite Difference Method. Calculation of radioactive decay and ingrowth within radionuclide chains is included. Linear equilibrium sorption and solubility limits are regarded. For all calculations GRAPOS, version 1.01 is used.

8 Far-field model and data

8.1 Far-field model

For modelling the radionuclide transport through the geosphere the radionuclide migration is assumed to be affected by the following processes:

- advection
- dispersion
- sorption
- matrix diffusion
- radioactive decay
- dilution.

Other processes such as chemical reactions, precipitation/dissolution, and colloid-facilitated transport may also affect the radionuclide transport but are not considered in the present safety analysis.

The transport of the radionuclides from the repository to the biosphere may take place along many possible flowpaths, depending on the location of release from the repository and the pattern of the groundwater flow. But in general the transport is assumed to occur through the low-permeability domain into the major water-conducting faults, upwards to the higher-permeabilty domain into a sedimentary cover or a highly weathered granitic zone near the surface. Since the radionuclide travel times from the repository to the biosphere are essentially determined by the travel times in the low-permeability domain, in the reference case only the transport through this domain is taken into account. The impact of the zones with higher permeability consists of a dilution of the radionuclide concentrations entering from domains of lower permeability.

The transport through the low-permeability domain is assumed to occur within a network of water-conducting features with potentially different properties. However, in the transport model only a single flowpath is considered, and the different transport characteristics of the water-conducting features are reduced to a few model parameters. The different

properties of the water-conducting features are included in the analysis by means of grouping the water-conducting features into three representative classes: 1) single, planar fractures representing fractured dykes and aplitic gneisses, 2) mulitiple, planar fractures representing cataclastic and jointed zones whose internal structures consist of subparallel, partially filled up fractures surrounded by an altered matrix, 3) crushed zones representing fractured zones with fill. Concerning the transport modelling, the first two classes of water-conducting features can be considered as a system with open fractures, whereas the third class leads to a model for filled-up fractures.

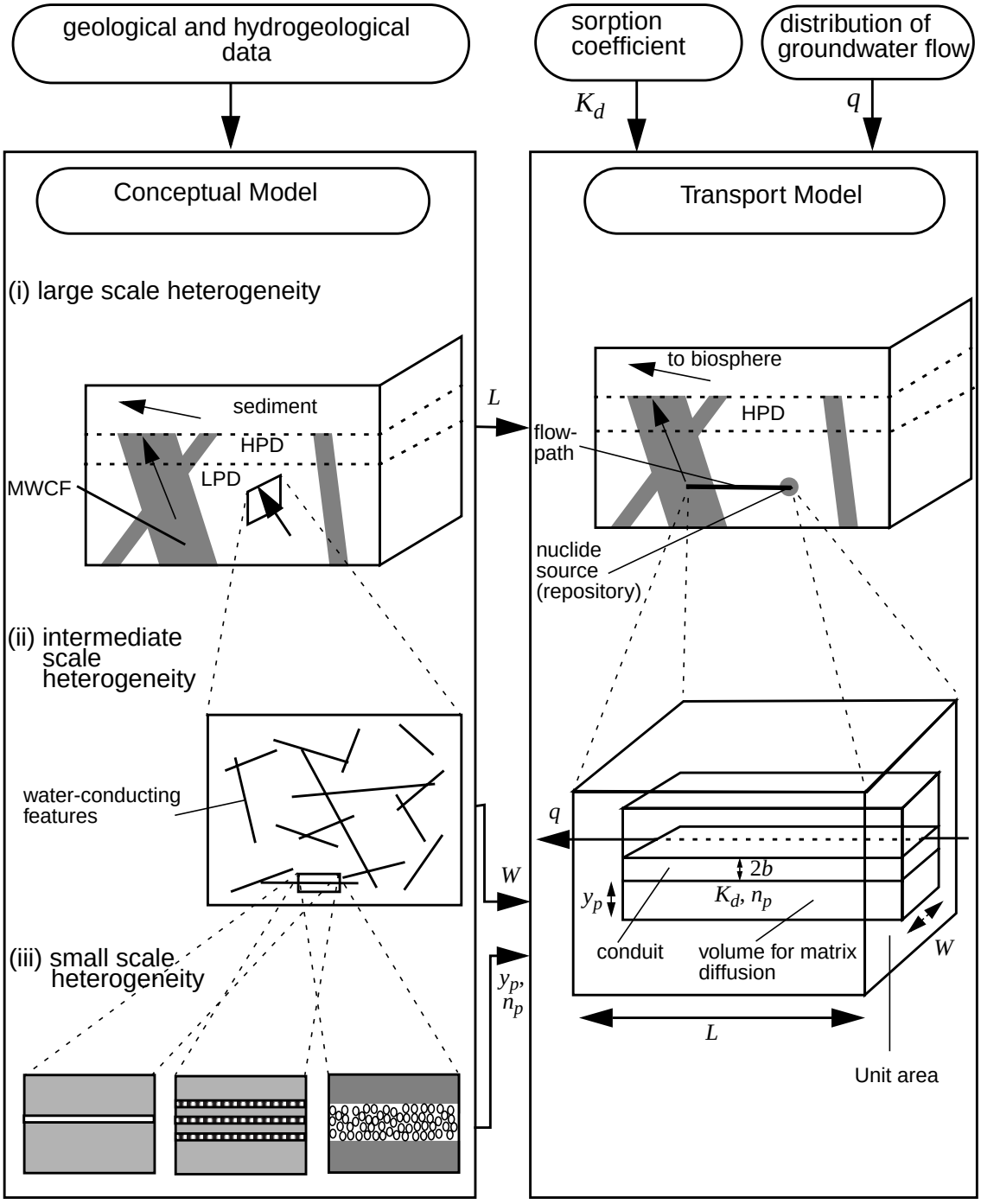

Fig. 8.1: Derivation of a transport model from a conceptual model based on field data and groundwater flow modelling and a modified figure from [32] (LPD: low permeability domain, MWCF: major water-conducting faults)

The transport of the radionuclides through the granitic rock is described by an advective-dispersion equation coupled to the equation describing the diffusion in the rock matrix:

$$\frac{\partial}{\partial t} R_f^i C_f^i = -v_f \frac{\partial C_f^i}{\partial z} + D \frac{\partial^2 C_f^i}{\partial z^2} + \frac{1}{b} \frac{n_p}{n_f} D_p \frac{\partial C_p^i}{\partial y}\Bigg|_{|y| = b} - \lambda^i \left(R_f^i C_f^i - \sum_k R_f^k C_f^k \right) \qquad (17)$$

$$\frac{\partial}{\partial t} R_p^i C_p^i = D_p \frac{\partial^2 C_p^i}{\partial y^2}\Bigg|_{|y| \le y_p} - \lambda^i \left(R_p^i C_p^i - \sum_k R_p^k C_p^k \right) , \qquad (18)$$

with

C_f^i concentration of radionuclide i in the water-conducting zones [Bq/m^3]

C_p^i concentration of radionuclide i in the stagnant matrix water [Bq/m^3]

v_f advective velocity of the radionuclides [m/y]

D dispersion/diffusion coefficient [m^2/y]

b half aperture [m]

y_p penetration depth [m]

n_p matrix porosity

D_p matrix diffusivity [m^2/y]

k indices of precursors of radionuklide i

λ^i radioactive decay constant of radionuclide i [1/y].

8.1.1 Initial and boundary conditions

The initial conditions are given by

$$C_f^i(t,\ z) \quad = \quad C_p^i(t,\ y) \quad = \quad 0; \qquad\qquad \forall y,\ z; t \leq t_0 \qquad (19)$$

where t_0 is given for example by the time of failure of the first canister or the time of repository closure.

The mass inflow from the near-field to the far-field is modelled by a source term $F_{\text{in}}^i(t)$ [Bq/y]. The boundary at $z = 0$ is assumed to be closed for mass flux:

$$\left[v_f C_f^i \ - \ D \frac{\partial C_f^i}{\partial z} \right] \Bigg|_{z \ = \ 0} \quad = \quad 0 . \qquad (20)$$

Corresponding to high dilution in either the major water-conducting faults or the upper sedimentary domain a zero concentration of the outer medium is assumed. Therefore, the outflow boundary condition is given by

$$C_f^i(t,\ z) \Big|_{z \ = \ L} \quad = \quad 0; \qquad\qquad t \ > \ t_0 . \qquad (21)$$

The total flux across the outflow boundary from the inner to the outer medium is calculated by

$$F_{\text{out}}^i(t) \quad = \quad \left[v_f C_f^i \ - \ D \frac{\partial C_f^i}{\partial z} \right] \Bigg|_{z \ = \ L} . \qquad (22)$$

The solute concentration across the boundary between the advective zone and the rock matrix is assumed to be continuous. This leads to the boundary condition:

$$C_f^i(t,\ z) \quad = \quad C_p^i(t,\ z,\ \pm b); \qquad\qquad \forall z,\ \forall t \qquad (23)$$

The limited penetration depth of the diffusion into the rock matrix is considered by a no-flow boundary condition:

$$\left.\frac{\partial C_p^i}{\partial y}\right|_{|y| \ = \ y_p} \quad = \quad 0\,. \qquad (24)$$

8.1.2 Advection and dispersion

The first term on the right side of equation (17) describes the advective flow through the channel within the small-scale water-conducting features of the low-permeability domain. The advective velocity depends on

- the total flow of water through a water-conducting feature
- the total volume of open channels within the water-conducting features.

The water-conducting features consist of a set of partially filled parallel fractures with discrete open channels in which groundwater flow is confined. A zone of altered wall rock is adjacent to the fractures. In the transport model the geometries of the fractures are described by means of the following parameters:

- total width of open flow channels per rock area W
- aperture of the fractures $2b$
- advective porosity of the fractures n_f.

The advective velocity within the channels is then calculated from the Darcy velocity q:

$$v_f \quad = \quad \frac{q}{2bWn_f}\,. \qquad (25)$$

The quantity W [m/m^2] determines the total trace length or the width of open channels over a unit area in a plane perpendicular to the flow direction. It is a measure of the average density of open channels in the domain of the host rock. The quantity $2W$ is sometimes referred to as the “specific surface area of fractures” or the “specific surface area for matrix diffusion” [35]. It is one of the main characteristics of the granitic rock. The porosity n_f describes the volume fraction of the water-bearing zones available for advective flow and is used in equation (28) to modell the (surface) sorption within the advective zones. Note that in the case of sorption in the water-bearing zones, i. e. $n_f < 1$, the parameter b has to be modified to $b + \delta$.

The dispersive term of equation (17) consists of the mechanical dispersion and the molecular diffusion. The mechanical dispersion is given by the product of the longitudinal dispersion length α_L and the pore velocity v_f. Generally, the dispersion length is considered to be dependent on the mean travel length. The ratio between the advective and dispersive flow is characterized by the Peclet-number Pe:

$$Pe = \frac{v_f L}{\alpha_L v_f} = \frac{L}{\alpha_L}, \qquad (26)$$

where L [m] is the transport distance. In the case of strong retardation by diffusion into the matrix the dispersion can have a significant influence on the transport of the radionuclides. This means that an increase in dispersion leads to an increase in the radionuclide release rates into the biosphere [19, 35].

8.1.3 Matrix diffusion and sorption

Two mechanisms of retardation of radionuclides in the water-conducting zones are taken into account in the transport model:

- Diffusion into the rock matrix accompanied by linear equilibrium sorption on the rock matrix, and
- linear equilibrium sorption on the surface of fracture walls, and sorption within the fracture fill, respectively.

The matrix diffusion term in equations (17) and (18) is calculated normal to the direction of advective flow. Basically, the whole rock matrix adjacent to a water-conducting zone is accessible via diffusion. Beyond a certain distance from the advective zone however, the effective diffusivity of the radionuclides is reduced significantly. Therefore, the region of the matrix available for diffusion is assumed to be limited. This region is determined by the so-called penetration depth y_p. Using large values for the penetration depth is of minor importance since most of the radionuclides will not diffuse deeply into the rock matrix in the course of a few million years.

The sorption onto the rock matrix is modelled assuming linear equilibrium sorption. This leads to a retardation factor R_p^i:

$$R_p^i = 1 + \frac{1 - n_p}{n_p} \rho K_d^{e(i)}, \qquad (27)$$

where

ρ rock density [kg/m^3]
$K_d^{e(i)}$ element-specific sorption coefficient for radionuclide i.

The retardation factor R_f^i describes the sorption in the water-bearing zones. This sorption process can arise either from the sorption onto the fracture wall surfaces, or from sorption within zones with fracture fill or strongly altered regions which are readily accessible via diffusion. In the code CHETMAD the retardation factor R_f^i is given by

$$R_f^i = 1 + \frac{1 - n_f}{n_f} (1 - n_p) \rho K_d^{e(i)}, \qquad (28)$$

where the porosity n_f describes the volume fraction of the water-bearing zones available for advective flow. In the case of an open fracture with half aperture b and "depth" of surface sorption δ, the parameter n_f is defined by

$$n_f = \frac{b}{b + \delta}. \qquad (29)$$

Hereby, the retardation factor is given in the familiar form:

$$R_f^i = 1 + \frac{(1 - n_p)\rho K_d^{e(i)}}{b}\delta . \qquad (30)$$

In the reference case the sorption on the surfaces of the channels will be neglected, thus assuming no retardation in the advective zone, i.e.

$$R_f^i = 1 . \qquad (31)$$

8.2 Far-field data

8.2.1 Sorption data

The sorption data of granite for the Swiss study Kristallin-I have been determined by Stenhouse [36]. The best estimate and the conservative data for crystalline rock are shown in table 8.1. These data are used in our study. Rb, Mo and Sm were not considered in Kristallin-I. Their distribution coefficients have been derived from chemical homologous elements as indicated in table 8.1.

Table 8.1: Distribution coefficients in granite in [m^3/kg] after [27] and [36]

element	reference	conserv.	element	reference	conserv.
Cl	0	0	Sn	$5.0 \cdot 10^{-1}$	$5.0 \cdot 10^{-2}$
C	$1.0 \cdot 10^{-3}$	0	Cs	$4.2 \cdot 10^{-2}$	$8.4 \cdot 10^{-3}$
Ca	$1.0 \cdot 10^{-2}$	$1.0 \cdot 10^{-3}$	Sm[a]	$5.0 \cdot 10^{+0}$	$5.0 \cdot 10^{-1}$
I	$1.0 \cdot 10^{-3}$	0	Ra	$5.0 \cdot 10^{-1}$	$1.0 \cdot 10^{-1}$
Ni	$5.0 \cdot 10^{-1}$	$5.0 \cdot 10^{-2}$	U	$1.0 \cdot 10^{+0}$	$5.0 \cdot 10^{-2}$
Se	$1.0 \cdot 10^{-2}$	$1.0 \cdot 10^{-3}$	Am	$5.0 \cdot 10^{+0}$	$1.0 \cdot 10^{+0}$
Rb[b]	$4.2 \cdot 10^{-2}$	$8.4 \cdot 10^{-3}$	Cm	$5.0 \cdot 10^{+0}$	$5.0 \cdot 10^{-1}$
Sr	$1.0 \cdot 10^{-2}$	$1.0 \cdot 10^{-3}$	Pu	$5.0 \cdot 10^{+0}$	$5.0 \cdot 10^{-1}$
Zr	$1.0 \cdot 10^{+0}$	$1.0 \cdot 10^{-1}$	Np	$1.0 \cdot 10^{+0}$	$5.0 \cdot 10^{-2}$
Nb	$1.0 \cdot 10^{+0}$	$1.0 \cdot 10^{-1}$	Th	$1.0 \cdot 10^{+0}$	$1.0 \cdot 10^{-1}$
Mo[c]	$1.0 \cdot 10^{-2}$	$1.0 \cdot 10^{-3}$	Pa	$1.0 \cdot 10^{+0}$	$1.0 \cdot 10^{-1}$
Tc	$5.0 \cdot 10^{-1}$	$5.0 \cdot 10^{-2}$	Pb	$5.0 \cdot 10^{-1}$	$5.0 \cdot 10^{-2}$
Pd	$5.0 \cdot 10^{-1}$	$5.0 \cdot 10^{-2}$			

a. Data of the tetravalent actinides are used.
b. Data of Cs are used.
c. Mo is assumed to be in the anionic state as MoO_4^{2-} and weakly sorbing. Data of Se (SeO_3^{2-}) are used.

8.2.2 Characterization of the geometry of water-conducting features

In the present safety analysis, the following model geometries for the water-conducting features of the low-permeability domain are taken into account:

(1) simple planar fracture according to fractured dykes

(2) multiple planar fractures which are partially filled up and surrounded by an altered matrix block according to cataclastic and joint zones

(3) a crushed zone modelled as a planar fracture with fill of spherical grains of uniform radius.

The model parameters and assumptions concerning the different kinds of water-conducting features are listed in table 8.2. The parameters for the geometry of the cataclastic or joint zones correspond essentially to the geometry and respective model parameters used in the reference case of the KRISTALLIN-I safety analysis.

Table 8.2: Geosphere model parameters for different kinds of water-conducting features

Parameter	fractured dykes (1)	Cataclastic or joint zones (2)	Crushed zones (3)
W [m/m^2]	$1 \cdot 10^{-2}$	$3 \cdot 10^{-3}$	$5 \cdot 10^{-2}$
$2b$ [m]	$8 \cdot 10^{-4}$	$1 \cdot 10^{-3}$	0.3
n_f	1.0	1.0	0.3
y_m [m]	0.02	0.05	0.05
n_p	$5.0 \cdot 10^{-3}$	$5.0 \cdot 10^{-2}$	$5.0 \cdot 10^{-3}$

8.2.3 Geosphere model assumptions and parameters for the reference case

The geosphere model assumptions and respective parameters are summarised in table 8.3. The value for the Darcy velocity is obtained by an assumed transmissivity of the water-conducting features in the low-permeability domain of $1.1 \cdot 10^{-9}$ m^2/s with a density per unit rock area of 0.05 m^{-1}, and an estimated hydraulic gradient of 0.02. These data give a slightly higher Darcy velocity than that assumed for the Area West in the KRISTALLIN-I study. In the reference case the water-conducting features of the low-permeability domain are supposed to consist of fractured dykes (see table 8.2). The transport parameters used result in a value for the transport resistance WL/q of about $6 \cdot 10^4$ y/m.

Table 8.3: Geosphere model assumptions and parameters for the reference case

Model assumption/parameter	Reference case assumption/value
Area of the repository A	$4 \cdot 10^6$ m^2
Transport pathway length L	200 m
Darcy-velocity q	$3.5 \cdot 10^{-5}$ m/y
Peclet-number Pe	10
Matrix density ρ	2600 kg/m^3
Pore diffusion coefficient D_m	$1.0 \cdot 10^{-3}$ m^2/y
Geometry of water-conducting features	fractured dykes, see table 8.2
Sorption parameters	see table 8.1

8.3 The far-field code CHETMAD

For the calculations of the radionuclide transport through the far-field the computer code CHETMAD version 1.01 is used. The CHETMAD code numerically solves the transport equations (17) and (18). The implemented solution procedure is based on the method of Finite Differences and was developed from the one-dimensional transport code CHET1 [24]. The code CHETMAD is implemented as a module in the integrated performance assessment code EMOS [39]. The following physical and chemical processes are included:

- The pathway of the radionuclide transport can be inhomogeneous. Therefore, the pathway can be divided into different regions characterized by the transport and sorption parameters and the properties of the geometry. The shape of the matrix blocks of a region are either planar or cylindrical. Alternatively, a region can be modelled as a one-dimensional porous system.

- Advection of radionuclides through the geosphere is assumed to occur through a set of parallel water-conduction zones. The groundwater flow can be considered time-dependent but constant in each region. Longitudinal dispersion and molecular diffusion spreads dissolved radionuclides along the direction of flow. Transverse dispersion is not taken into account.

- Diffusion in the rock matrix occurs perpendicular to the wall of the advective zones. The penetration deep of diffusion into the rock matrix is limited. Unlimited matrix diffusion is modelled by choosing a sufficiently large value for the penetration depth.

- Retardation of the radionuclides by sorption on fracture surfaces and sorption within the diffusive accessible matrix are modelled as a linear equilibrium sorption. The sorption parameters are element-specific.

- Dilution of radionuclide concentrations caused by entry into highly advective zones are modelled with a dilution factor.

- Radioactive decay and ingrowth of radionuclide chains are considered.

9 Biosphere model and data

In the following, a description of the biosphere model used in the reference case of our safety analysis for a repository in granite is given. All biosphere calculations are performed with the computer code EXMAS, version 1.01.

The application of this German biosphere model in long-term performance assessments is mandatory under the government regulations published in [1]. The key indicator for safety assessment is the dose. The German acceptation criteria for repositories of radioactive waste require proof that the effective dose rate does not exceed $3 \cdot 10^{-4}$ Sv/y for adults and small children.

Within the SPA project an alternative scenario, WELL-96, shall be investigated in order to have a common basis for comparison of the results of all SPA participants.

9.1 Biosphere model

9.1.1 Exposition pathways

After transport through the granitic formations radionuclides can reach near-surface aquifers, consisting of 20 - 100 m thick sandy sediments or highly weathered crystalline material. The surface area considered in biosphere modelling corresponds to the region in which the radionuclide flux from the most relevant transport pathway through the geosphere is released. The concentration in the aquifer system is given by the nuclide release rates and the groundwater flow in the aquifer. It is assumed that a group of the population is supplied exclusively with contaminated water from near-surface wells drilled into this aquifer. No capillary effects in the soil are considered. Additionally it is assumed that the water is used for different applications without any further dilution. The model is based on the living habits of the present population in a typical area of northern Germany. Since changes of living habits cannot be predicted accurately, no changes are presupposed for the future.

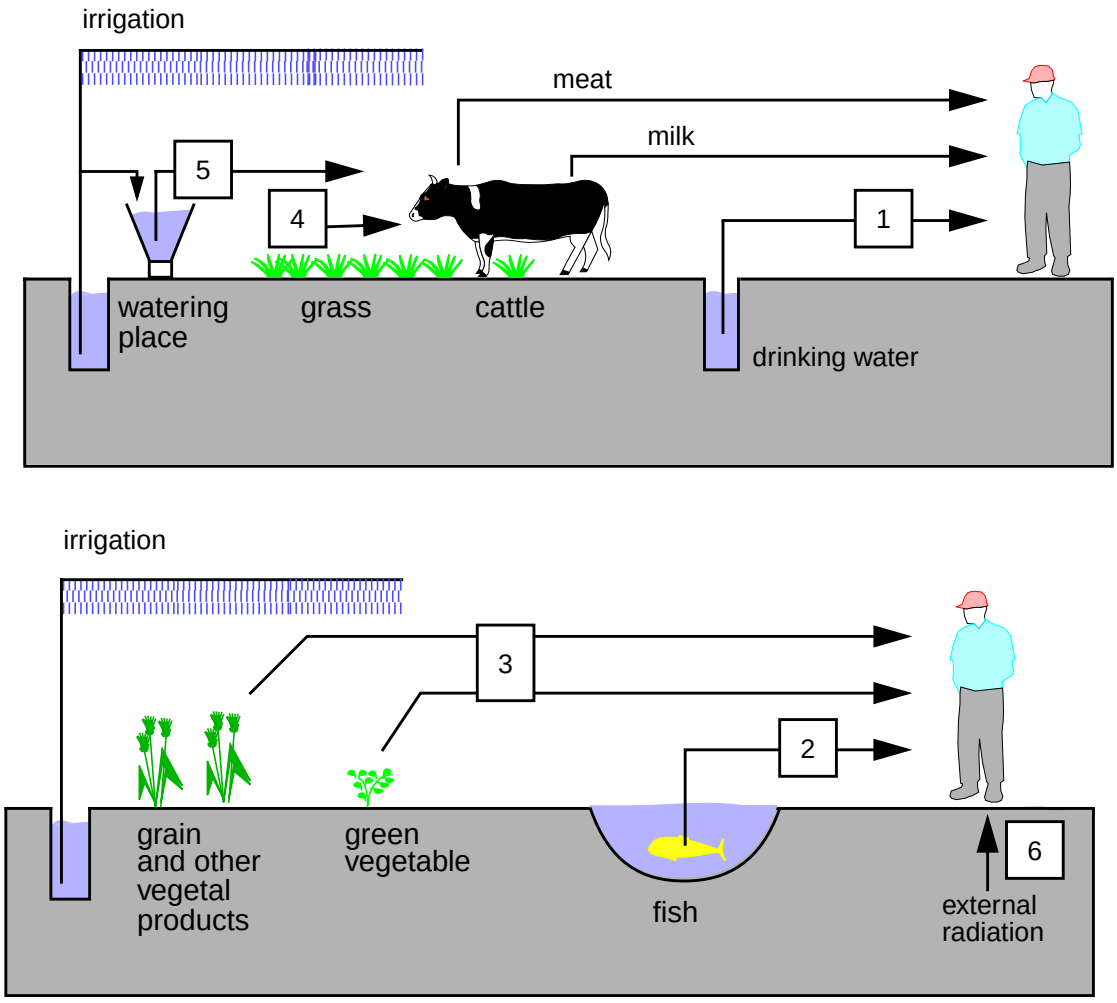

Fig. 9.1: Exposition pathways in the biosphere (AVV [1])

In Germany the biosphere model and all data for its use in long-term performance assessments are given by the AVV [1]. The following exposition pathways schematically shown in figure 9.1 have to be included:

(1) uptake of drinking water
(2) ingestion of fresh water fish from ponds
(3) ingestion of plants irrigated with contaminated water
(4) ingestion of milk and meat from cattle whose feed has been irrigated with contaminated water
(5) ingestion of milk and meat from cattle maintained with contaminated water
(6) external radiation by dwelling on inundated areas.

9.1.1.1 Drinking water

It is assumed that drinking water is taken directly from the well. Dilution effects or possible changes of the activity concentration by treatment of drinking water are not considered.

9.1.1.2 Fish from ponds

The contaminated groundwater is used for artificial ponds with fish cultures, i.e. the nuclide concentration in the pond water and in the groundwater are the same. It is assumed that all fresh water fish eaten by man are taken from those ponds. The nuclide concentration in the fish C_i^{fi} [Bq kg^{-1}] is determined by

$$C_i^{fi} = C_i^w T_i^{fi} , \qquad (32)$$

with the concentration in the groundwater C_i^w [Bq·l^{-1}] and the transfer factors T_i^{fi} [l·kg^{-1}].

9.1.1.3 Irrigation

The irrigation with contaminated well-water affects primarily the plants. In a second step the animal products, milk and meat get contaminated since pasture plants or dry fodder are consumed by animals.

Irrigation of plants

The plants are irrigated with contaminated well-water. Three different types of plants, denoted by index n, are delineated by within the AVV:

- pasture plants ($n=pp$)
- green vegetables ($n=gp$)
- other plants: grains, fruits, root vegetables ($n=op$).

Two mechanisms are responsible for the contamination of the plants - on the one hand radionuclide deposition on foliage, denoted by index *f*, on the other hand radionuclide uptake from the soil by the roots of the plant, denoted by index *s*.

$C_i^{n,\ f}$ [Bq·kg^{-1}], the nuclide concentration in the plant due to deposition on foliage, is calculated for all nuclides except C-14 by use of the equation

$$C_i^{n,\ f} = C_i^w \frac{W f_w}{y^n (\lambda_r^f + \lambda_i)} (1 - \exp(-(\lambda_r^f + \lambda_i) t_g^n)) , \qquad (33)$$

with

n index for plant type: pasture plants ($n=pp$), green vegetables ($n=gp$), and other plants ($n=op$)

W irrigation rate [l·m^{-2}·s^{-1}]
f_w fraction of activity deposited on leaves during irrigation [-]
y^n produce yields for different types of plants n [kg·m^{-2}]
λ_r^f weathering rate of nuclides on the foliage of the plant [s^{-1}]
λ_i radioactive decay constant for nuclide i [s^{-1}]
t_g^n time during which plants n are contaminated by irrigation (growth period) [s].

$C_i^{n,\ s}$ [Bq·kg^{-1}], the nuclide concentration of the plant due to uptake by roots from the soil, is calculated by considering the contamination of soil and with nuclide-specific soil/plant transfer factor. This transfer factor describes the ratio of activity in plant to the activity in soil. The contamination of the soil results from the annual input by irrigation. The activity in the soil is decreased by radioactive decay and leaching of nuclides into deeper soil layers that are unattainable through root growth. Leaching rates are dependent on soil type and element type. Two different soil types (arable land and pasture land) are distinguished. The contamination is calculated for all nuclides except C-14 as follows:

$$C_i^{n,\,s} = C_i^w \left(\frac{W T_i^n t_R}{p^m (\lambda_{r,\,i}^s + \lambda_i)} (1 - \exp(-(\lambda_{r,\,i}^s + \lambda_i) t_a)) \right), \qquad (34)$$

with

m index for soil type: arable land ($m=a$) and pasture land ($m=p$)
t_R ratio of the number of days of irrigation to the number of days in a year [-]
p^m dry mass of root-reachable soil m per area [kg·m^{-2}]
$\lambda_{r,\,i}^s$ loss rate of nuclides i from the rooting zone [s^{-1}]
T_i^n transfer factors soil/plant for different types of plants n and nuclide i [-]
t_a accumulation time for nuclides in the soil [s].

The accumulation of nuclides in the soil is considered over a period of $1 \cdot 10^5$ years. The total concentration of nuclide i in plants C_i^n is given by the sum of both processes, $C_i^{n,\,f}$ and $C_i^{n,\,s}$.

In the case of C-14 it is assumed that the C-14-activity in the irrigation water is completely released as gaseous $^{14}CO_2$ and uptaken from the plant by photosynthesis. The specific activity of plants, C_{C14}^n has to be calculated by using

$$C_{C14}^n = \frac{W C_{C14}^w f_C^n}{V_c}, \qquad (35)$$

with

f_C^n mass fraction of carbon in plants [-]
C_{C14}^w concentration of C-14 in the well-water [Bq l^{-1}]
V_c assimilation rate of the plant [kg·m^{-2}·s^{-1}].

Contamination of animal products by irrigation

The contamination of animal products by the irrigation pathway (*ir*) occurs because animals consume contaminated plants. For the accumulation of nuclides in meat and milk, element-specific transfer factors are used which describe the equilibrium ratio of radionuclide concentrations in milk and meat, respectively, and the daily uptake of the respective radionuclides. The nuclide concentration in meat $C_i^{me,\ ir}$, and milk $C_i^{mi,\ ir}$, in [Bq·kg^{-1}] is described by the following equation:

$$C_i^{me,\ ir} = C_i^{fo} \dot{M}_{fo} T_i^{me} , \qquad (36)$$

with

$\dot{M}_{fo}$ daily uptake of pasture for cattle [kg·d^{-1}]
T_i^{me} transfer factor pasture/meat [d·kg^{-1}]
C_i^{fo} The nuclide concentration in animal food [Bq·kg^{-1}] is calculated by using

$$C_i^{fo} = f_p C_i^{pp} + (1 - f_p) C_i^{df} , \qquad (37)$$

with f_p [-] denoting the part of the year that cattle graze on pasture land. The concentration for fresh pasture plants C_i^{pp} is calculated as described above. For calculating the concentration in winter feed C_i^{df} [Bq·kg^{-1}] a storage time t_c^{df} [s] has to be considered:

$$C_i^{df} = C_i^{pp} \exp(-\lambda_i t_c^{df}) . \qquad (38)$$

The nuclide concentration in milk is derived from

$$C_i^{mi,\ ir} = C_i^{fo} \dot{M}_{fo} T_i^{mi} , \qquad (39)$$

where T_i^{mi} [d·kg^{-1}] denotes the transfer factor pasture/milk.

9.1.1.4 Watering places

Another pathway for contamination of the animal products meat and milk is the watering place (*wp*). The concentration in meat and milk is calculated based on the daily consumption rate of water L [l·d^{-1}] by cattle. It is assumed that the well-water is used at the watering places without dilution. This means that for the contamination of meat $C_i^{me,\ wp}$ [Bq·kg^{-1}]:

$$C_i^{me,\ wp} = C_i^w L T_i^{me}, \qquad (40)$$

and for the contamination of milk $C_i^{mi,\ wp}$ [Bq·l^{-1}]:

$$C_i^{mi,\ wp} = C_i^w L T_i^{mi}. \qquad (41)$$

9.1.1.5 External radiation

It is assumed that a reference person is dwelling on areas inundated by contaminated water. The nuclide concentration in the soil of these areas is reduced by nuclide transport into deep sediment layers. The annual dose by external radiation D_i^{ex} [Sv·y^{-1}] is then calculated via the equation

$$D_i^{ex} = K_{e,\ i} t_d C_i^w g_{s,\ i} \frac{\ln 2}{\lambda_r^{in} + \lambda_i} (1 - \exp(\lambda_r^{in} + \lambda_i) t_{se}), \qquad (42)$$

with

$K_{e,i}$ transfer constant for nuclide i [l·m^{-2}·s^{-1}]
t_d annual dwelling time of persons from critical group on flooded areas [s·y^{-1}]
λ_r^{in} loss rate of nuclides on inundated areas [s^{-1}]
$g_{s,i}$ dose factor for external in radiation from soil for nuclide i [(Sv·s^{-1})/(Bq·m^{-2})]
t_{se} sedimentation time [s].

9.1.2 Daughter nuclides

The effect of daughter nuclides is considered for two of the pathways where nuclide accumulation over long timeframes occurs:

- irrigation pathway: nuclide uptake from the soil
- external radiation from inundated areas.

In general, for continuous deposition in the soil the activity of the parent nuclide is calculated by using the expression:

$$A_M(t) = \int_0^t \dot{A}_M(t') \exp(-(\lambda_m + \lambda_{rm})(t - t'))dt' , \quad (43)$$

with

A_M activity of mother nuclide in soil corresponding to 1 m^2 of land [Bq·m^{-2}]
$\dot{A}_M$ inflow rate of parent nuclide [Bq m^{-2} s^{-1}]
λ_m decay constant of parent nuclide *m* [s^{-1}]
λ_{rm} dwelling constant of parent nuclide *m* [s^{-1}].

The activity of the *n*th daughter nuclide $A_n(t)$ is given by the equation:

$$A_n(t) = \lambda_n \int_0^t \dot{A}_{n-1}(t') \exp(-(\lambda_n + \lambda_{rn})(t - t'))dt' , \quad (44)$$

with

A_n activity of *n*th daughter nuclide in soil corresponding to 1 m^2 of land [Bq·m^{-2}]
$\dot{A}_{n-1}$ activity of (*n*-1)th daughter nuclide in soil corresponding to 1 m^2 of land [Bq·m^{-2}]
λ_n decay constant of daughter nuclide *n* [s^{-1}]
λ_r dwelling constant of nuclide *n* [s^{-1}].

The contamination of plants by daughter nuclides is calculated using the respective transfer factors of the daughter nuclides. The effect of daughter nuclides on external radiation dose is calculated with the respective transfer and dwelling constants as well as the dose factors for external soil radiation for the daughter nuclides.

For these calculations a large number of radionuclides not listed in the data tables of this paper has to be considered. The necessary data such as ingestion dose factors as well as dose factors for external radiation exposition for all nuclides are taken from [6] and are available for 830 nuclides as Excel file [30].

9.1.3 Individual dose

The individual dose rate D_i [Sv·y^{-1}] due to radionuclide i is calculated as the sum over all pathways:

$$\begin{aligned} D_i \;=\; & (U^{dw} C_i^{w} \;+\; U^{fi} C_i^{fi} \;+\; U^{gp} C_i^{gp} \;+\; U^{op} C_i^{op} \\ & + U^{mi} C_i^{mi} \;+\; U^{me} C_i^{me}) H_i \;+\; D_i^{ex} \,, \end{aligned} \qquad (45)$$

where $H_{i,t}$ denotes the ingestion dose factor of nuclide i and U^x the consumption rates for different foods (d*w* = drinking water, *fi* = fresh water fish, *gp* = green vegetables, *op* = other plants, *mi* = milk and *me* = meat). The concentrations in meat C_i^{me}, and milk C_i^{mi}, are given by summing up the contributions from both pathways: irrigation, and watering places.

9.2 Data

9.2.1 Sorption data

Sorption data are needed for calculating the mobile concentrations in the biosphere of daughter nuclides which were not considered in geosphere calculations. It is assumed that the sorption values for highly weathered granite are similar to those for sandy aquifers. Consequently K_d-values of the overburden from SAM study are taken [9].

Table 9.1: distribution coefficients [m^3/kg] for overlying sediment (highly weathered granitic layer).

element	K_d-value	lower limit	upper limit	element	K_d-value	upper limit	lower limit
C	$5.0.\cdot10^{-03}$	$5.0\cdot10^{-04}$	$5.0\cdot10^{-02}$	Cs	$1.0\cdot10^{-03}$	$1.0\cdot10^{-04}$	$1.0\cdot10^{-02}$
Cl	$5.0\cdot10^{-04}$	$1.0\cdot10^{-04}$	$2.5\cdot10^{-03}$	Sm	$1.0\cdot10^{+00}$	$1.0\cdot10^{+00}$	$1.0\cdot10^{+00}$
Ca	$5.0\cdot10^{-04}$	$1.0\cdot10^{-04}$	$2.0\cdot10^{-03}$	Eu	$1.0\cdot10^{+00}$	$1.0\cdot10^{+00}$	$1.0\cdot10^{+00}$
Ni	$1.0\cdot10^{-02}$	$1.0\cdot10^{-03}$	$1.0\cdot10^{-01}$	Pu	$1.0\cdot10^{+00}$	$1.0\cdot10^{+00}$	$1.0\cdot10^{+00}$
Se	$3.0\cdot10^{-04}$	$1.0\cdot10^{-04}$	$9.0\cdot10^{-04}$	U	$2.0\cdot10^{-03}$	$2.0\cdot10^{-04}$	$2.0\cdot10^{-02}$
Rb	$1.0\cdot10^{-03}$	$1.0\cdot10^{-04}$	$1.0\cdot10^{-02}$	Th	$3.0\cdot10^{-01}$	$1.0\cdot10^{-01}$	$1.0\cdot10^{+00}$
Sr	$5.0\cdot10^{-04}$	$1.0\cdot10^{-04}$	$2.0\cdot10^{-03}$	Np	$3.0\cdot10^{-02}$	$1.0\cdot10^{-03}$	$1.0\cdot10^{+00}$
Zr	$1.0\cdot10^{-01}$	$1.0\cdot10^{-02}$	$1.0\cdot10^{00}$	Ra	$9.0\cdot10^{-04}$	$4.0\cdot10^{-04}$	$2.0\cdot10^{-03}$
Mo	$1.0\cdot10^{-03}$	$1.0\cdot10^{-04}$	$1.0\cdot10^{-02}$	Am	$1.0\cdot10^{+00}$	$1.0\cdot10^{+00}$	$1.0\cdot10^{+00}$
Nb	$1.0\cdot10^{-01}$	$1.0\cdot10^{-02}$	$1.0\cdot10^{00}$	Pa	$1.0\cdot10^{+00}$	$1.0\cdot10^{+00}$	$1.0\cdot10^{+00}$
Tc	$7.0\cdot10^{-03}$	$1.6\cdot10^{-04}$	$3.0\cdot10^{-01}$	Pb	$4.0\cdot10^{-02}$	$3.0\cdot10^{-03}$	$5.0\cdot10^{-01}$
Pd	$1.0\cdot10^{-02}$	$1.0\cdot10^{-03}$	$1.5\cdot10^{-01}$	Po	$1.0\cdot10^{+00}$	$1.0\cdot10^{+00}$	$1.0\cdot10^{+00}$
Sn	$2.0\cdot10^{-01}$	$1.3\cdot10^{-01}$	$3.0\cdot10^{-01}$	Ac	$1.0\cdot10^{+00}$	$1.0\cdot10^{+00}$	$1.0\cdot10^{+00}$
I	$5.0\cdot10^{-04}$	$1.0\cdot10^{-04}$	$2.5\cdot10^{-03}$				

9.2.2 General data

All data used for modelling are summarised in the following tables. The data are given by [1] and [29].

Table 9.2: General data for biosphere modelling

symbol	explanation	value	unit
f_W	activity fraction deposited on leaves of plants	0.3	[-]
f_p	fraction of the year cattle graze on pasture	0.5	[-]
f_C^n	mass fraction of carbon in plants $n = pp$: pasture plants $n = pl$: other plants	 0.09 0.18	[-]
$K_{e,i}$	transfer constant for Sr, Tc, Ra, Nb Cs, I Co, Zr, Ni, actinides	 $2 \cdot 10^{-5}$ $2 \cdot 10^{-3}$ $5 \cdot 10^{-3}$	$[l \cdot m^{-2}\ s^{-1}]$
L	daily water consumption rate for cattle	75	$[l \cdot d^{-1}]$
$\dot{M}_{fo}$	daily rate of uptake of pasture for cattle	65	$[kg \cdot d^{-1}]$
p^m	dry mass of the soil reachable by plant roots $m = a$: arable land $m = p$: pasture land	 280 120	$[kg \cdot m^{-2}]$
t_a	accumulation time of nuclides in the soil	$3.152 \cdot 10^{12}$	[s]
t_d	annual dwelling time on inundated areas	$3.6 \cdot 10^6$	$[s \cdot y^{-1}]$
t_R	ratio of number of days of irrigation to the number of days in a year	180/365	$[d \cdot d^{-1}]$
t_{se}	sedimentation time	$1.57 \cdot 10^9$	[s]
t_c^{df}	storage time of dry fodder	$5.2 \cdot 10^6$	[s]

Table 9.2: General data for biosphere modelling

symbol	explanation	value	unit
t_g^n	time during which plants are contaminated by irrigation (growth period) n = *pp*: pasture plants n = *op*: other plants	 $2.6 \cdot 10^6$ $5.2 \cdot 10^6$	[s]
V_c	carbon assimilation rate for plants	10^{-7}	[kg·m^{-2} s^{-1}]
W	irrigation rate	$1.2 \cdot 10^{-5}$	[l·m^{-2} s^{-1}]
y^n	produce yields n = *gp*: green vegetables n = *op*: other plants n = *pp*: pasture plants	 1.6 2.4 0.85	[kg·m^{-2}]
λ_i	decay constant of nuclide i		[s^{-1}]
λ_r^{in}	loss rate on flooded areas	$3 \cdot 10^{-9}$	[s^{-1}]
λ_r^f	weathering rate of nuclides on plant foliage	$5.7 \cdot 10^{-7}$	[s^{-1}]
$\lambda_{r,\ i}^s$	loss rate of nuclides from the rooting zone: Tc, Cl (arable land) (pasture land Ca, Sr, Ru, I (arable land) (pasture land) actinides and other elements (arable land) (pasture land)	 $1.0 \cdot 10^{-8}$ $2.0 \cdot 10^{-8}$ $1.0 \cdot 10^{-9}$ $2.0 \cdot 10^{-9}$ $1.0 \cdot 10^{-10}$ $2.0 \cdot 10^{-10}$	[s^{-1}]

9.2.3 Dose factors

The dose factors used in the German model are based on the models and data published in ICRP 30 and 48 [17], [18]. Some of these values have been upgraded with newer results. The actual dose factors are published in [6].

9.2.4 Dose conversion factors

Dose conversion factors were calculated via equation (45) assuming a nuclide concentration of 1 [Bq·l^{-1}] in well-water. These values are then used to directly calculate the dose via multiplication with the nuclide concentrations in the contaminated well-water.

Table 9.3: Concentration factor water/fish T_i^{fi} and transfer factors for soil/pasture plant T_i^{pp}, soil/plant T_i^{pl}, pasture/milk T_i^{mi}, and pasture/meat T_i^{me}. The transfer factors soil/plant describe the ratio of activity in the fresh plant mass to the activity in the dry soil mass.

element	T_i^{fi} [l/kg]	T_i^{pp} [-]	T_i^{pl} [-]	T_i^{mi} [d/kg]	T_i^{me} [d/kg]
C	8000	-	-	$2 \cdot 10^{-2}$	$4 \cdot 10^{-2}$
Cl	50 *)	$5 \cdot 10^{+0}$	$5 \cdot 10^{+0}$	$2 \cdot 10^{-2}$	$8 \cdot 10^{-2}$
Ca	40 *)	$2 \cdot 10^{-1}$	$6 \cdot 10^{-2}$	$2 \cdot 10^{-2}$	$1 \cdot 10^{-3}$
Co	100	$2 \cdot 10^{-2}$	$2 \cdot 10^{-2}$	$2 \cdot 10^{-4}$	$1 \cdot 10^{-2}$
Ni	100	$2 \cdot 10^{-2}$	$2 \cdot 10^{-2}$	$1 \cdot 10^{-2}$	$2 \cdot 10^{-3}$
Se	200	$5 \cdot 10^{-1}$	$5 \cdot 10^{-1}$	$4 \cdot 10^{-3}$ *)	$2 \cdot 10^{-2}$
Rb	2000	$9 \cdot 10^{-1}$	$9 \cdot 10^{-2}$	$6 \cdot 10^{-3}$	$1 \cdot 10^{-2}$
Sr	30	$4 \cdot 10^{-1}$	$4 \cdot 10^{-1}$	$2 \cdot 10^{-3}$	$6 \cdot 10^{-4}$
Zr	200	$1 \cdot 10^{-3}$	$3 \cdot 10^{-3}$	$5 \cdot 10^{-6}$	$2 \cdot 10^{-2}$
Nb	200	$1 \cdot 10^{-2}$	$1 \cdot 10^{-2}$	$3 \cdot 10^{-3}$	$3 \cdot 10^{-1}$
Mo	10 *)	$2 \cdot 10^{-1}$	$5 \cdot 10^{-2}$	$2 \cdot 10^{-3}$	$7 \cdot 10^{-3}$
Tc	80	$3 \cdot 10^{+0}$	$3 \cdot 10^{+0}$	$1 \cdot 10^{-5}$	$4 \cdot 10^{-2}$
Pd	10 *)	$2 \cdot 10^{-2}$	$2 \cdot 10^{-2}$	$1 \cdot 10^{-2}$	$4 \cdot 10^{-3}$
Sn	3000	$2 \cdot 10^{-1}$	$2 \cdot 10^{-1}$	$3 \cdot 10^{-3}$	$8 \cdot 10^{-2}$
Sb	100	$1 \cdot 10^{-1}$	$2 \cdot 10^{-2}$	$2 \cdot 10^{-3}$	$1 \cdot 10^{-3}$
I	50	$1 \cdot 10^{-1}$	$2 \cdot 10^{-2}$	$3 \cdot 10^{-3}$	$1 \cdot 10^{-2}$
Cs	1500	$5 \cdot 10^{-2}$	$5 \cdot 10^{-2}$	$5 \cdot 10^{-3}$	$3 \cdot 10^{-2}$
Sm	25	$3 \cdot 10^{-3}$	$3 \cdot 10^{-3}$	$2 \cdot 10^{-5}$	$5 \cdot 10^{-3}$
Eu	25	$3 \cdot 10^{-3}$	$3 \cdot 10^{-3}$	$2 \cdot 10^{-5}$	$5 \cdot 10^{-3}$
Pb	60	$8 \cdot 10^{-2}$	$8 \cdot 10^{-2}$	$3 \cdot 10^{-4}$	$4 \cdot 10^{-4}$
Po	300	$9 \cdot 10^{-3}$	$9 \cdot 10^{-3}$	$3 \cdot 10^{-4}$	$5 \cdot 10^{-3}$
Ra	10	$3 \cdot 10^{-2}$	$9 \cdot 10^{-2}$	$3 \cdot 10^{-3}$	$9 \cdot 10^{-4}$
Th	30	$5 \cdot 10^{-3}$	$5 \cdot 10^{-3}$	$5 \cdot 10^{-6}$	$2 \cdot 10^{-4}$
U	2	$5 \cdot 10^{-2}$	$5 \cdot 10^{-3}$	$5 \cdot 10^{-4}$	$4 \cdot 10^{-4}$
Np	10	$2 \cdot 10^{-2}$	$2 \cdot 10^{-2}$	$5 \cdot 10^{-6}$	$2 \cdot 10^{-4}$
Pu	8	$8 \cdot 10^{-5}$	$4 \cdot 10^{-4}$	$1 \cdot 10^{-7}$	$3 \cdot 10^{-4}$
Am	25	$3 \cdot 10^{-4}$	$3 \cdot 10^{-4}$	$2 \cdot 10^{-5}$	$5 \cdot 10^{-4}$
Cm	25	$3 \cdot 10^{-4}$	$3 \cdot 10^{-4}$	$2 \cdot 10^{-5}$	$5 \cdot 10^{-4}$
Pa	11 *)	$3 \cdot 10^{-3}$	$3 \cdot 10^{-3}$	$3 \cdot 10^{-2}$	$3 \cdot 10^{-2}$
Ac	25 *)	$3 \cdot 10^{-2}$	$3 \cdot 10^{-2}$	$5 \cdot 10^{-6}$	$5 \cdot 10^{-3}$

Table 9.4: Annual consumption habits U^x of adults and children [1]

	annual consumption	
	adults	children
drinking water	800 l	250 l
fish (fresh water)	20 kg	-
milk and milk products	330 kg	200 kg
meat	150 kg	20 kg
plant products	500 kg	60 kg
- grain (*op*)	190 kg	15 kg
- fruits (*op*)	100 kg	20 kg
- root vegetables (*op*)	170 kg	15 kg
- green vegetables (*gp*)	40 kg	10 kg

Table 9.7 shows the contribution of the different pathways to the dose factor for relevant nuclides. The nuclides in this table are ranked according to their contribution to the drinking water pathway. For most of the nuclides the main contribution stems from the irrigation pathway. There are only a few exceptions.

For some of the nuclides like Sn-126, U-235, Ni- 59, Cs-137 or Zr-93, which are high-energy gamma emitters or which have high-energy gamma-emitting daughters, the external radiation is the most important pathway.

The dose conversion factors of C-14 and Cs-135 are dominated by the fish consumption. Both nuclides exhibit large concentration factors for water/fish. The contribution of the watering places is far below 10% for all nuclides and highest for Nb-94 because of the high value of its pasture/meat transfer factor.

Within the irrigation pathway, for many nuclides, e.g. Sn-126, C-14, Se-79, Cs-137, Zr-93, the contribution from vegetal food (plants) is of the same order of magnitude as the contribution from food-animals. Only for Nb-94 is the contribution from the food-animals much higher than the contribution from vegetal food. This is due to its relatively large transfer factor pasture/meat. On the other hand there are a number of elements like Ra-

Table 9.5: Ingestion dose factors for adults H_i [Sv/Bq] and dose factors for external radiation $g_{s,i}$ [(Sv·s^{-1})/(Bq·m^{-2})] [6]

nuclide	H_i	$g_{s,i}$	nuclide	H_i	$g_{s,i}$
activation and fission products			Th-228	$1.1\cdot10^{-07}$	$2.4\cdot10^{-18}$
C- 14	$5.7\cdot10^{-10}$	0.0	Ra-228	$3.8\cdot10^{-07}$	0.0
Cl- 36	$8.2\cdot10^{-10}$	0.0	Cm-245	$1.0\cdot10^{-06}$	$8.5\cdot10^{-17}$
Co-60	$2.8\cdot10^{-09}$	$2.3\cdot10^{-15}$	Pu-241	$1.8\cdot10^{-08}$	0.0
Ni- 59	$5.7\cdot10^{-11}$	$2.8\cdot10^{-19}$	Am-241	$9.8\cdot10^{-07}$	$2.6\cdot10^{-17}$
Ni- 63	$1.6\cdot10^{-10}$	0.0	Np-237	$1.2\cdot10^{-06}$	$2.9\cdot10^{-17}$
Se- 79	$2.4\cdot10^{-09}$	0.0	U-233	$7.8\cdot10^{-08}$	$7.5\cdot10^{-19}$
Rb- 87	$1.3\cdot10^{-09}$	0.0	Th-229	$9.5\cdot10^{-07}$	$8.4\cdot10^{-17}$
Sr- 90	$3.5\cdot10^{-08}$	0.0	Ra-225	$1.0\cdot10^{-07}$	$1.3\cdot10^{-17}$
Zr- 93	$4.5\cdot10^{-10}$	0.0	Ac-225	$3.0\cdot10^{-08}$	$1.6\cdot10^{-17}$
Nb- 94	$1.9\cdot10^{-09}$	$1.5\cdot10^{-15}$	Cm-246	$5.4\cdot10^{-07}$	$8.5\cdot10^{-19}$
Mo- 93	$3.3\cdot10^{-10}$	$5.6\cdot10^{-18}$	Am-242m	$9.5\cdot10^{-07}$	$3.2\cdot10^{-18}$
Tc- 99	$3.9\cdot10^{-10}$	0.0	Pu-242	$2.5\cdot10^{-06}$	$7.3\cdot10^{-19}$
Pd-107	$4.0\cdot10^{-11}$	0.0	U-238	$6.9\cdot10^{-08}$	$6.3\cdot10^{-19}$
Sn-126	$5.3\cdot10^{-09}$	$5.4\cdot10^{-17}$	Pu-238	$8.6\cdot10^{-07}$	$9.2\cdot10^{-19}$
I-129	$6.7\cdot10^{-08}$	$2.6\cdot10^{-17}$	U-234	$7.7\cdot10^{-08}$	$8.3\cdot10^{-19}$
Cs-135	$1.9\cdot10^{-09}$	0.0	Th-230	$1.4\cdot10^{-07}$	$8.1\cdot10^{-19}$
Cs-137	$1.4\cdot10^{-08}$	0.0	Ra-226	$3.6\cdot10^{-07}$	$6.4\cdot10^{-18}$
Sm-147	$5.0\cdot10^{-08}$	0.0	Pb-210	$1.5\cdot10^{-06}$	$1.9\cdot10^{-16}$
Sm-151	$1.0\cdot10^{-10}$	0.0	Po-210	$5.1\cdot10^{-07}$	0.0
Eu-154	$2.8\cdot10^{-09}$	$1.1\cdot10^{-15}$	Am-243	$9.8\cdot10^{-07}$	$5.1\cdot10^{-17}$
nuclides from decay chains			Pu-239	$9.5\cdot10^{-07}$	$3.2\cdot10^{-18}$
Cm-244	$5.4\cdot10^{-06}$	$9.5\cdot10^{-19}$	U-235	$7.2\cdot10^{-08}$	$1.5\cdot10^{-16}$
Pu-240	$9.6\cdot10^{-07}$	$8.8\cdot10^{-19}$	Pa-231	$2.9\cdot10^{-06}$	$4.1\cdot10^{-17}$
U-236	$7.3\cdot10^{-08}$	$7.3\cdot10^{-19}$	Th-227	$1.0\cdot10^{-08}$	$9.9\cdot10^{-17}$
Th-232	$7.4\cdot10^{-07}$	$6.2\cdot10^{-19}$	Ac-227	$3.8\cdot10^{-06}$	0.0
U-232	$3.5\cdot10^{-07}$	$1.1\cdot10^{-18}$	Ra-223	$1.8\cdot10^{-07}$	$1.3\cdot10^{-16}$

226 or actinides with significantly higher contributions from vegetable foods than from food-animals due to the relatively small transfer factors pasture/milk, and pasture/meat, respectively.

Table 9.6: Dose conversion factors (DCF) of relevant nuclides for adults in $[(Sv \cdot y^{-1})/(Bq \cdot m^{-3})]$. *) The contribution of daughter nuclides is included [29].

nuclide	DCF	nuclide	DCF	nuclide	DCF
fission/activation products		Cs-135	$8.6 \cdot 10^{-08}$	Ra-225 *)	$2.0 \cdot 10^{-07}$
C- 14	$1.0 \cdot 10^{-07}$	Cs-137 *)	$1.3 \cdot 10^{-06}$	Ac-225 *)	$1.3 \cdot 10^{-07}$
Cl- 36	$2.6 \cdot 10^{-08}$	Sm-147	$1.6 \cdot 10^{-07}$	Am-242m *)	$2.6 \cdot 10^{-06}$
Ca- 41	$3.1 \cdot 10^{-09}$	Sm-151	$3.0 \cdot 10^{-10}$	U-238 *)	$3.1 \cdot 10^{-07}$
Co- 60	$4.0 \cdot 10^{-08}$	nuclides from decay chains		Pu-238 *)	$2.0 \cdot 10^{-06}$
Ni- 59	$1.7 \cdot 10^{-09}$	Cm-244 *)	$1.4 \cdot 10^{-06}$	U-234 *)	$2.4 \cdot 10^{-07}$
Ni- 63	$1.1 \cdot 10^{-09}$	Pu-240 *)	$2.2 \cdot 10^{-06}$	Th-230 *)	$2.4 \cdot 10^{-06}$
Se- 79	$2.3 \cdot 10^{-07}$	U-236 *)	$2.2 \cdot 10^{-07}$	Ra-226 *)	$1.5 \cdot 10^{-05}$
Rb- 87	$1.3 \cdot 10^{-07}$	Th-232 *)	$1.1 \cdot 10^{-05}$	Pb-210 *)	$6.3 \cdot 10^{-06}$
Sr- 90 *)	$2.0 \cdot 10^{-07}$	U-232 *)	$5.2 \cdot 10^{-06}$	Po-210 *)	$4.3 \cdot 10^{-06}$
Zr- 93 *)	$6.0 \cdot 10^{-09}$	Th-228 *)	$1.5 \cdot 10^{-06}$	Am-243 *)	$3.5 \cdot 10^{-06}$
Nb- 94	$9.2 \cdot 10^{-08}$	Ra-228 *)	$1.2 \cdot 10^{-06}$	Pu-239 *)	$2.2 \cdot 10^{-06}$
Mo- 93	$2.8 \cdot 10^{-08}$	Cm-245 *)	$3.0 \cdot 10^{-06}$	U-235 *)	$9.4 \cdot 10^{-07}$
Tc- 99	$4.9 \cdot 10^{-09}$	Pu-241 *)	$4.3 \cdot 10^{-08}$	Pa-231 *)	$1.3 \cdot 10^{-05}$
Pd-107	$3.0 \cdot 10^{-10}$	Am-241 *)	$2.7 \cdot 10^{-06}$	Ac-227 *)	$2.7 \cdot 10^{-05}$
Sb-125 *)	$8.1 \cdot 10^{-09}$	Np-237 *)	$6.2 \cdot 10^{-06}$	Th-227 *)	$3.2 \cdot 10^{-08}$
Sn-126 *)	$8.7 \cdot 10^{-06}$	U-233 *)	$2.8 \cdot 10^{-07}$	Ra-223 *)	$3.5 \cdot 10^{-07}$
I-129	$3.7 \cdot 10^{-07}$	Th-229 *)	$5.4 \cdot 10^{-06}$		

Table 9.7: Contribution of the exposition pathways to the dose conversion factors for relevant nuclides for adults (The contribution of daughter nuclides is included) [29]

parent nuclide	contribution of the exposition pathway in [%]					
	drinking water	fish	irrigation		watering place	external exposition
			plant	animal		
C-14	0.4	88.2	6.0	4.8	0.6	0.0
Sn-126	0.5	3.6	1.4	2.8	0.6	92.0
Se-79	0.8	4.2	56.6	38.0	0.4	0.0
Cs-137	0.9	33.7	2.1	3.8	0.5	58.9
Nb-94	1.7	8.3	4.7	50.8	7.2	27.2
Cs-135	1.8	66.6	14.6	16.0	1.0	0.0
Ra-226	1.9	0.5	93.1	4.1	0.2	0.2
Cl-36	2.5	3.2	20.8	69.1	4.4	0.0
Ni-59	2.7	6.8	11.6	8.5	0.9	69.5
Th-230	4.8	3.5	88.8	1.5	0.0	1.4
Zr-93	6.0	30.1	14.4	24.0	1.7	23.8
U-235	6.1	0.2	16.5	2.6	0.2	74.4
Tc-99	6.4	12.9	35.9	41.2	3.6	0.0
Pd-107	10.8	2.7	46.0	36.5	3.9	0.0
Ni-63	11.6	29.0	28.3	27.2	3.9	0.0
Sr-90	13.8	10.4	63.9	10.9	1.0	0.0
I-129	14.6	18.3	27.6	24.3	3.4	11.8
Np-237	15.4	3.8	65.7	0.4	0.1	14.6
Pa-231	17.4	4.8	54.9	17.8	1.3	3.8
U-238	17.9	0.9	41.6	5.9	0.4	33.4
U-233	22.4	1.2	66.5	7.9	0.5	1.6
U-234	26.1	1.3	61.8	8.7	0.6	1.5
Sm-151	26.3	16.4	45.7	9.7	1.9	0.0
Cm-245	26.4	16.5	44.3	0.4	0.1	12.3
U-236	26.8	1.3	61.1	8.9	0.5	1.4
Am-243	27.5	14.1	37.3	0.9	0.2	25.1
Am-241	28.9	18.1	47.4	1.1	0.2	3.9
Pu-241	33.6	6.8	56.0	0.7	0.1	2.8
Pu-240	34.5	6.9	57.6	0.7	0.1	0.2
Pu-239	34.5	6.9	57.7	0.7	0.1	0.1
Pu-238	34.9	7.0	57.1	0.7	0.1	0.2

10 Reference case calculations and parameter variations

10.1 Reference case

10.1.1 Near-field

The maximum release rates of the radionuclides from the waste forms into the canister interior ("volume of dissolution") and from the near-field into the geosphere are presented in table 10.1. The release rates into the geosphere are shown in figures 10.1 - 10.3. The results are presented for a group of 3900 canisters each containing 1.602 t_{hm}. The radionuclide release rates from this group of canisters, corresponding to 25 % of the total number of disposed canisters and a repository area of 1 km^2, define the portion of mass which enters into the most relevant flow pathway between the repository and the biosphere.

For all nuclides except Th-229, the maximum release rates of the waste forms (gap, metal parts, fuel matrix) occur at the time of canister failure (1000 years). This peak is caused by the instantaneous released fraction (IRF) from the gap. After 2100 years the release rates from the waste forms are controlled by the matrix-released fraction (MRF) whose inventory contains for most nuclides the main part of the waste. The release rates and the inventories of some daughter nuclides in the actinide chains continue to increase beyond 2100 years due to the decay of precursors.

The near-field results for the reference scenario lead to the following conclusions:

- The maximum release rates from the near-field into the geosphere are dominated by C-14, Ni-59, Mo-93, and Ra-226.

- The instantaneous release pulses from the waste forms of the non-solubility-limited and non- or weakly-sorbing nuclides, Cl-36, C-14, I-129, and Mo-93, are reduced by diffusion through the bentonite buffer before entering the geosphere. For example, the maximum annual release rate of I-129 is $3.8 \cdot 10^{-4}$ times the IRF inventory.

- The release rates of Se, Zr, Tc, Pd, Ra, U, Pu, Np, Th, and Pa are governed by the solubility limits. In the cases of Zr, Tc, Pd, U, Np, and Pa major portions of the nuclides released from the waste forms precipitate in the canister interior.

- The solubility limits of Ca, Nb, Sr, Mo, Sn, Sm, Am, and Cm are so high that they do not affect the release rates significantly.

- The maximum release rates of Ra-226 and Pa-231 originate from the decay of their parents Th-230 and U-235, respectively. The decay of Th-230 and U-235 released from the waste forms but precipitated in the canister interior results in nearly constant release rates for the daughter nuclides even after the complete degradation of the waste forms.

Table 10.1: Maximum release rates from the waste forms and from the near-field into the geosphere in the reference scenario

Nuclide	Release from waste forms			Release from near-field	
	IRF [Bq/y]	$t_{max,MRF}$ [y]	MRF [Bq/y]	t_{max} [y]	[Bq/y]
C -14	$1.6 \cdot 10^{12}$	$2.1 \cdot 10^{3}$	$6.0 \cdot 10^{7}$	$2.1 \cdot 10^{3}$	$2.1 \cdot 10^{9}$
Cl-36	$1.9 \cdot 10^{11}$	$2.1 \cdot 10^{3}$	$3.6 \cdot 10^{6}$	$1.0 \cdot 10^{3}$	$9.5 \cdot 10^{7}$
Ca-41	$1.9 \cdot 10^{9}$	$2.1 \cdot 10^{3}$	$1.8 \cdot 10^{5}$	$1.3 \cdot 10^{5}$	$7.0 \cdot 10^{3}$
Ni-59	$1.9 \cdot 10^{13}$	--	--	$1.4 \cdot 10^{4}$	$3.7 \cdot 10^{8}$
Ni-63	$9.2 \cdot 10^{11}$	--	--	$2.0 \cdot 10^{3}$	$7.1 \cdot 10^{0}$
Se-79	$1.2 \cdot 10^{12}$	$2.1 \cdot 10^{3}$	$1.1 \cdot 10^{8}$	$1.7 \cdot 10^{3}$	$7.9 \cdot 10^{6}$
Rb-87	$3.3 \cdot 10^{8}$	$2.1 \cdot 10^{3}$	$6.2 \cdot 10^{3}$	$2.2 \cdot 10^{3}$	$6.2 \cdot 10^{3}$
Sr-90	$2.6 \cdot 10^{6}$	--	--	$1.0 \cdot 10^{3}$	$5.8 \cdot 10^{0}$
Zr-93	$2.8 \cdot 10^{13}$	$2.1 \cdot 10^{3}$	$5.3 \cdot 10^{8}$	$1.1 \cdot 10^{5}$	$1.7 \cdot 10^{5}$
Mo-93	$1.3 \cdot 10^{11}$	--	--	$2.0 \cdot 10^{3}$	$4.6 \cdot 10^{8}$
Nb-94	$3.1 \cdot 10^{12}$	--	--	$1.1 \cdot 10^{4}$	$4.5 \cdot 10^{7}$
Tc-99	$8.0 \cdot 10^{13}$	$2.1 \cdot 10^{3}$	$3.9 \cdot 10^{9}$	$1.2 \cdot 10^{4}$	$2.4 \cdot 10^{7}$
Pd-107	$6.5 \cdot 10^{11}$	$2.1 \cdot 10^{3}$	$3.2 \cdot 10^{7}$	$1.4 \cdot 10^{5}$	$7.9 \cdot 10^{1}$
Sn-126	$3.5 \cdot 10^{12}$	$2.1 \cdot 10^{3}$	$1.7 \cdot 10^{8}$	$1.1 \cdot 10^{5}$	$1.4 \cdot 10^{6}$
I-129	$4.8 \cdot 10^{11}$	$2.1 \cdot 10^{3}$	$9.0 \cdot 10^{6}$	$1.1 \cdot 10^{3}$	$1.2 \cdot 10^{7}$
Cs-135	$4.8 \cdot 10^{12}$	$2.1 \cdot 10^{3}$	$9.1 \cdot 10^{7}$	$1.8 \cdot 10^{5}$	$8.4 \cdot 10^{7}$
Cs-137	$3.9 \cdot 10^{7}$	--	--	$1.0 \cdot 10^{3}$	$8.9 \cdot 10^{1}$
Sm-147	$4.2 \cdot 10^{6}$	$2.1 \cdot 10^{3}$	$4.1 \cdot 10^{2}$	$1.0 \cdot 10^{6}$	$4.5 \cdot 10^{1}$
Sm-151	$2.2 \cdot 10^{11}$	$2.1 \cdot 10^{3}$	$4.0 \cdot 10^{3}$	--	--

Table 10.1: Maximum release rates from the waste forms and from the near-field into the geosphere in the reference scenario

Nuclide	Release from waste forms			Release from near-field	
	IRF [Bq/y]	$t_{max,MRF}$ [y]	MRF [Bq/y]	t_{max} [y]	[Bq/y]
Cm-248	$9.1 \cdot 10^{6}$	$2.1 \cdot 10^{3}$	$1.8 \cdot 10^{3}$	$5.1 \cdot 10^{5}$	$8.5 \cdot 10^{0}$
Pu 244	$1.4 \cdot 10^{6}$	$5.3 \cdot 10^{5}$	$2.7 \cdot 10^{2}$	$1.6 \cdot 10^{6}$	$7.4 \cdot 10^{0}$
Pu-240	$6.8 \cdot 10^{14}$	$2.1 \cdot 10^{3}$	$1.2 \cdot 10^{11}$	$2.4 \cdot 10^{4}$	$2.4 \cdot 10^{5}$
U-236	$3.9 \cdot 10^{11}$	$3.7 \cdot 10^{4}$	$1.2 \cdot 10^{8}$	$4.5 \cdot 10^{5}$	$1.8 \cdot 10^{3}$
Th-232	$2.0 \cdot 10^{4}$	$9.8 \cdot 10^{5}$	$5.6 \cdot 10^{3}$	$1.0 \cdot 10^{7}$	$1.8 \cdot 10^{1}$
U-232	$9.0 \cdot 10^{5}$	--	--	--	--
Cm-245	$4.9 \cdot 10^{11}$	$2.1 \cdot 10^{3}$	$8.8 \cdot 10^{7}$	$2.6 \cdot 10^{4}$	$3.0 \cdot 10^{3}$
Pu-241	$4.9 \cdot 10^{11}$	$2.1 \cdot 10^{3}$	$8.9 \cdot 10^{7}$	$2.6 \cdot 10^{4}$	$3.0 \cdot 10^{3}$
Am-241	$1.2 \cdot 10^{15}$	$2.1 \cdot 10^{3}$	$3.9 \cdot 10^{10}$	$2.6 \cdot 10^{4}$	$3.1 \cdot 10^{3}$
Np-237	$1.5 \cdot 10^{12}$	$4.1 \cdot 10^{3}$	$3.5 \cdot 10^{8}$	$5.0 \cdot 10^{5}$	$2.3 \cdot 10^{3}$
U-233	$5.4 \cdot 10^{9}$	$5.9 \cdot 10^{5}$	$2.9 \cdot 10^{8}$	$7.3 \cdot 10^{5}$	$3.8 \cdot 10^{3}$
Th-229	$2.3 \cdot 10^{8}$	$6.0 \cdot 10^{5}$	$2.9 \cdot 10^{8}$	$1.6 \cdot 10^{5}$	$7.0 \cdot 10^{4}$
Cm-246	$1.1 \cdot 10^{12}$	$2.1 \cdot 10^{3}$	$1.9 \cdot 10^{8}$	$1.8 \cdot 10^{4}$	$1.8 \cdot 10^{3}$
Pu-242	$3.6 \cdot 10^{12}$	$2.1 \cdot 10^{3}$	$7.1 \cdot 10^{8}$	$5.4 \cdot 10^{5}$	$1.1 \cdot 10^{6}$
Am-242	$4.8 \cdot 10^{10}$	$2.1 \cdot 10^{3}$	$5.7 \cdot 10^{4}$	--	--
U-238	$3.6 \cdot 10^{11}$	$2.3 \cdot 10^{4}$	$7.2 \cdot 10^{7}$	$7.5 \cdot 10^{5}$	$1.1 \cdot 10^{3}$
Pu-238	$1.3 \cdot 10^{12}$	$2.1 \cdot 10^{3}$	$1.7 \cdot 10^{5}$	--	--
U-234	$2.8 \cdot 10^{12}$	$2.1 \cdot 10^{3}$	$5.5 \cdot 10^{8}$	$1.8 \cdot 10^{5}$	$4.7 \cdot 10^{3}$
Th-230	$2.4 \cdot 10^{10}$	$2.0 \cdot 10^{5}$	$3.4 \cdot 10^{8}$	$2.2 \cdot 10^{5}$	$9.7 \cdot 10^{5}$
Ra-226	$4.6 \cdot 10^{9}$	$2.0 \cdot 10^{5}$	$3.4 \cdot 10^{8}$	$5.4 \cdot 10^{5}$	$1.5 \cdot 10^{9}$
Cm-247	$2.9 \cdot 10^{6}$	$2.1 \cdot 10^{3}$	$5.8 \cdot 10^{2}$	$1.0 \cdot 10^{6}$	$1.5 \cdot 10^{1}$
Am-243	$3.8 \cdot 10^{13}$	$2.1 \cdot 10^{3}$	$6.7 \cdot 10^{9}$	$2.3 \cdot 10^{4}$	$1.7 \cdot 10^{5}$
Pu-239	$4.0 \cdot 10^{14}$	$2.1 \cdot 10^{3}$	$7.7 \cdot 10^{10}$	$6.4 \cdot 10^{4}$	$2.5 \cdot 10^{6}$
U-235	$1.6 \cdot 10^{10}$	$2.0 \cdot 10^{5}$	$5.9 \cdot 10^{6}$	$1.3 \cdot 10^{5}$	$2.8 \cdot 10^{2}$
Pa-231	$3.8 \cdot 10^{8}$	$3.5 \cdot 10^{5}$	$5.9 \cdot 10^{6}$	$2.2 \cdot 10^{5}$	$1.1 \cdot 10^{5}$

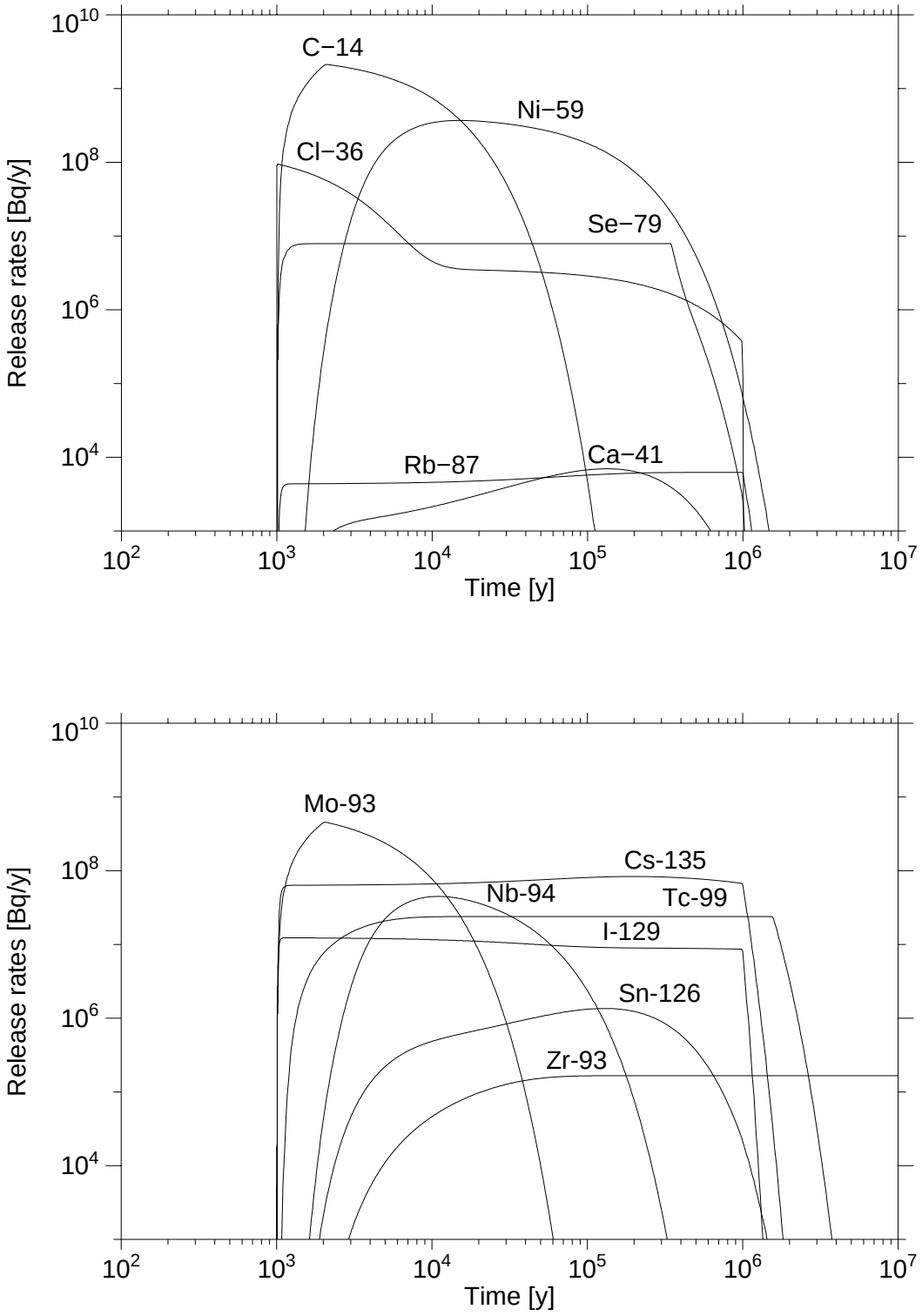

Fig. 10.1: Release rates of fission and activation products from the near-field into the geosphere in the reference scenario

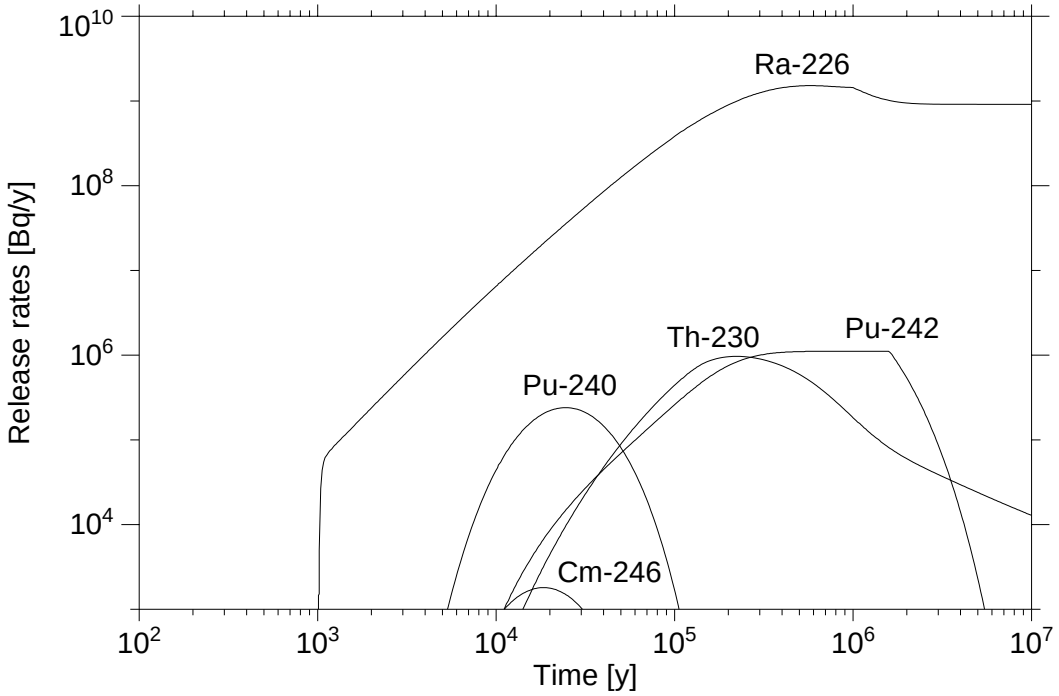

Fig. 10.2: Release rates of the radionuclides in the 4N and 4N+2 nuclide chains from the near-field into the geosphere in the reference scenario

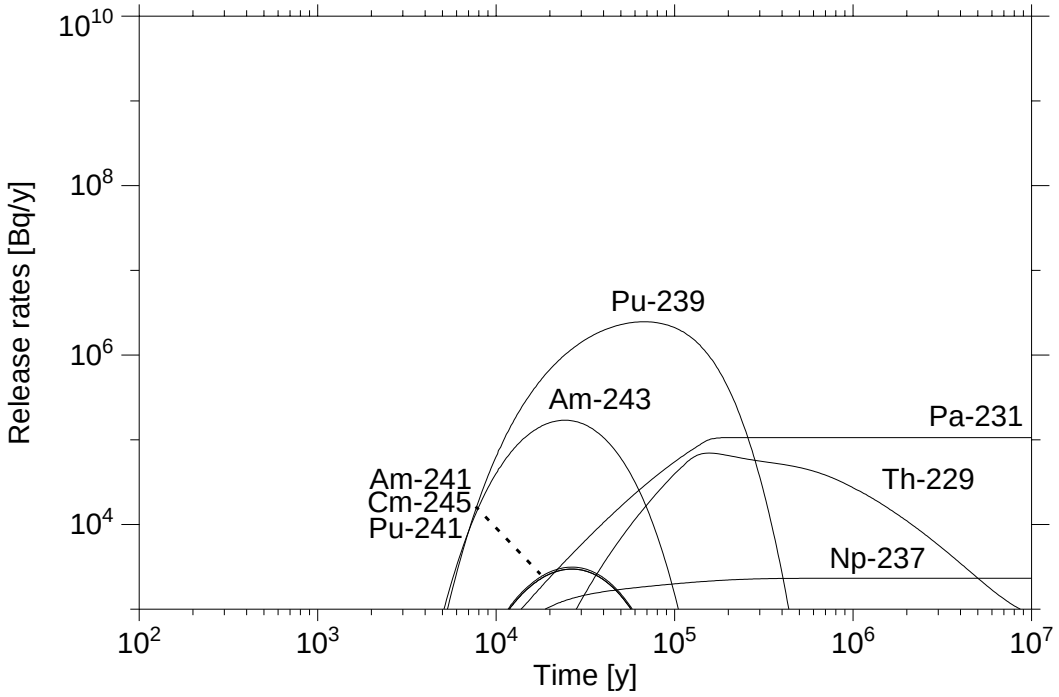

Fig. 10.3: Release rates of the radionuclides in the 4N+1 and 4N+3 nuclide chains from the near-field into the geosphere in the reference scenario

10.1.2 Far-field and biosphere

The maximum release rates from the geosphere into the biosphere and the maximum individual dose rates are given in table 10.1. Some short-lived nuclides (Ac-225, Ac-227, Ra-225, Ra-228, Pb-210) are considered in the biosphere calculations only. Their dose rates are calculated by means of the dose rates of their parent nuclides assuming both to be in radioactive equilibrium. The release rates from the geosphere into the biosphere and the individual dose rates are shown in fig. 10.4 and fig. 10.5, respectively.

The calculations for the reference scenario yield the following results:

- The maxima of the total dose rates are determined by the contributions of activation and fission products like C-14, Cl-36, I-129, Se-79, and Cs-135.

- In the case of the non-sorbing or weakly sorbing fission products (C-14, Cl-36, Ca-41, Se-79, Pd-107 I-129, Cs-135) the barrier function of the geosphere plays a minor role resulting in maximum release rates and times of occurrence which are only slightly affected by the transport through the geosphere.

- The geosphere is an important transport barrier for the well-sorbing nuclides such as the actinides and their daughter products. The release rates for some of these nuclides are still increasing after 10^7 years. As a consequence, the maximum dose rates from the nuclides of the four decay chains are some orders of magnitude lower than those of the relevant activation and fission products.

Table 10.2: Maximum release rates from the near-field and geosphere, and maximum dose rates in the reference scenario

Nuclide	Release from near-field		Release from far-field		Maximum dose rates [mSv/y]
	t_{max} [y]	[Bq/y]	t_{max} [y]	[Bq/y]	
C -14	$2.1 \cdot 10^{3}$	$2.1 \cdot 10^{9}$	$8.2 \cdot 10^{3}$	$7.7 \cdot 10^{8}$	$9.6 \cdot 10^{-3}$
Cl-36	$1.0 \cdot 10^{3}$	$9.5 \cdot 10^{7}$	$1.3 \cdot 10^{3}$	$8.7 \cdot 10^{7}$	$2.8 \cdot 10^{-4}$
Ca-41	$1.3 \cdot 10^{5}$	$7.0 \cdot 10^{3}$	$1.9 \cdot 10^{5}$	$4.9 \cdot 10^{3}$	$1.9 \cdot 10^{-9}$
Ni-59	$1.4 \cdot 10^{4}$	$3.7 \cdot 10^{8}$	$6.1 \cdot 10^{5}$	$7.6 \cdot 10^{3}$	$1.6 \cdot 10^{-9}$
Se-79	$1.7 \cdot 10^{3}$	$7.9 \cdot 10^{6}$	$1.7 \cdot 10^{5}$	$4.7 \cdot 10^{6}$	$1.3 \cdot 10^{-4}$
Rb-87	$4.3 \cdot 10^{5}$	$6.2 \cdot 10^{3}$	$9.5 \cdot 10^{5}$	$6.3 \cdot 10^{3}$	$1.0 \cdot 10^{-7}$
Zr-93	$1.1 \cdot 10^{5}$	$1.7 \cdot 10^{5}$	$1.0 \cdot 10^{7}$	$2.5 \cdot 10^{4}$	$1.8 \cdot 10^{-8}$
Mo-93	$2.0 \cdot 10^{3}$	$4.6 \cdot 10^{8}$	$2.4 \cdot 10^{4}$	$2.9 \cdot 10^{5}$	$1.0 \cdot 10^{-6}$
Nb-94	$1.1 \cdot 10^{4}$	$4.5 \cdot 10^{7}$	--	--	--
Tc-99	$1.2 \cdot 10^{4}$	$2.4 \cdot 10^{7}$	$2.0 \cdot 10^{6}$	$1.5 \cdot 10^{5}$	$8.9 \cdot 10^{-8}$
Pd-107	$1.4 \cdot 10^{5}$	$7.9 \cdot 10^{1}$	$1.0 \cdot 10^{7}$	$6.0 \cdot 10^{1}$	$2.3 \cdot 10^{-12}$
Sn-126	$1.1 \cdot 10^{5}$	$1.4 \cdot 10^{6}$	$8.4 \cdot 10^{5}$	$1.9 \cdot 10^{2}$	$2.1 \cdot 10^{-7}$
I-129	$1.1 \cdot 10^{3}$	$1.2 \cdot 10^{7}$	$1.4 \cdot 10^{5}$	$1.2 \cdot 10^{7}$	$5.4 \cdot 10^{-4}$
Cs-135	$1.8 \cdot 10^{5}$	$8.4 \cdot 10^{7}$	$5.1 \cdot 10^{5}$	$7.5 \cdot 10^{7}$	$8.1 \cdot 10^{-4}$
Sm-147	$1.1 \cdot 10^{6}$	$1.1 \cdot 10^{1}$	$1.0 \cdot 10^{7}$	0.36	$7.3 \cdot 10^{-12}$
Pu-240	$2.4 \cdot 10^{4}$	$2.4 \cdot 10^{5}$	--	--	--
U-236	$4.5 \cdot 10^{5}$	$1.8 \cdot 10^{3}$	$9.6 \cdot 10^{6}$	$1.3 \cdot 10^{3}$	$3.5 \cdot 10^{-8}$
Th-232	$1.0 \cdot 10^{7}$	$1.8 \cdot 10^{1}$	$1.0 \cdot 10^{7}$	$1.7 \cdot 10^{1}$	$2.4 \cdot 10^{-8}$
Ra-228					$7.9 \cdot 10^{-7}$
Cm-245	$2.6 \cdot 10^{4}$	$3.0 \cdot 10^{3}$	--	--	--
Pu-241	$2.6 \cdot 10^{4}$	$3.0 \cdot 10^{3}$	--	--	--
Am-241	$2.6 \cdot 10^{4}$	$3.1 \cdot 10^{3}$	--	--	--
Np-237	$5.0 \cdot 10^{5}$	$2.3 \cdot 10^{3}$	$1.0 \cdot 10^{7}$	$5.5 \cdot 10^{2}$	$4.3 \cdot 10^{-7}$
U-233	$7.3 \cdot 10^{5}$	$3.8 \cdot 10^{3}$	$1.0 \cdot 10^{7}$	$6.0 \cdot 10^{2}$	$2.1 \cdot 10^{-8}$
Th-229	$1.6 \cdot 10^{5}$	$7.0 \cdot 10^{4}$	$1.0 \cdot 10^{7}$	$6.0 \cdot 10^{2}$	$4.0 \cdot 10^{-7}$
Ra-225					$4.5 \cdot 10^{-6}$
Ac-225					$2.9 \cdot 10^{-9}$
Cm-246	$1.8 \cdot 10^{4}$	$1.8 \cdot 10^{3}$	--	--	--
Pu-242	$5.4 \cdot 10^{5}$	$1.1 \cdot 10^{6}$	$4.0 \cdot 10^{6}$	1.3	$3.4 \cdot 10^{-10}$
U-238	$7.5 \cdot 10^{5}$	$1.1 \cdot 10^{3}$	$1.1 \cdot 10^{7}$	$1.1 \cdot 10^{3}$	$4.3 \cdot 10^{-8}$
U-234	$1.8 \cdot 10^{5}$	$4.7 \cdot 10^{3}$	$1.1 \cdot 10^{7}$	$1.1 \cdot 10^{3}$	$3.3 \cdot 10^{-8}$

Table 10.2: Maximum release rates from the near-field and geosphere, and maximum dose rates in the reference scenario

Nuclide	Release from near-field		Release from far-field		Maximum dose rates [mSv/y]
	t_{max} [y]	[Bq/y]	t_{max} [y]	[Bq/y]	
Th-230	$2.2 \cdot 10^{5}$	$9.7 \cdot 10^{5}$	$1.1 \cdot 10^{7}$	$1.1 \cdot 10^{3}$	$3.3 \cdot 10^{-7}$
Ra-226	$5.4 \cdot 10^{5}$	$1.5 \cdot 10^{9}$	$1.1 \cdot 10^{7}$	$2.2 \cdot 10^{3}$	$4.1 \cdot 10^{-6}$
Pb-210					$4.3 \cdot 10^{-8}$
Cm-247	$1.0 \cdot 10^{6}$	$1.5 \cdot 10^{1}$	$1.0 \cdot 10^{7}$	0.32	$1.5 \cdot 10^{-10}$
Am-243	$2.3 \cdot 10^{4}$	$1.7 \cdot 10^{5}$	$1.0 \cdot 10^{7}$	0.32	$1.4 \cdot 10^{-10}$
Pu-239	$6.4 \cdot 10^{4}$	$2.5 \cdot 10^{6}$	$1.0 \cdot 10^{7}$	0.33	$8.9 \cdot 10^{-11}$
U-235	$1.3 \cdot 10^{5}$	$2.8 \cdot 10^{2}$	$1.1 \cdot 10^{7}$	$8.9 \cdot 10^{1}$	$1.0 \cdot 10^{-8}$
Pa-231	$2.2 \cdot 10^{5}$	$1.1 \cdot 10^{5}$	$1.1 \cdot 10^{7}$	$8.9 \cdot 10^{1}$	$1.4 \cdot 10^{-7}$
Ac-227					$3.0 \cdot 10^{-7}$

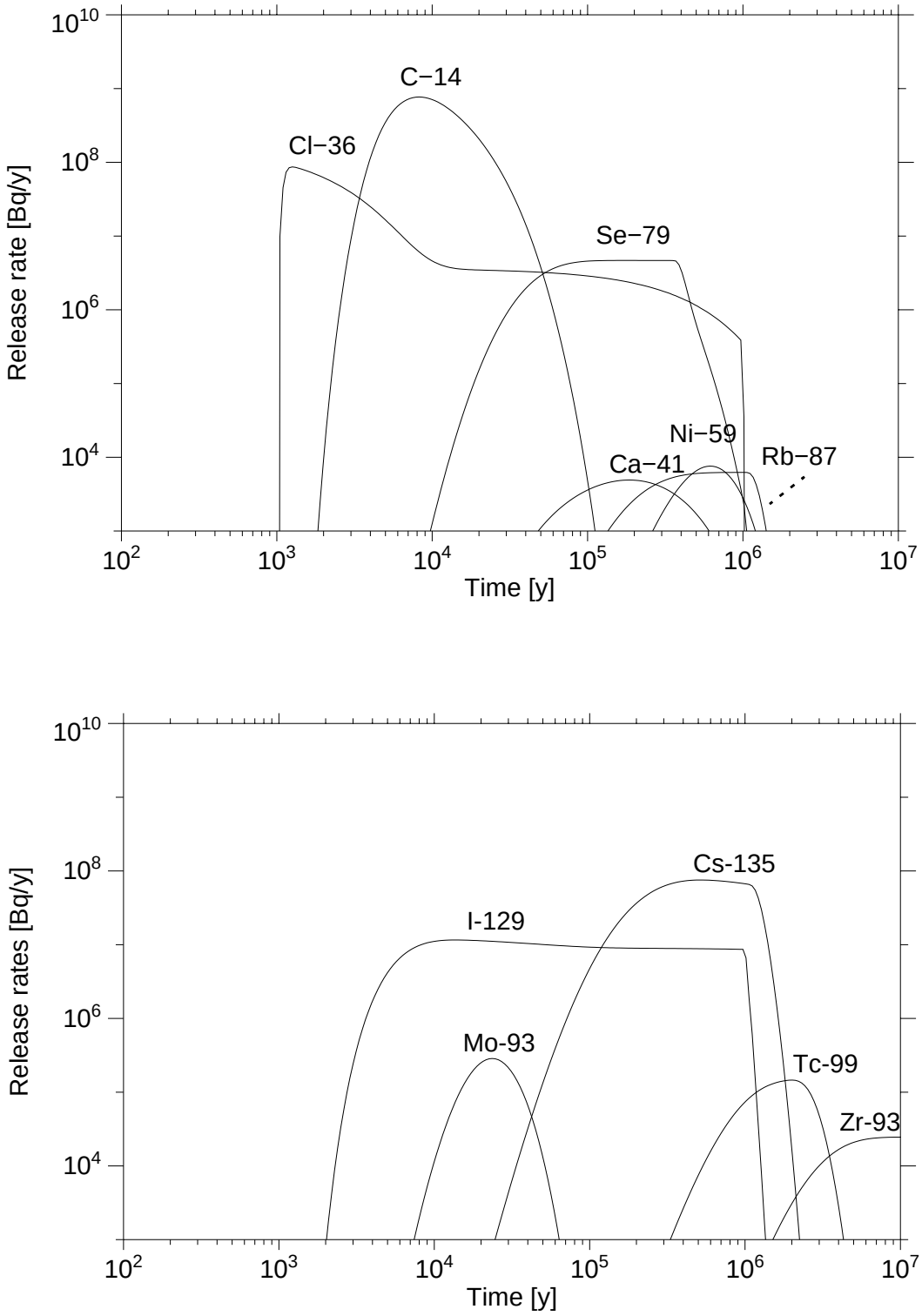

Fig. 10.4: Release rates of fission and activation products from the geosphere into the biosphere in the reference case

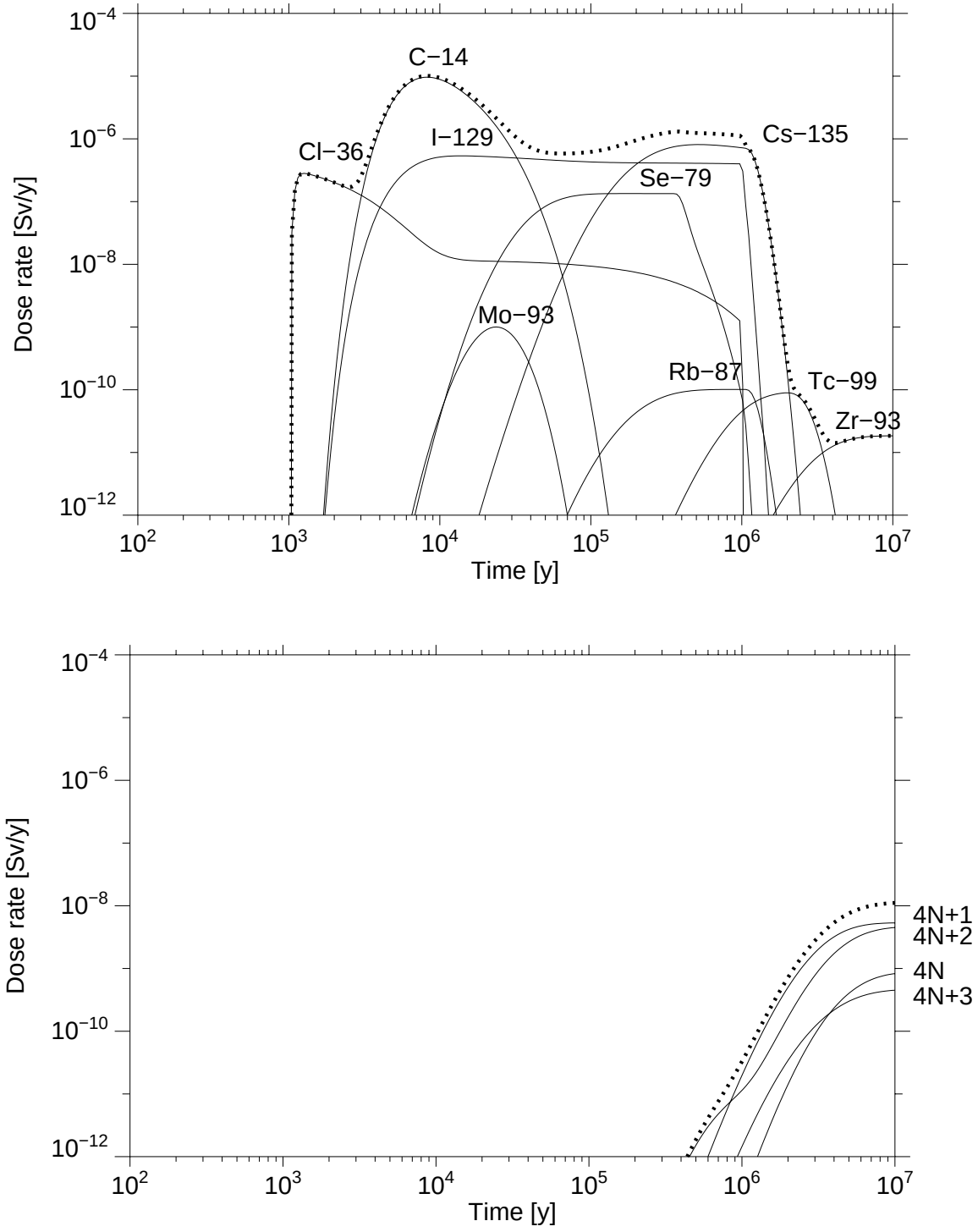

Fig. 10.5: Dose rates due to activation and fission products and nuclide chains in the reference scenario. The dotted lines give the sum over the dose rates due to activation/fission products, and nuclides in the decay chains

10.1.3 Behaviour of the multi-barrier system

This section focuses upon the general behaviour of radionuclide transport through a multi-barrier systems as considered in our safety analysis. For this prupose the transport behaviour of Tc-99 is investigated. Tc-99 represents a medium sorbing, solubility limited and decaying radionuclide. The distribution of the Tc-99 inventory among the different components of the repository system versus time and the release rates of Tc-99 from different components (waste forms, near-field, far-field) as a function of time are given in Fig. 10.6.

The release rates from the waste forms are characterized by the instantaneous released fraction, the released fraction from the metal parts, and the released fraction from the matrix. After the matrix dissolution time of one million years the Tc-99 inventory is mobilized. Within the first $1.5 \cdot 10^6$ years, most of the inventory released from the waste forms precipitates in the volume of dissolution. For the next 500,000 years the main part of Tc-99 inventory is dissolved or sorbed within the bentonite buffer. From 2 to 3 million years the main part of the Tc-99 inventory in the repository system is transported through the geosphere. After 3 million years the Tc-99 inventory having already entered the biosphere represents the main part of the remaining inventory. However, the total amount of Tc-99 inventory which enters the biosphere is more than four orders of magnitude less than that originally emplaced.

The impact of the multi-barrier system can be seen in the second part of Figure 10.6. The peak release rates of the instantaneous released fraction and the released fraction from the metal parts are lowered by diffusion through the bentonite. During diffusive transport through the bentonite the Tc-99 concentration is also reduced by radioactive decay. Because of this, its release rate from the near-field into the geosphere is about two orders of magnitude lower than the release rate from the fuel matrix, which is nearly constant over several 10^5 years. The Tc-99 flux from the near-field into the fractured system of the geosphere is reduced during its transport through the far-field. Diffusion into the adjacent matrix with immobile pore water and sorption onto the matrix surfaces increase the transport time through the far-field and the effect of radioactive decay. Because of these processes the release rate of Tc-99 representing a medium sorbing nuclide decreases during its transport through the far-field by approximately two orders of magnitude.

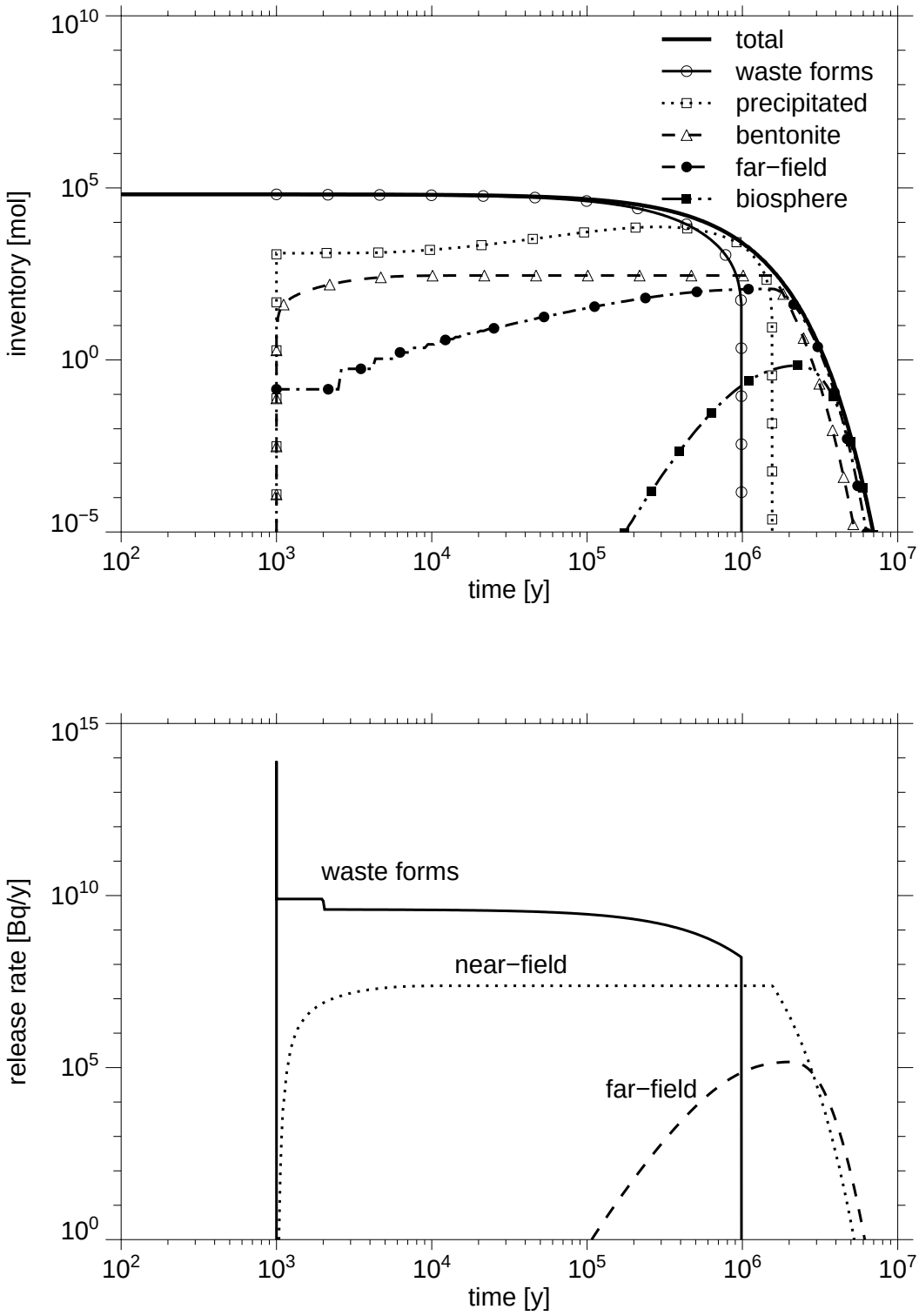

Fig. 10.6: Distribution of Tc-99 inventory among the different components of the repository system; release rates of Tc-99 from different components (waste forms, near-field, far-field) as a function of time

Firstly, beside the general transport mechanisms during passage of the radionuclides through the engineered and geological barriers, the radionuclides are jointly affected by

- radioactive decay and
- element-specific solubility.

In Fig. 10.7 the release rates from the waste forms for radionuclides of the neptunium-chain are given. The ingrowth of U-233 and Th-229 through the decay of the parent nuclides Np-237 and U-233, respectively, results in an increase in the release rates from the fuel matrix with time. Because of decay processes the concentrations of many daughter nuclides are controlled by the concentrations of their precursors in the different components of the multi-barrier system.

Secondly, the radionuclides are affected by each other because of element-specific solubility limits. Fig. 10.8 presents the concentrations in the ‘volume of dissolution’ for different Pu radionuclides as a function of time. The maximum sum of dissolved plutonium isotopes is limited by their solubility of 10^{-5} mol/m^3. This mutual solubility limit results, for example, in an increase of dissolved Pu-242 concentration by one order of magnitude after the disappearance of the shorter-lived plutonium nuclides Pu-239 and Pu-240.

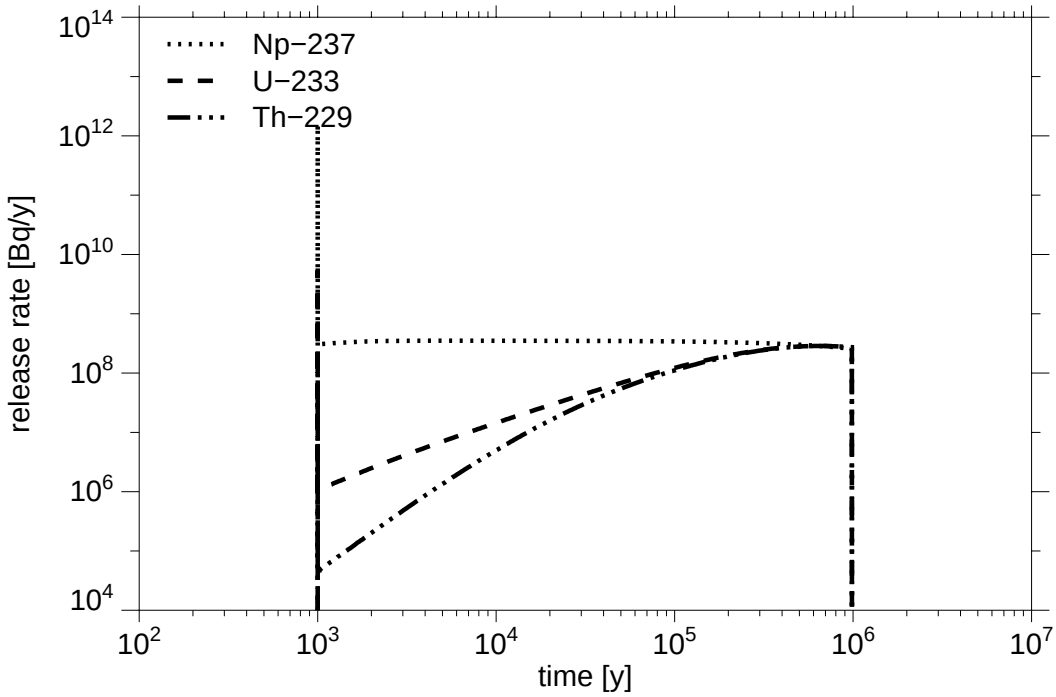

Fig. 10.7: Release rates versus time for radionuclides of the neptunium decay chain

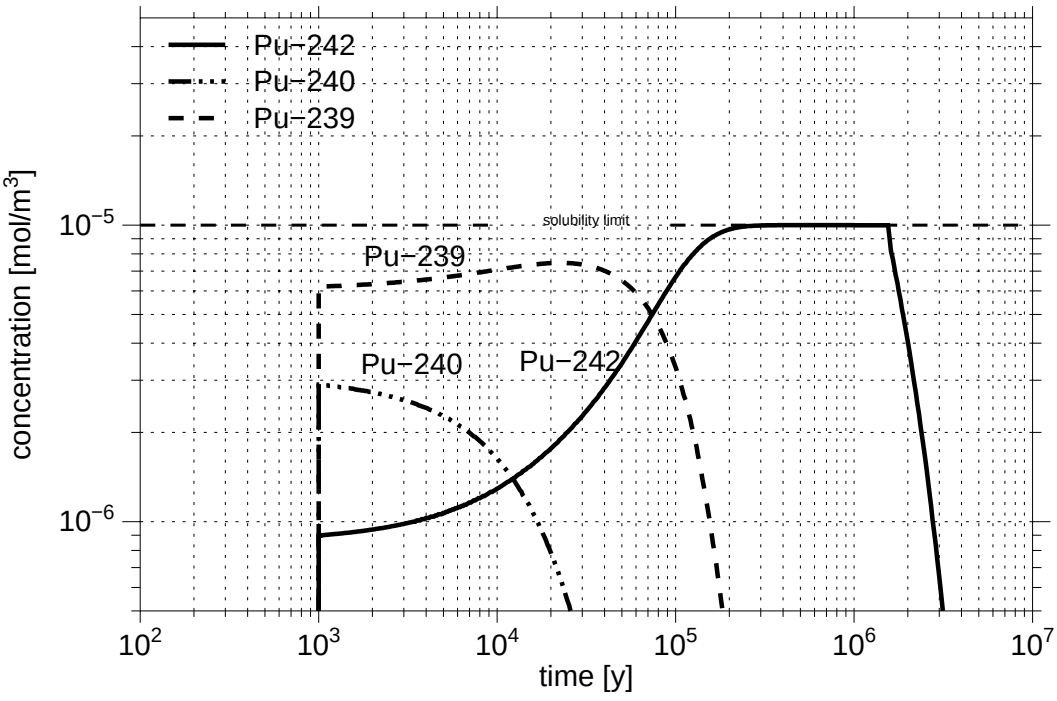

Fig. 10.8: Distribution of concentration in the “volume of dissolution” for different Pu radionuclides as a function of time

10.2 Sensitivity analysis

For the reference scenario a local sensitivity analysis is performed by means of parameter variations. Within each variation a single parameter or a single set of parameters are varied, while the others are held constant. The varied parameters are divided into two groups:

- element-specific parameters
- other parameters.

The impact of the element-specific parameters on the total dose rates is investigated by comparison of the maximum dose rates for all nuclides. For the other parameters only the maximum total dose rates and the maximum dose rates of the most relevant nuclides are evaluated. It has to be mentioned that the impact of non element-specific parameter variations is different for each nuclide.

10.2.1 Efficiency and sensitivity of the near-field barrier

The efficiency of the near-field barrier is shown in the hypothetical scenario with direct release from the near-field into the biosphere neglecting retardation and decay in the far-field. With the exception of Ra-226 the near-field barrier is sufficient to guarantee maximum total dose rates below $3 \cdot 10^{-4}$ Sv/y.

In the case of non element-specific parameter variations, the values of the water flow rate through the EDZ and the number of canisters which are assumed to be connected with the relevant transport pathways to the biosphere are the most sensitive parameters. An increase and decrease, respectively, of water flow through the EDZ by a factor of 10 results in almost an order of magnitude increase and decrease in the dose rates, respectively. The maximum total dose rates after variation of element-specific parameters show the following behaviour:

- **Conservative solubility limits:** Conservative solubilities affect significantly the dose rates of nuclides such as Se, Zr, Tc, Pd, U, Np, Th, and Ra which are limited by the solubility. Additionally, the release rates of daughter nuclides from solubility-limited parents are sensitive to the solubilities.

- **Conservative sorption constants:** The influence of conservative sorption constants for bentonite compared to reference sorption constants is shown in fig. 10.12. The maximum dose rate increases by a factor of 17, which is the result of the higher C-14 dose rate. For the other relevant nuclides, only the maximum dose rate of I-129 is influenced by the use of lower sorption constants. The impact of conservative sorption parameters for the actinides and their daughters is negligible.

- **Oxidizing conditions:** For the case of oxidizing conditions in the bentonite buffer, the dose rates of elements like Ni, Se, Tc, and U increase because of the low sorption values and/or high solubility limits. However, the most sensitive parameter is the high solubility of uranium which results in strongly increasing dose rates for the daughters of the uranium nuclides. The total dose rate is dominated by the dose rate of Ra-226.

- **Source term:** The parameter variations for the source term are performed by varying the dissolution rates for the different waste forms. A significantly higher total dose rate is only reached if the matrix dissolution rate is increased by a factor of 1000. In this case, the higher release rates of I-129 from the waste forms are responsible for the increase of the total dose rates. A degradation rate of the metal parts of 10^{-4} 1/y results in decreased maximum total dose rates because of the reduced C-14 release rates. The waste fraction in the gap is not a sensitive parameter with respect to the maximum total dose rates since the peak from the gap is significantly lowered by diffusion through the bentonite.

10.2.2 Efficiency and sensitivity of the far-field barrier

The release rates of nuclides from the near-field are lowered by retardation and decay during the transport through the far-field. Therefore, the geosphere is only an effective barrier for the higher sorbing or short-lived nuclides. Considering the reference case, the maximum dose rates of the most relevant nuclides such as C-14, Cs-135, I-129, Cl-36, and Se-79 are reduced at most by a factor of 2.7 (C-14) during transport through the geosphere. This shows that the impact of conservative far-field parameters on the maximum dose rates is limited. However, less conservative assumptions such as increased penetration depth, increased transport pathway, increased total width of open channels per rock area, and decreased water flow result in significantly lower dose rates, particularly for C-14, and consequently significantly lower maximum total dose rates. Insensitive parameters concerning the far-field barrier are the longitudinal dispersion length, the matrix diffusivity and the matrix porosity.

- **Conservative sorption constants:** For the most relevant nuclides the geosphere represents a weak barrier. Therefore, conservative sorption constants lead only to slightly higher maximum total dose rates compared to the realistic values. However, for nuclides such as Ni-59, Mo-93, Tc-99, Sn-126, which are short-lived with respect to the transport time, as well as some actinides with their daughter products, the maximum dose rates increase by several orders of magnitude.

10.2.3 Sensitivity of the biosphere parameter values

Besides the dose conversion factors which have not been varied, the relevant and sensitive parameter for the biosphere modelling is the dilution of contaminant concentrations entering the near-surface aquifers. Since in our calculations no dilution effect is considered during the transport through the geosphere, the nuclide concentration in the near-surface aquifer depends linearly on the groundwater flow rate in that layer.

The sorption constants are only taken into account for dose calculations of short-lived daughter nuclides and are insensitive with respect to the total dose rates.

10.2.4 Tables and figures

Table 10.3: Parameter variations for the near-field model data

Near-field parameter variations	
Name	**Description**
RS-Nrmi10	degradation rate of metal parts increased by a factor of 10
RS-Nrmd10	degradation rate of metal parts decreased by a factor of 10
RS-Nrsi100	spent fuel matrix dissolution rate increased by a factor of 100
RS-Nrsd10	spent fuel matrix dissolution rate decreased by a factor of 10
RS-Nfgi2	fraction of elements in the gap increased by a factor of 2
RS-Nfgd2	fraction of elements in the gap decreased by a factor of 2
RS-Nvdi5	volume of dissolution increased by a factor of 5
RS-Nvdd5	volume of dissolution decreased by a factor of 5
RS-Nslc	conservative solubility limits
RS-Nscc	conservative sorption constants in bentonite
RS-Ndci5	increased diffusion constant by a factor of 5
RS-Ndcd5	decreased diffusion constant by a factor of 5
RS-Ncco	oxidizing conditions in the near-field
RS-Nbti2	increased bentonite thickness by a factor of 2
RS-Nbtd2	decreased bentonite thickness by a factor of 2
RS-Nfei10	increased water flow through EDZ by a factor of 10
RS-Nfed10	decreased water flow through EDZ by a factor of 10
RS-Ncll	canister lifetime between 1000 - 2000 years
RS-Ncle	1% of the canisters with early failures
RS-Nnci4	number of canisters associated with “conservative” geosphere pathways increased by a factor of 4
RS-Nncd4	number of canisters associated with “conservative” geosphere pathways decreased by a factor of 4
RS-Ndrb	hypothetical case of direct release from near-field into the biosphere

Table 10.4: Parameter variations for geosphere and biosphere model data

Geosphere parameter variations	
Name	**Description**
RS-Gfli2	LPD flow path length increased by a factor of 2
RS-Gfld2	LPD flow path length decreased by a factor of 2
RS-Gfri10	increased flow rate by factor of 10
RS-Gfrd10	decreased flow rate by a factor of 10
RS-Gtwi10	total width of open channels per rock area increased by a factor of 10
RS-Gscc	conservative sorption constants in granite
RS-Gdcd5	decreased diffusion constant by a factor of 5
RS-Gdii5	increased dispersion by a factor of 5
RS-Gdnd	no dispersion
RS-Gpd10	penetration depth of 10 cm for matrix diffusion
RS-Gpd1	penetration depth of 1 cm for matrix diffusion
RS-Gmpi4	increased matrix porosity by a factor of 4
Alternative geometrical model assumptions	
Name	**Description**
RS-Gmdu	unlimited matrix diffusion
RS-Gcjz	cataclastic zones or jointed zones with broad, widely-spaced channels, matrix diffusion in altered rock (KRISTALLIN-I, Reference case)
RS-Gczi	crushed zone with spherical grain fill
Parameter variations affecting near-field and geosphere	
Name	**Description**
RS-NGfri10	groundwater flow rate increased by factor of 10: combination of RS-Nfei10 and RS-Gfri10
RS-NGfrd10	groundwater flow rate decreased by factor of 10: combination of RS-Nfed10 and RS-Gfrd10
Biosphere parameter variations	
Name	**Description**
RS-Bsci	increased sorption constants of near-surface layers
RS-Bscd	decreased sorption values of near-surface layers
RS-Bdii10	increased dilution in near-surface layers by a factor of 10
RS-Bdid10	decreased dilution in near-surface layers by a factor of 10

Table 10.5: Maximum dose rates for the total dose and the most important nuclides

	t_{max} [y]	S_{max} [Sv/y]	1st nuclide	max [Sv/y]	2nd nuclide	max [Sv/y]	3rd nuclide	max [Sv/y]
Reference	**$8.2 \cdot 10^{3}$**	**$1.0 \cdot 10^{-5}$**	**C-14**	**$9.6 \cdot 10^{-6}$**	**Cs-135**	**$8.1 \cdot 10^{-7}$**	**I-129**	**$5.4 \cdot 10^{-7}$**
RS-Nrmi10	$7.9 \cdot 10^{3}$	$1.1 \cdot 10^{-5}$	C-14	$1.0 \cdot 10^{-5}$	Cs-135	$8.1 \cdot 10^{-7}$	I-129	$5.4 \cdot 10^{-7}$
RS-Nrmd10	$1.4 \cdot 10^{4}$	$5.2 \cdot 10^{-6}$	C-14	$4.6 \cdot 10^{-6}$	Cs-135	$8.1 \cdot 10^{-7}$	I-129	$5.4 \cdot 10^{-7}$
RS-Nrsi100	$1.1 \cdot 10^{4}$	$1.6 \cdot 10^{-5}$	C-14	$1.1 \cdot 10^{-5}$	I-129	$9.1 \cdot 10^{-6}$	Cs-135	$3.5 \cdot 10^{-6}$
RS-Nrsd10	$8.2 \cdot 10^{3}$	$1.0 \cdot 10^{-5}$	C-14	$9.6 \cdot 10^{-6}$	I-129	$4.8 \cdot 10^{-7}$	Cl-36	$2.8 \cdot 10^{-7}$
RS-Nfgi2	$8.2 \cdot 10^{3}$	$1.1 \cdot 10^{-5}$	C-14	$9.7 \cdot 10^{-6}$	I-129	$1.0 \cdot 10^{-6}$	Cs-135	$8.2 \cdot 10^{-7}$
RS-Nfgd2	$8.2 \cdot 10^{3}$	$9.8 \cdot 10^{-6}$	C-14	$9.6 \cdot 10^{-6}$	Cs-135	$8.2 \cdot 10^{-7}$	I-129	$4.2 \cdot 10^{-7}$
RS-Nvdi5	$8.2 \cdot 10^{3}$	$9.9 \cdot 10^{-6}$	C-14	$9.4 \cdot 10^{-6}$	Cs-135	$8.1 \cdot 10^{-7}$	I-129	$5.2 \cdot 10^{-7}$
RS-Nvdd5	$8.2 \cdot 10^{3}$	$1.0 \cdot 10^{-5}$	C-14	$9.6 \cdot 10^{-6}$	Cs-135	$8.1 \cdot 10^{-7}$	I-129	$5.4 \cdot 10^{-7}$
RS-Nslc	$8.2 \cdot 10^{3}$	$1.0 \cdot 10^{-5}$	C-14	$9.6 \cdot 10^{-6}$	Ra-226	$2.9 \cdot 10^{-6}$	Se-79	$8.4 \cdot 10^{-7}$
RS-Nscc	$6.6 \cdot 10^{3}$	$1.7 \cdot 10^{-4}$	C-14	$1.7 \cdot 10^{-4}$	I-129	$3.5 \cdot 10^{-6}$	Cs-135	$8.4 \cdot 10^{-7}$
RS-Ndci5	$8.2 \cdot 10^{3}$	$1.0 \cdot 10^{-5}$	C-14	$9.6 \cdot 10^{-6}$	Cs-135	$8.1 \cdot 10^{-7}$	I-129	$5.4 \cdot 10^{-7}$
RS-Ndcd5	$8.2 \cdot 10^{3}$	$9.8 \cdot 10^{-6}$	C-14	$9.3 \cdot 10^{-6}$	Cs-135	$8.1 \cdot 10^{-7}$	I-129	$5.3 \cdot 10^{-7}$
RS-Ncco	$4.4 \cdot 10^{6}$	$6.6 \cdot 10^{-5}$	Ra-226	$5.3 \cdot 10^{-5}$	C-14	$9.6 \cdot 10^{-6}$	Th-230	$4.2 \cdot 10^{-6}$
RS-Nbti2	$8.6 \cdot 10^{3}$	$3.7 \cdot 10^{-6}$	C-14	$3.5 \cdot 10^{-6}$	Cs-135	$7.2 \cdot 10^{-7}$	I-129	$4.1 \cdot 10^{-7}$
RS-Nbtd2	$8.2 \cdot 10^{3}$	$2.4 \cdot 10^{-5}$	C-14	$2.3 \cdot 10^{-5}$	I-129	$1.1 \cdot 10^{-6}$	Cs-135	$8.3 \cdot 10^{-7}$
RS-Nfei10	$7.5 \cdot 10^{3}$	$7.7 \cdot 10^{-5}$	C-14	$7.4 \cdot 10^{-5}$	I-129	$2.6 \cdot 10^{-6}$	Cl-36	$1.9 \cdot 10^{-6}$
RS-Nfed10	$8.6 \cdot 10^{3}$	$1.1 \cdot 10^{-6}$	C-14	$9.9 \cdot 10^{-7}$	Cs-135	$4.9 \cdot 10^{-7}$	I-129	$3.7 \cdot 10^{-7}$
RS-Ncll	$8.6 \cdot 10^{3}$	$1.0 \cdot 10^{-5}$	C-14	$9.6 \cdot 10^{-6}$	Cs-135	$8.1 \cdot 10^{-7}$	I-129	$5.4 \cdot 10^{-7}$
RS-Ncle	$8.2 \cdot 10^{3}$	$1.1 \cdot 10^{-5}$	C-14	$1.0 \cdot 10^{-5}$	Cs-135	$8.1 \cdot 10^{-7}$	I-129	$5.4 \cdot 10^{-7}$
RS-Nnci4	$8.2 \cdot 10^{3}$	$4.0 \cdot 10^{-5}$	C-14	$3.8 \cdot 10^{-5}$	Cs-135	$3.2 \cdot 10^{-6}$	I-129	$2.1 \cdot 10^{-6}$
RS-Nncd4	$8.2 \cdot 10^{3}$	$2.5 \cdot 10^{-6}$	C-14	$2.4 \cdot 10^{-6}$	Cs-135	$2.0 \cdot 10^{-7}$	I-129	$1.3 \cdot 10^{-7}$
RS-Ndrb	$5.4 \cdot 10^{3}$	$2.9 \cdot 10^{-3}$	Ra-226	$2.9 \cdot 10^{-3}$	Pb-210	$3.0 \cdot 10^{-5}$	C-14	$2.7 \cdot 10^{-5}$
RS-Gfli2	$1.3 \cdot 10^{4}$	$4.9 \cdot 10^{-6}$	C-14	$4.5 \cdot 10^{-6}$	Cs-135	$7.2 \cdot 10^{-7}$	I-129	$5.2 \cdot 10^{-7}$
RS-Gfld2	$5.7 \cdot 10^{3}$	$1.6 \cdot 10^{-5}$	C-14	$1.5 \cdot 10^{-5}$	Cs-135	$8.6 \cdot 10^{-7}$	I-129	$5.5 \cdot 10^{-7}$
RS-Gfri10	$2.9 \cdot 10^{3}$	$2.4 \cdot 10^{-5}$	C-14	$2.3 \cdot 10^{-5}$	Cs-135	$8.9 \cdot 10^{-7}$	Ra-226	$7.1 \cdot 10^{-7}$
RS-Gfrd10	$1.0 \cdot 10^{5}$	$4.5 \cdot 10^{-7}$	I-129	$4.4 \cdot 10^{-7}$	Cs-135	$2.5 \cdot 10^{-7}$	Cl-36	$2.0 \cdot 10^{-7}$
RS-Gtwi10	$1.0 \cdot 10^{5}$	$4.5 \cdot 10^{-7}$	I-129	$4.4 \cdot 10^{-7}$	Cs-135	$2.5 \cdot 10^{-7}$	Cl-36	$2.0 \cdot 10^{-7}$
RS-Gscc	$2.3 \cdot 10^{3}$	$2.7 \cdot 10^{-5}$	C-14	$2.6 \cdot 10^{-5}$	Cs-135	$8.9 \cdot 10^{-7}$	I-129	$5.7 \cdot 10^{-7}$
RS-Gdcd5	$8.2 \cdot 10^{3}$	$9.9 \cdot 10^{-6}$	C-14	$9.4 \cdot 10^{-6}$	Cs-135	$8.0 \cdot 10^{-7}$	I-129	$5.3 \cdot 10^{-7}$
RS-Gdii5	$9.0 \cdot 10^{3}$	$1.0 \cdot 10^{-5}$	C-14	$9.8 \cdot 10^{-6}$	Cs-135	$8.3 \cdot 10^{-7}$	I-129	$5.5 \cdot 10^{-7}$
RS-Gdnd	$9.5 \cdot 10^{3}$	$1.0 \cdot 10^{-5}$	C-14	$9.9 \cdot 10^{-6}$	Cs-135	$8.3 \cdot 10^{-7}$	I-129	$5.5 \cdot 10^{-7}$
RS-Gpd10	$2.0 \cdot 10^{4}$	$1.1 \cdot 10^{-6}$	C-14	$9.5 \cdot 10^{-7}$	I-129	$4.7 \cdot 10^{-7}$	Cs-135	$4.3 \cdot 10^{-7}$
RS-Gpd1	$5.5 \cdot 10^{3}$	$1.6 \cdot 10^{-5}$	C-14	$1.5 \cdot 10^{-5}$	Cs-135	$8.6 \cdot 10^{-7}$	I-129	$5.5 \cdot 10^{-7}$
RS-Gmpi4	$8.2 \cdot 10^{3}$	$1.0 \cdot 10^{-5}$	C-14	$9.6 \cdot 10^{-6}$	Cs-135	$8.1 \cdot 10^{-7}$	I-129	$5.4 \cdot 10^{-7}$
RS-Gmdu	$9.7 \cdot 10^{3}$	$4.3 \cdot 10^{-7}$	C-14	$3.3 \cdot 10^{-7}$	I-129	$3.2 \cdot 10^{-7}$	Cs-135	$1.2 \cdot 10^{-7}$
RS-Gcjz	$6.9 \cdot 10^{3}$	$1.3 \cdot 10^{-5}$	C-14	$1.2 \cdot 10^{-5}$	Cs-135	$8.4 \cdot 10^{-7}$	I-129	$5.4 \cdot 10^{-7}$
RS-Gczi	$4.9 \cdot 10^{5}$	$4.1 \cdot 10^{-7}$	I-129	$4.1 \cdot 10^{-7}$	Cs-135	$3.4 \cdot 10^{-8}$	Cl-36	$3.0 \cdot 10^{-8}$
RS-NGfri10	$2.7 \cdot 10^{3}$	$2.2 \cdot 10^{-4}$	C-14	$2.1 \cdot 10^{-4}$	Ra-226	$6.0 \cdot 10^{-6}$	I-129	$4.7 \cdot 10^{-6}$

Table 10.5: Maximum dose rates for the total dose and the most important nuclides

	t_{max} [y]	S_{max} [Sv/y]	1st nuclide	max [Sv/y]	2nd nuclide	max [Sv/y]	3rd nuclide	max [Sv/y]
RS-NGfrd10	$1.0 \cdot 10^{6}$	$3.8 \cdot 10^{-7}$	I-129	$3.7 \cdot 10^{-7}$	Cs-135	$1.6 \cdot 10^{-7}$	Cl-36	$2.9 \cdot 10^{-8}$
RS-Bsci	$8.2 \cdot 10^{3}$	$1.0 \cdot 10^{-5}$	C-14	$9.6 \cdot 10^{-6}$	Cs-135	$8.1 \cdot 10^{-7}$	I-129	$5.4 \cdot 10^{-7}$
RS-Bscd	$8.2 \cdot 10^{3}$	$1.0 \cdot 10^{-5}$	C-14	$9.6 \cdot 10^{-6}$	Cs-135	$8.1 \cdot 10^{-7}$	I-129	$5.4 \cdot 10^{-7}$
RS-Bdii10	$8.2 \cdot 10^{-3}$	$1.0 \cdot 10^{-6}$	C-14	$9.6 \cdot 10^{-7}$	Cs-135	$8.1 \cdot 10^{-8}$	I-129	$5.4 \cdot 10^{-8}$
RS-Bdid10	$8.2 \cdot 10^{-3}$	$1.0 \cdot 10^{-4}$	C-14	$9.6 \cdot 10^{-5}$	Cs-135	$8.1 \cdot 10^{-6}$	I-129	$5.4 \cdot 10^{-6}$

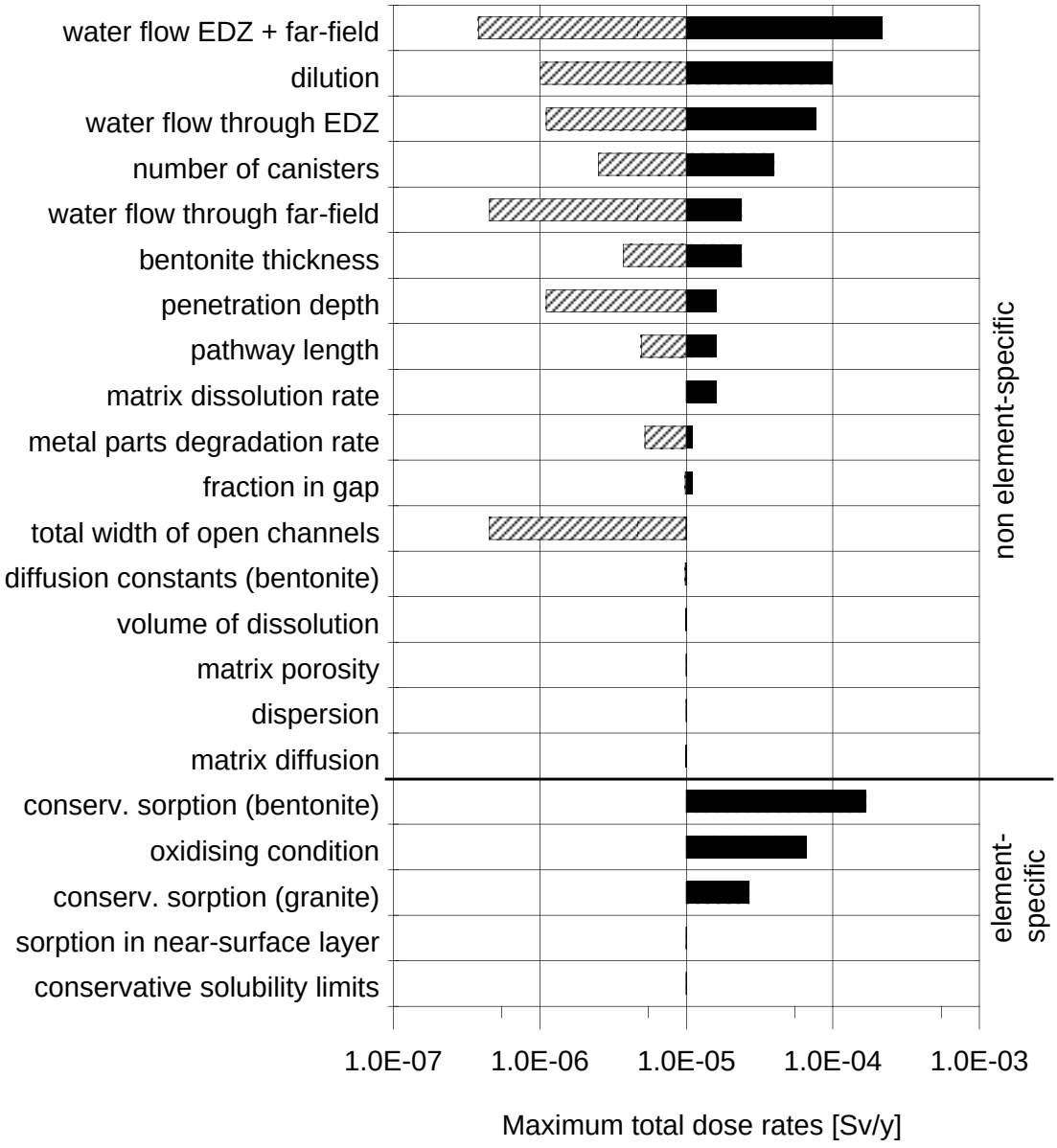

Fig. 10.9: Range of maximum total dose rates obtained by variation of single model parameters

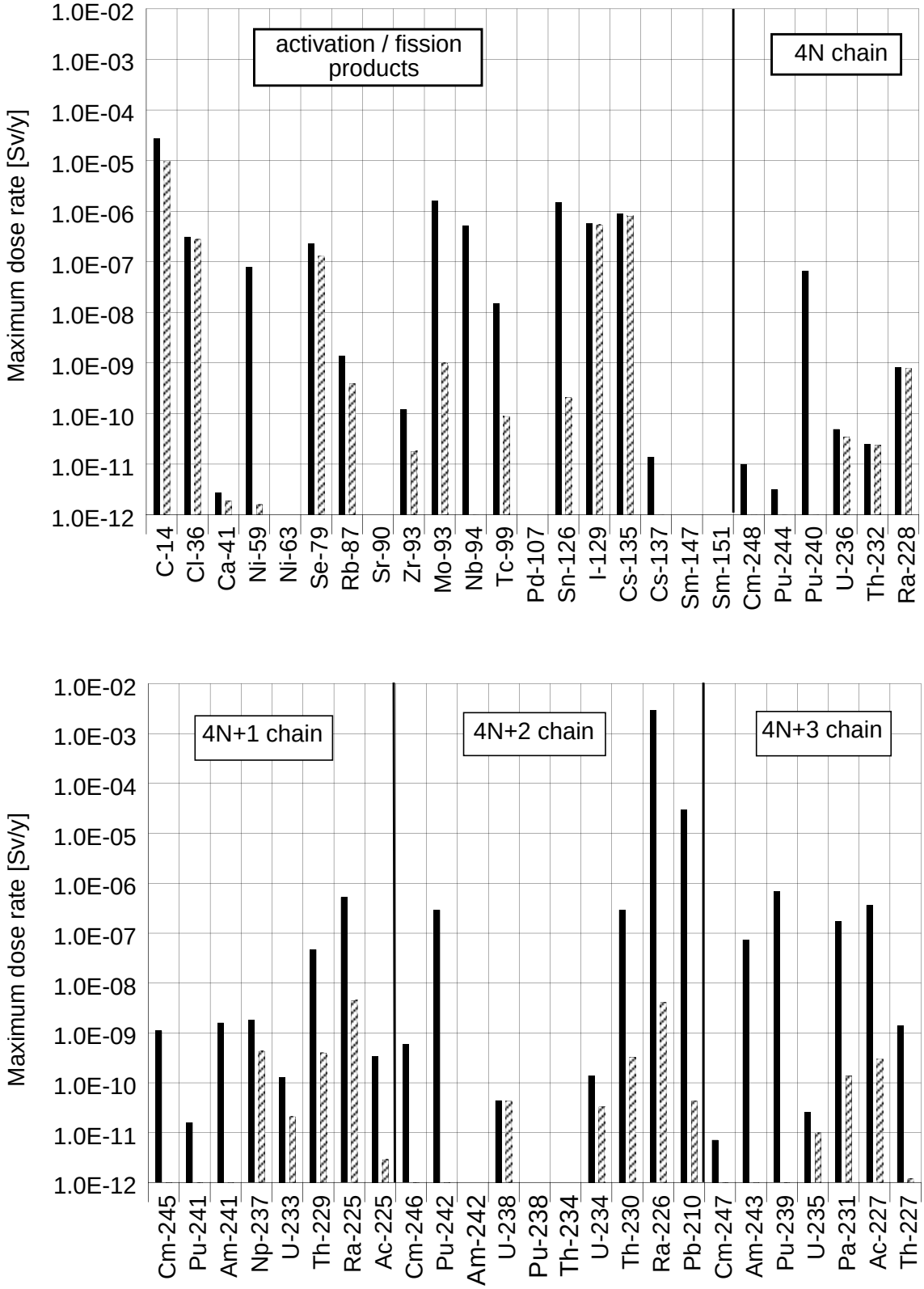

Fig. 10.10: Maximum dose rates for direct release from the near-field into the biosphere (solid lines) and for the reference case (dashed lines)

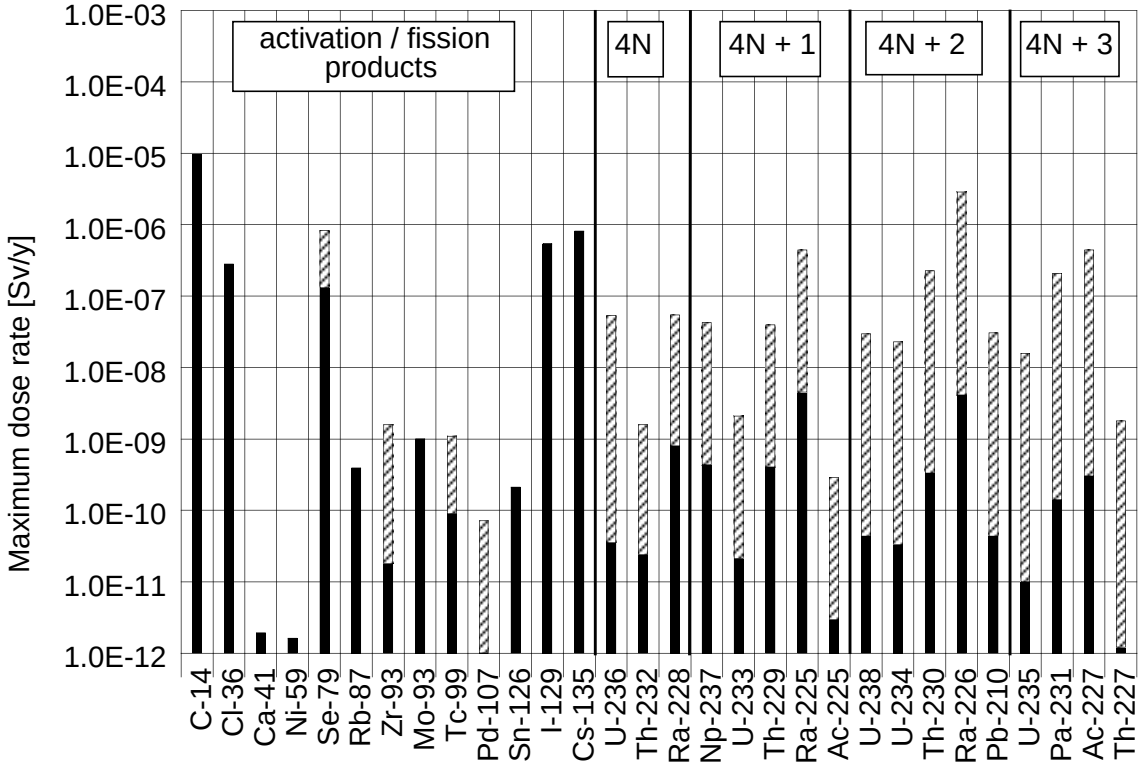

Fig. 10.11: Maximum dose rates of the relevant nuclides for the reference case (solid lines) and in the case of conservative solubility limits (dashed lines)

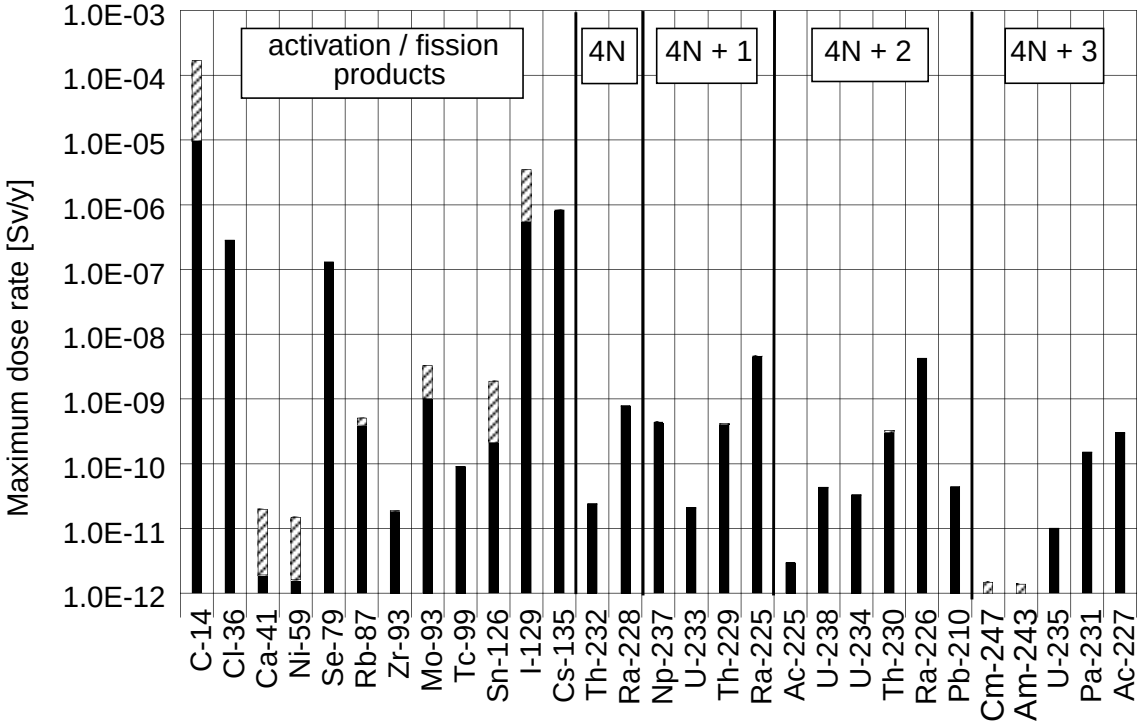

Fig. 10.12: Maximum dose rates for the reference case (solid lines) and in the case of conservative sorption constants for the bentonite (dashed lines)

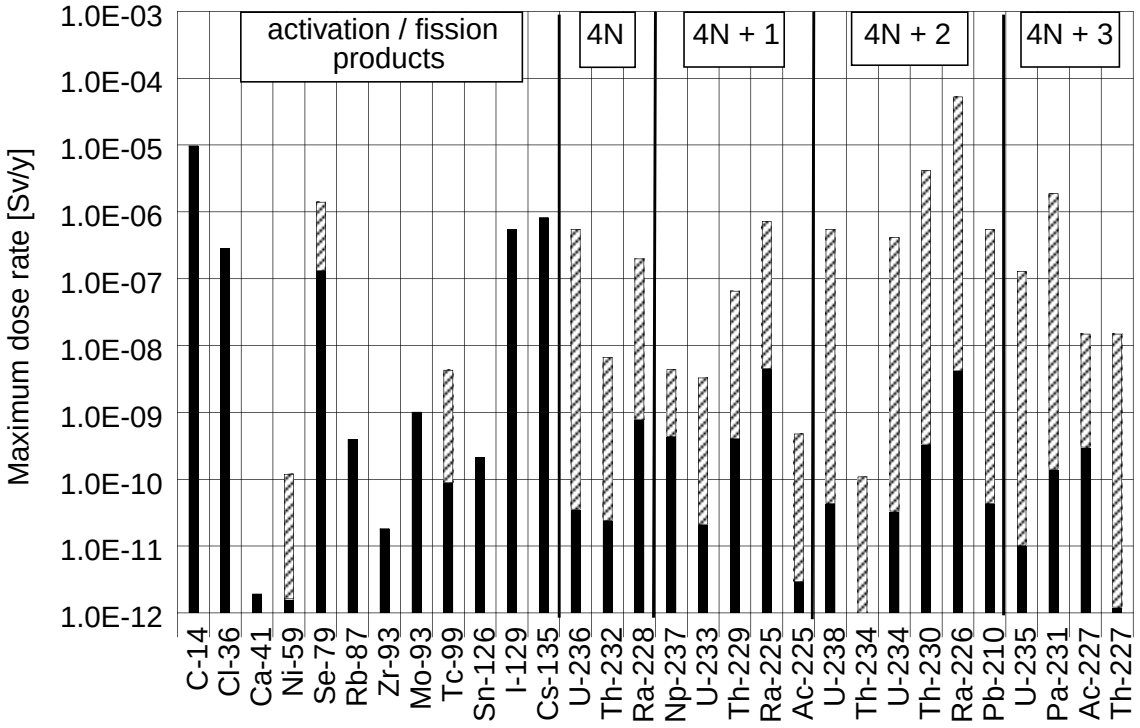

Fig. 10.13: Maximum dose rates of the relevant nuclides for the reference case (solid lines) and in the case of oxidizing conditions in the near-field (dashed)

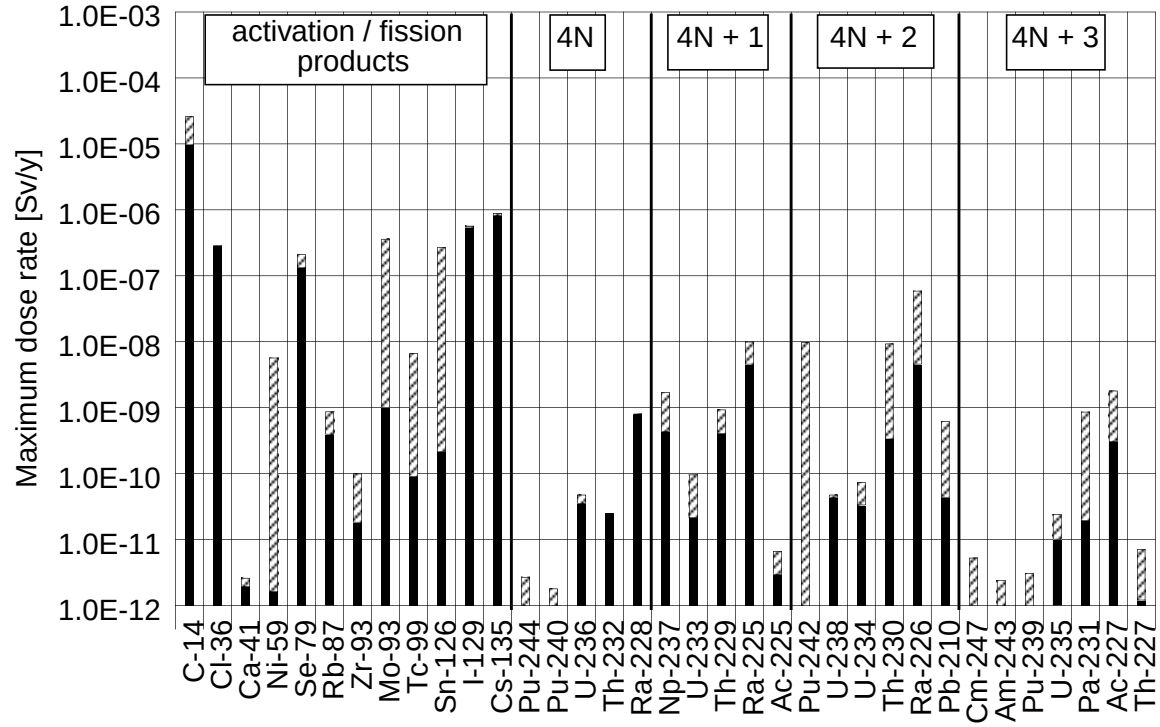

Fig. 10.14: Maximum dose rates for the reference case (solid lines) and for the case of conservative sorption constants for the granite (dashed lines)

11 Calculations for alternative model assumptions and scenarios

11.1 Other scenarios

11.1.1 Deep groundwater well (WELL-97)

As an alternative scenario the release of radionuclides from the repository into the catchment area of wells for extraction of deep groundwater is considered. The conceptual differences between the reference biosphere and the deep-well scenario are: The reference biosphere considers a region of farmland requiring a large amount of water which can easily be extracted by wells from near-surface aquifers. On the other hand, in the deep-well scenario a region non-favourable to agriculture is assumed because of a lack of water. Thus, the groundwater drawn from deep wells entails relatively high costs and is only used as drinking water.

The dose conversion factors are derived according to the WELL-97 scenario [41]. This scenario is based upon the assumption that the annual releases from the repository into the biosphere are diluted in 100,000 m^3 of water and that an individual drinks 500 litres of contaminated water per year. An effective dilution volume of 100,000 m^3/y is obtained, for example, if 1% of the total release from the repository into the biosphere ends up in a well and the pumping rate of the well is 1000 m^3/y. Drinking water is considered the only exposure pathway. This assumption means that an individual in the critical group ingests annually a fraction $5 \cdot 10^{-6}$ of the radionuclides released from the repository into the biosphere. The dose conversion factor of a radionuclide is thus $5 \cdot 10^{-6}$ times its ingestion dose coefficient.

Fig. 11.1 shows the dose rates of the most relevant fission and activation products, and of the decay chains. Mo-93 and Rb-87 are not considered in WELL-97. In contrast to the reference case, I-129 is the first, and C-14 only the second, most relevant nuclide with respect to the maximum dose rates. Additionally, the dose rates of the nuclide chains are roughly an order of magnitude higher for the WELL-97 scenario. The differences can be explained as follows: The effective dilution volume in the WELL-97 scenario is assumed

to be by a factor of 80 lower than in the reference biosphere (10^5 instead of $8 \cdot 10^6$ m^3/y). This results in increased dose rates from nuclides like I-129 and most of the actinides for which the drinking of water is one of the main contributions to the exposition pathways. Practically no change in the maximum dose rates occurs from nuclides for which drinking water contributes only about 1-2% to the total exposition, e. g. Cs-135 and Cl-36. In the case of C-14 the maximum dose rates are lower in the WELL-97 scenario than in the reference case since eating fish is the main exposition pathway and the drinking of water contributes only 0.4% to the exposition for man in the reference scenario.

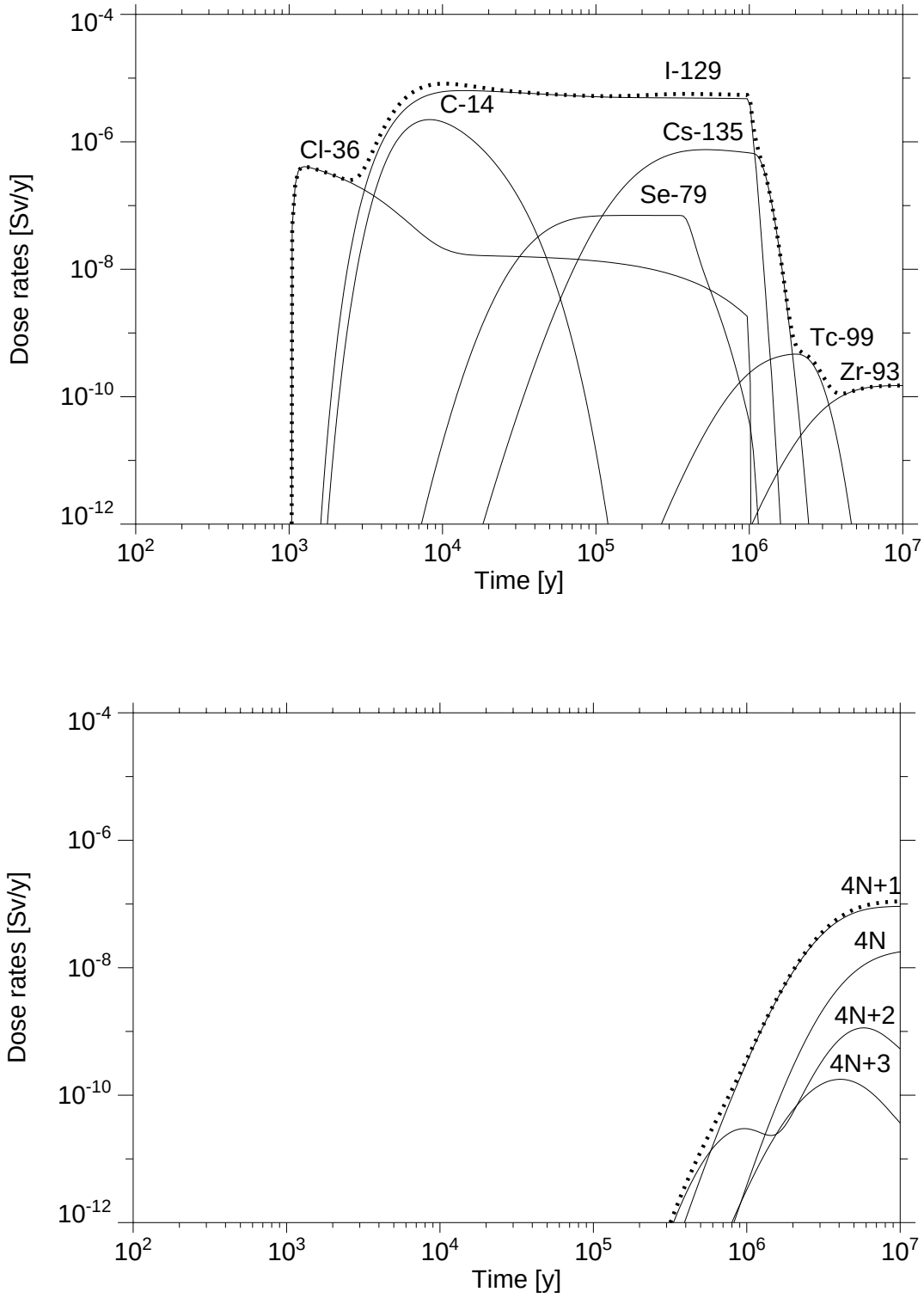

Fig. 11.1: Dose rates due to activation and fission products, and from the nuclide chains for the deep groundwater well (WELL-97) scenario. The dotted lines represents the total dose rate resulting from the activation/fisson products and the nuclides in the decay chains, respectively.

11.1.2 RN transport along EDZs of tunnels and shaft

After closure of the repository, the access tunnels and shafts will be backfilled. In the following scenario a continuously connected excavation-disturbed zone surrounding the tunnels and shafts is considered which may have significantly higher hydraulic conductivities than the adjacent undisturbed host rock. Therefore, a rapid transport pathway from the repository to the biosphere is assumed.

The modelling of the nuclide transport along EDZs of tunnels and shafts corresponds to the proceeding of the KRISTALLIN-I study. The relevant repository area of 1 km^2 (25% of the total repository area) is modelled as a disk of radius R = 560 m located inside a homogeneous porous medium with hydraulic conductivity $K = 1.75 \cdot 10^{-3}$ m/y (large-scale hydraulic conductivity for a low-permeability domain). According to the approach used in KRISTALLIN-I, the flux into the repository is given approximately by $8K\Delta hR$ with a hydraulic head Δh between the repository tunnel system and the undisturbed host rock of 100 m. Based on this, the total flow into the repository and through the shaft is estimated to be 784 m^3 per year.

The length of the flow path is estimated by the vertical distance from the repository to the higher-permeability domain of the crystalline basement and has a value of 500 m. The shaft has a diameter of 7.5 m ([28]). The thickness of its excavation-disturbed zone is assumed to be about one shaft radius, which results in an area of 133 m^2. Therefore, the Darcy velocity through the surrounding excavation-disturbed zone is estimated to be 5.9 m/y.

The transport along the excavation-disturbed zone is modelled (see NAGRA [27]) as an equivalent porous medium. Diffusion of nuclides into the adjacent rock matrix is neglected. The porosity ε of the EDZ is supposed to be so low that the approximation $\varepsilon R_f = \rho K_d$ is valid. Sorption properties of the undisturbed host rock are also applied for the excavation-disturbed zone with $K_d = 10^{-5}$ m^3/kg for non-sorbing nuclides.

11.1.3 Barrier effects of a sedimentary cover

In the reference scenario the transport through the low-permeability domain is assumed to represent the main barrier effect of the geosphere. In this scenario, additionally, the transport through a sedimentary cover is taken into account. Conservatively, the water flow rate through the sedimentary cover is assumed to be identical to the flow rate of $8 \cdot 10^6$ m^3/y supposed to occur within the near-surface layers. As a basis for the sorption at the sediment matrix the upper values of sorption constants, listed in table 9.1, are taken. For the transport calculations, a porosity of 20%, a bulk density of 2500 kg/m^3, and a transport pathway length of 200 m are used. The cross section for the water flow is assumed to be $4 \cdot 10^6$ m^2.

11.1.4 Total dose rates of the alternative scenarios

In fig. 11.2 the total dose rate as a function of the time is presented both for the reference scenario and for the alternative scenario. The maximum total dose rate and maximum dose rates of the most relevant nuclide are listed in table 11.1. The calculations show the following results:

- In the case of radionuclide transport through the EDZs surrounding the tunnels and shafts the geosphere is not a barrier to long-lived nuclides or weakly sorbed nuclides as, for instance, C-14, I-129 and Cs-135. Almost no delay of the arrival time of the maximum dose rates to the biosphere compared with the arrival times of the maximum peaks from the near-field into the geosphere can be observed. However, the dose rates of the actinides and their daughter products are significantly reduced during the transport along the considered migration pathway.

- The consideration of the transport through the sedimentary cover reduces the maximum dose rate of C-14 and the arrival time of its peak by about 25%. No additional barrier effect can be obtained for long-lived nuclides like Cs-135 and I-129.

Compared with the reference case, the differences concerning the total dose rates for the WELL-97 scenario arise from the reduced dilution and the fact that drinking water is the only exposure pathway to man. These assumptions for nuclides for which drinking water is the main exposure pathway result in an increase of the dose rates. For nuclides for which the eating of fish is the main exposure pathway a reduction of the dose rates is obtained.

Table 11.1: Maximum total dose rate for the different scenarios and the maximum dose rate for each of the most important nuclides

	t_{max} [y]	S_{max} [Sv/y]	1st nuclide	max [Sv/y]	2st nuclide	max [Sv/y]	3st nuclide	max [Sv/y]
Ref	$\mathbf{8.2 \cdot 10^{3}}$	$\mathbf{1.0 \cdot 10^{-5}}$	**C-14**	$\mathbf{9.6 \cdot 10^{-6}}$	**Cs-135**	$\mathbf{8.1 \cdot 10^{-7}}$	**I-129**	$\mathbf{5.4 \cdot 10^{-7}}$
AS-TTS	$2.4 \cdot 10^{3}$	$2.6 \cdot 10^{-5}$	C-14	$2.5 \cdot 10^{-5}$	Cs-135	$8.6 \cdot 10^{-7}$	Mo-93	$8.2 \cdot 10^{-7}$
AS-TSC	$1.1 \cdot 10^{4}$	$7.6 \cdot 10^{-6}$	C-14	$7.0 \cdot 10^{-6}$	Cs-135	$8.1 \cdot 10^{-7}$	I-129	$5.4 \cdot 10^{-7}$
AS-DGW	$1.0 \cdot 10^{4}$	$8.2 \cdot 10^{-6}$	I-129	$6.4 \cdot 10^{-6}$	C-14	$2.2 \cdot 10^{-6}$	Cs-135	$7.5 \cdot 10^{-7}$

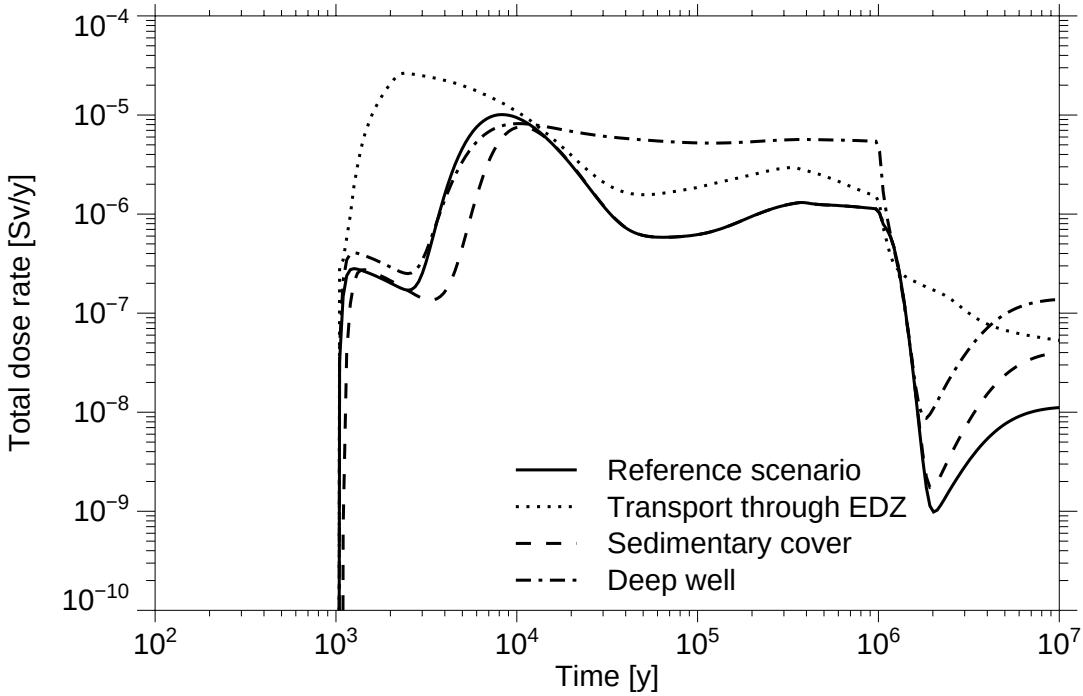

Fig. 11.2: Total dose rates for the reference scenario and alternative scenarios.

12 Results and conclusions

12.1 Comparison with other IPAs for crystalline formations

This chapter focuses on the studies performed for repositories for spent fuel in granite formations in the SPA project and on a comparison with the Swiss study Kristallin I for a repository with vitrified high level waste.

12.1.1 Safety analyses by SPA participants

Within the SPA project repositories in granite formations have been considered by ENRESA, GRS, IPSN and VTT. Each organisation has considered its own geological formation, disposal site, repository design, waste volume and applied its own modelling tools. However, the general approach and the assessment method were largely common.

The results of the deterministic calculation for the reference case from the different participants are given in Figure 12.1. In all cases the common source term model (s. chapter 7.2.2) was used and the normal evolution of the repository system is considered. For all the exercises a release into a well is assumed, which in general gives higher dose rates as the release into a river.

Differences in the results especially reflect differences in the assumptions for the container and for the modelling of the retention and dilution in the geosphere. In the Finnish analyses only one copper-iron container is assumed to fail and disappear after ten thousand years, whereas all other participants assume failure of all containers after thousand years. In the French and Spanish analyses the average groundwater travel times are assumed to be about some ten thousand years. In the Finnish and German analyses the groundwater travel times are assumed to be only some ten of years. This results in much earlier radiation exposure in the biosphere compared to the results from ENRESA and IPSN. The GRS assumption, that 25% of the containers are connected to fast pathways in the granite is conservative and has to be refined in future investigations of the geological structure and hydrogeological conditions in German granite formations.

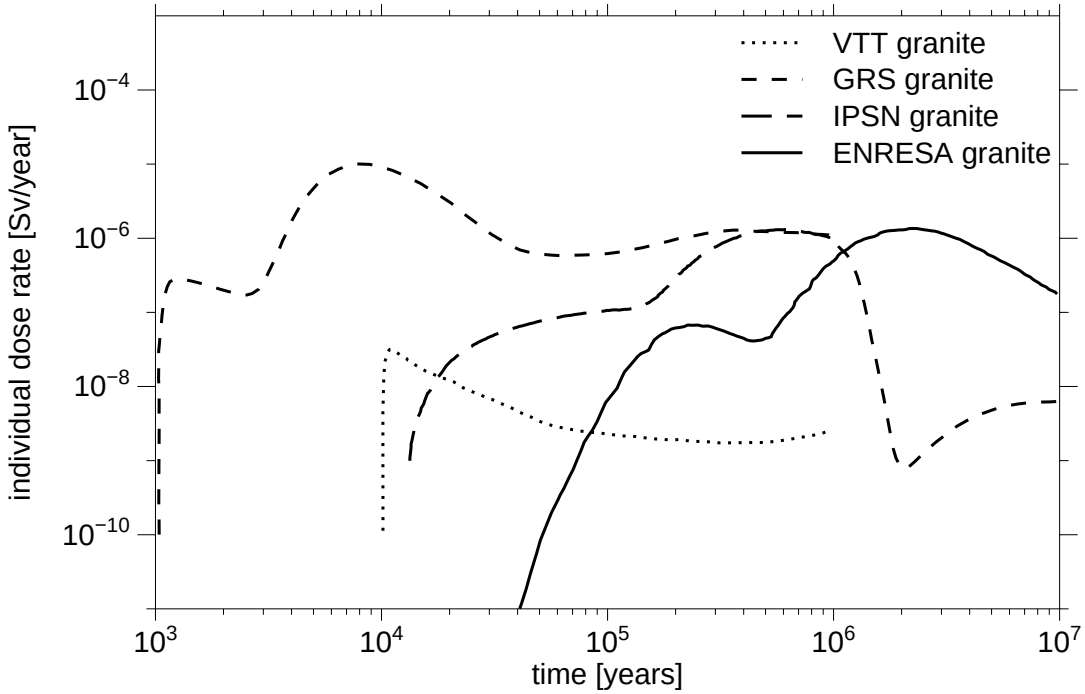

Fig. 12.1: Dose rates from deterministic calculations of four participants in SPA project

Furthermore the nuclide C-14 dominates the dose rate in the German case. This is due to a travel time which is in the same order of magnitude as the half life of the nuclide. For ENRESA and IPSN C-14 play only a minor role since the travel time is much longer and a significant amount of the nuclide is decayed. In case of longer groundwater travel times in the geosphere the C-14 peak observed by GRS would be significantly reduced.

Looking at the importance of radionuclides, I-129 turned out as very important if not the most important contributor to the radiological impact in all performance assessments, independent from the formation. This is due to its unique properties which are highly soluble, weakly sorbed added to its long half-life. Other fission and activation products can also play a dominant role but their level of importance varies from one participant to another. Besides C-14 this is the case for Cl-36, Se-79, Sn-126 and Cs-135. The relevance of actinides compared to fission and activation products is different for the participants. In the French and Spanish analyses the actinides cause a higher dose rate whereas in

the German calculation the activation and fission products are found to dominate the dose rate. This effect could be explained mainly by the lower solubility limits considered by GRS for uranium and neptunium.

Biosphere assumptions can also influence the dose rates of nuclides significantly. Biosphere conversion factors can vary by orders of magnitude, which is obvious for different model assumptions, e.g. if drinking water is considered as the only exposition pathway, as in the Finnish study [41] compared to a model where additionally irrigation, cattle feed and fish ponds are considered, as in the German study [1]. Due to this, C-14 plays a more important role in the German than in the Finnish case. However, besides these assumptions the amount of dilution of the contaminated water is a very important biosphere parameter.

The calculated dose rates are in all cases well below the national regulatory limits. The results for the SPA project do not differ so much from the PAGIS results [38], i.e. the much higher inventory of actinides in the spent-fuel compared to the vitrified waste does not lead to higher doses. This is due to the solubility limits of the actinides which in both cases control the release from the near field.

12.1.2 KRISTALLIN-I study

In this section, the KRISTALLIN-I safety assessment of a repository for vitrified high-level radioactive waste is compared with the results of GRS safety analysis for a spent fuel repository. Both integrated performance assessments are based on similar approaches and models. Additionally, because of the similarity between the geological situation in the Northern Switzerland and the granitic sites of Germany such as the Black Forest, many of the data for the near-field and far-field models used in GRS IPA are taken from the KRISTALLIN-I study. This situation allows a good comparison to be made between the results of the two different safety analyses.

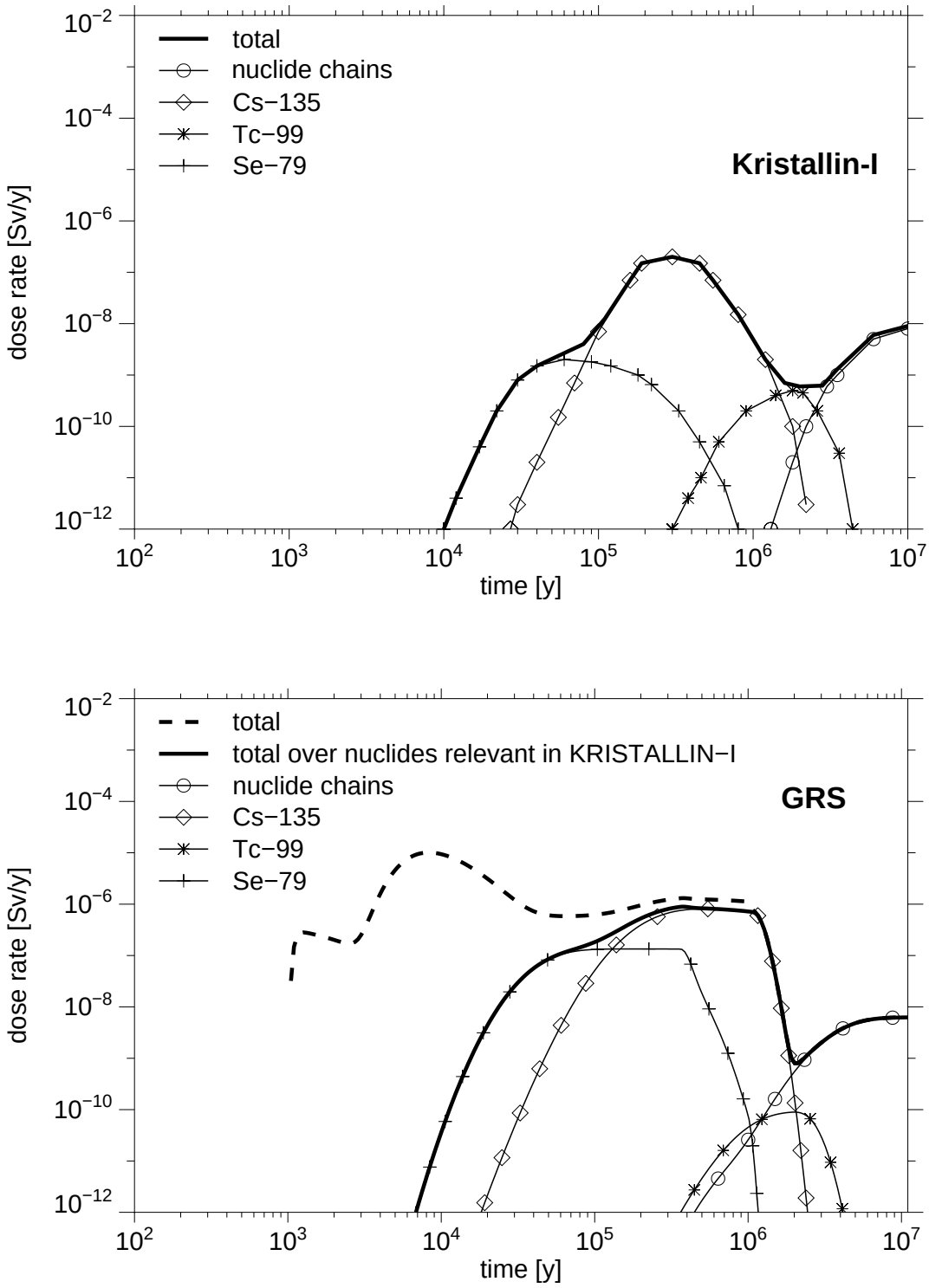

Fig. 12.2: Comparison between the results for the KRISTALLIN-I reference case (top) and GRS reference scenario (bottom). For the total dose rate over nuclides relevant in KRISTALLIN-I the dose rates from C-14, Cl-36 and I-129 are neglected.

In Figure 12.2 the dose rates for the corresponding reference case calculations are presented. The main difference between both studies results from the different types of waste regarded: vitrified HLW in case of Kristallin-I and spent fuel in case of GRS. Therefore, C-14 and I-129 inventories orders of magnitude lower compared to that of the GRS study are considered in Kristallin-I. Additionally no Cl-36 inventory is considered in Kristallin-I. Those three nuclides are the main contributors to the early dose rate peaks in the GRS study, which do not occur in Kristallin-I. Looking at the relevant nuclides of the Swiss study the dose rate curves show a similar behaviour and the maximum dose rates are within one or two orders of magnitude. Further differences between the reference case calculations of the Swiss and German study are the following:

- the higher radionuclide inventory assumed in the hypothetical repository presented in the German study,

- the lower thickness of the bentonite barrier in the German case proposed within the national GEISHA Project,

- the difference of some dose conversion factors used in the biosphere modelling, e.g. the 8 - 10 times higher values for Cs-135 and Se-79 used in the German study and the 10 times higher value for Tc-99 used in the NAGRA study.

12.2 Conclusions and outlook

Within the SPA-Project GRS has performed an integrated performance assessment for a repository in a crystalline formation for the first time. Accordingly the main areas of work carried out in the project can be divided into two different classes:

- development and adaption of models and numerical tools
- performance of calculations and evaluation of the results.

The capability to perform a first IPA for a repository in crystalline formations has been realised in the following steps:

- review of literature concerning long-term safety analyses for repositories in granitic host rock
- working out of conceptual models
- adaption and development of numerical models
- compilation of necessary data
- verification and intercomparison of computer codes for near-field and far-field calculations
- integration of near-field code GRAPOS, far-field code CHETMAD and biosphere model EXCON within the IPA package EMOS using its graphical interfaces and Monte-Carlo frame for stochastical calculations.

Within the SPA-Project GRS has performed deterministic calculations only. The results of the calculations demonstrate the safety of the repository system of the assumed design, the engineered barriers and the geological situation. The total dose rates are dominated by the activation and fission products C-14, Cl-36, I-129, Se-79 and Cs-135 whereas the actinides and their daughter products are strongly retarded by the multi-barrier system. Besides calculations for the reference scenario the following work was carried out with the SPA-Project:

- comparison of conceptual model, on which IPAs for repositories in granitic host rock are based
- estimation and evaluation of barrier efficiency for the different components of the repository system by a local sensitivity analysis

As a consequence of the work done within the SPA-Project a first identification of processes and properties concerning the engineered and geological barriers which are relevant for performance assessment has been made. The results from sensitivity analyses indicate that repository layout and/or location of the repository as well as the bentonite buffer are important features of the system. The transport pathways in the far-field represent almost no barrier for weakly sorbed nuclides like C-14. However less conservative assumptions for the hydrogeological parameters of the granite could reduce the dose rate of the most important radionuclide C-14 significantly. Objectives for further investigations should be the long-term stability and optimization of engineered barriers and a more detailed description of the structure of the fractures in the geosphere.

Furthermore the codes for long term safety assessment will be further developed. A model which describes the influence of colloids on the nuclide transport will be integrated in the far-field code CHETMAD. It is well known that diffusion of nuclides into the rock matrix decreases with increasing distance from the fracture. Hence, this process should be included.

In the CEC-funded project “Bentonite Barriers in Integrated Performance Assessment” (BENIPA) the state of the art in the treatment of near-field processes in performance assessments will be evaluated. According to the outcome of this project, additional processes like the saturation of the bentonite have to be included into the near-field model GRAPOS.

13 References

[1] Allgemeine Verwaltungsvorschrift zu §45 Strahlenschutzverordnung: Ermittlung der Strahlenexposition durch die Ableitung radioaktiver Stoffe aus kerntechnischen Anlagen oder Einrichtungen (21. Februar 1990). Erschienen im Bundesanzeiger, 42. Jg., Nummer 64a (1990).

[2] Andrews, R. W., LaFleur, D. W., Pahwa, S. B.: Resaturation of backfilled tunnels in granite: NTB 86-27, NAGRA, Baden, 1986.

[3] Andersson, K.: Chemical and Physical Transport Parameters for SITE-94. SKI Report 96:2, February 1996.

[4] Baudoin P., Gay, D., Certes, C., Serres, C., Alonso, J., Lührmann, L., Martens, K.H., Dodd, D., Marivout, J., Vieno, T.: Spent Fuel Disposal Performance Assessment- SPA Project. Final Report. EC-contract Nr. FI4W-CT96-0018, Brussels 1999, to be published.

[5] Bechthold, W., Braun, W., Brückner, C.,Closs, K. D., Knapp, U., Papp, R.: Systemanalyse Mischkonzept, Abschlußbericht Hauptband. Kernforschungszentrum Karlsruhe. KWA 2190 A1. Dezember 1989.

[6] Bekanntmachung der Tabelle IV 1: Freigrenzen und abgeleitete Grenzwerte der Jahres-Aktivitätszufuhr für Inhalation und Ingestion einzelner Radionuklide; Bekanntmachung der Dosisfaktoren. Bundesanzeiger, Jahrgang 41, Nummer 185a, Bundesminister der Justiz, Bonn. 30. September 1989

[7] Berner, U.: Kristallin-I: Estimates of Solubility Limits for Safety Relevant Radionuclides. PSI-Report Nr. 95-07. Würrenlingen and Villigen 1995.

[8] Bräuer, V., Reh, M., Schulz, P., Schuster, P., Sprado, K.-H.: Endlagerung stark wärmeentwickelnder radioaktiver Abfälle in tiefen geologischen Formationen. Untersuchung und Bewertung von Regionen in nichtsalinaren Formationen. TGB. Nr. 12437/91, Hannover, November 1994.

[9] Buhmann, D., Nies, A., Storck, R.: Analyse der Langzeitsicherheit von Endlagerkonzepten für wärmeerzeugende radioaktive Abfälle. GSF-Bericht 27/91. GSF - Forschungszentrum für Umwelt und Gesundheit GmbH, Braunschweig 1991.

[10] Closs, K. D., Engelmann, H. J., Fürst, W., Loser, H., Mehling, O., Motoi, V., Papp, R.: Systemstudie Andere Entsorgungstechniken. Hauptband. KWA 2190/1, Kernforschungszentrum Karlsruhe, Dezember 1984.

[11] Curti, E.: Modelling bentonite pore waters for the Swiss high level waste repository. PSI-report 93-05. Würrenlingen and Villigen 1993.

[12] Freeze, R. A., Cherry, J. A.: Groundwater. Prentice-Hall, Inc., 1979.

[13] First annual report (01.05.1996 - 01.05.1997). Project Spent Fuel Performance Assessment (SPA), 1997.

[14] Grambow, B., Loida, A., Dressier, P., Geckeis, H., Gago, J., Casas, I., de Pablo, J., Gimenez, J., Torrero, M. E.: Chemical reaction of fabricated and high burn-up spent UO2 fuel with saline brines. EUR 17111 EN, Final Report 1997.

[15] Hadermann, J., Rösel, F.: Radionuclide chain transport in inhomogeneous crystalline rocks - Limited matrix diffusion and effective surface sorption. NTB 85-40, NAGRA, Baden, February 1985.

[16] Hirsekorn, R.-P., Nies, A., Rausch, H., Storck R.: Performance Assessment of Confinements for Medium-Level and Alpha-Contaminated Waste (PACOMA): Rock Salt Option. EUR 13634 EN, GSF-Bericht 12/91. Kommission der Europäischen Gemeinschaften, GSF - Forschungszentrum für Umwelt und Gesundheit GmbH, Brüssel-Luxemburg 1991.

[17] International Commission on Radiological Protection: Limits for intakes of radionuclides by workers. ICRP 30. Pergamon Press. Oxford, 1979.

[18] International Commission on Radiological Protection: The metabolism of plutonium and related elements. ICRP 48. Pergamon Press. Oxford, 1986.

[19] INTRACOIN International Nuclide Transport code Intercomparison Study Final Report Levels 2 and 3, SKI 86:2. Swedish Nuclear Power Inspectorate, Stockholm, Sweden, May 1986.

[20] Jakob, A., Hadermann, J., Rösel, F.: Radionuclide chain transport with matrix diffusion and non-linear sorption. NTB 90-13, NAGRA, Baden, February 1990.

[21] Kahr, G., Kraehenbuehl, f., Mueller-Vonmoos, M. Stoeckli, H. F.: Wasseraufnahme und Wasserbewegung in hochverdichtetem Bentonit. NTB 86-14, NAGRA, Baden, 1996.

[22] Kerntechnik, Anlagen in Deutschland. Deutsches Atomforum e. V. (ed.), Inforum Verlag. Bonn 1997.

[23] Kernthemen: Entsorgung der Kernkraftwerke. Deutsches Atomforum e. V. (ed.), Inforum Verlag. Bonn 1997.

[24] Kühle, T., Zude, F., Lührmann, L.: Das eindimensionale Transportprogramm CHET1 unter Berücksichtigung der Sorption nach dem K_d-Konzept. Gesellschaft für Anlagen- und Reaktorsicherheit (GRS) mbH, GRS-124, Braunschweig 1996.

[25] NAGRA: Endlager für hochaktive Abfälle: Das System der Sicherheitsbarrieren. Projektbericht NGB 85-04, Projekt Gewähr 1985, Wettingen, Januar 1985

[26] NAGRA: Geology and hydrogeology of the crystalline basement of northern Switzerland. NAGRA Technical Report NTB 93-01, Wettingen, May 1994.

[27] NAGRA: Kristallin-I. Safety Assessment Report. NAGRA Technical Report NTB 93-22, Wettingen, July 1994.

[28] Papp, R.: GEISHA: Gegenüberstellung von Endlagerkonzepten in Salz und Hartgestein. FZKA-PTE Nr. 3, Forschungszentrum Karlsruhe GmbH, Karlsruhe 1997.

[29] Pröhl, G., Baier, M.: Dosiskonversionsfaktoren zur Berechnung der Strahlenexposition in der Nachbetriebsphase von Endlagern nach den Allgemeinen Verwaltungsvorschriften zu §45 StrlSchV in Anlehnung an die Vorgehensweise im Rahmen des Planfeststellungsverfahrens des geplanten Endlagers Konrad. Bericht GSF, Januar 1998.

[30] Pröhl, G., Baier, M.: Ingestion factors and dose factors for external radiation exposition by soil radiation. Excel file, Status 06/1998.

[31] Rüegger, B.: NEA's sorption data base (SDB), version 2.0. OECD/NEA, Paris 1989.

[32] Smith, P. A., Gautschi, A., Vomvoris, S., Zuidema, P., Mazurek, M.: The development of a safety assessment model of the geosphere for a repository sited in the crystalline basement of northern Switzerland. J. Cont. Hydrol., 26, 1997 (309-324).

[33] Statens Kärnkraftinspektion: SKI Project-90. Volume I. SKI-TR 91:23, August 1991.

[34] Statens Kärnkraftinspektion: SKI Project-90. Volume II. SKI-TR 91:23, August 1991.

[35] Statens Kärnkraftinspektion: SKI Site-94, Deep Repository Performance Assessment Project, Volume II. SKI TR 91:23, Stockholm, December 1996.

[36] Stenhouse, M. J.: Sorption Database for Crystalline, Marl and Bentonite for Performance Assessment. NAGRA Technical Report NTB 93-06, Wettingen July 1995.

[37] Storck, R., Hossain, S., Podtschaske, T., Rimkus, D., Stelte, N., Weber, P.: Einzeluntersuchungen zur Radionuklidfreisetzung aus einem Modellsalzstock. In: Projekt Sicherheitsstudien Entsorgung (PSE), Abschlußbericht: Fachband 15. Hahn-Meitner Institut, Berlin 1985.

[38] Storck, R., Aschenbach, J., Hirsekorn, R.P., Nies, A., Stelte, N.: Performance Assessment of Geological Isolation Systems for Radioactive Waste (PAGIS): Disposal in Salt Formations. EUR 11 778 EN, GSF-Bericht 23/88. Commission of the European Communities, Gesellschaft für Strahlen- und Umweltforschung mbH München, Brussels-Luxembourg 1988.

[39] Storck, R., Buhmann, D., Hirsekorn, R.-P., Kühle, T., Lührmann, L.: Das Programmpaket EMOS zur Analyse der Langzeitsicherheit eines Endlagers für radioaktive Abfälle. Version 5. Gesellschaft für Anlagen- und Reaktorsicherheit (GRS) mbH, GRS-122, Braunschweig 1996.

[40] Vieno, T., Nordman, H.: Interim Report on Safety Assessment of Spent Fuel Disposal TILA-96. Posiva-96-17, Helsinki, December 1996.

[41] Vieno, T: WELL-97 - A stylized well scenario for indicative dose assessment of deep repositories. Espoo, VTT Energy, Technical Report SPAVTT-2/97, 1997.

[42] Wiese, D.: CORIGEN-Abbrandrechnungen. KfK 1985 und FZK 1997.

Appendix

A Near-field code intercomparison between RIP and GRAPOS

Contribution for the EU-project “Spent fuel Performance Assessment (SPA)” from
Gesellschaft für Anlagen- und Reaktorsicherheit (GRS) mbH
ENRESA

A1.1 Introduction and objectives

Within the SPA-project, ENRESA and GRS perform integrated performance assessments for repositories in granite. This includes the modelling of radionuclide mobilisation from the waste packages and transport through the bentonite barrier.

In the ENRESA and GRS approaches, the following processes are taken into consideration:

- canister failure
- radioactive decay and ingrowth in waste, canister, and bentonite
- release from the waste form
- element-specific dissolution and precipitation
- sorption onto the bentonite
- diffusion through the bentonite buffer
- transport of radionuclides from the bentonite buffer into the groundwater system.

The radionuclide transport model for the near-field is based on a one-dimensional transport equation using cylindrical coordinates. Advection through the bentonite backfill is in general assumed to be negligible, as its permeability is more than 10^2 times smaller than that of granite, and has not been considered in this comparison exercise. The interface for the mass transport between the bentonite buffer and the far-field is assumed to be the advection through the excavation-disturbed zone (EDZ).

The near-field model is performed by ENRESA with the code RIP, and by GRS with the code GRAPOS, respectively. For verification of the numerical models a code intercomparison has been performed. In this paper we report the intercomparison exercise and its results.

The conceptual model on which the near-field codes are based is described in chapter 2. In this chapter, also some information about the numerical methods will be given. In the next chapter, the applied near-field model assumptions and data used for the different test cases are defined. The presentation and discussion of the results of the calculations finalise this code intercomparison exercise.

A1.2 Model and code description

A1.2.1 Model description

The near-field models developed by ENRESA and GRS are very similar as they consider the same processes. The models include processes like radionuclide dissolution from the waste, diffusion of dissolved radionuclides through bentonite, sorption onto bentonite minerals, radioactive decay and dissolution and precipitation reactions in the bentonite.

A1.2.1.1 Geometry

The geometry of the near-field is shown in Figure 1.1. The cylindrical canisters (0.9 m diameter and 4.54 m length) are emplaced in horizontal galleries, inside a continuous liner of carbon steel with 0.95 m external diameter. The distance between the centres of two neighbouring canisters is 5.54 m (canisters are separated by 1 m of bentonite).

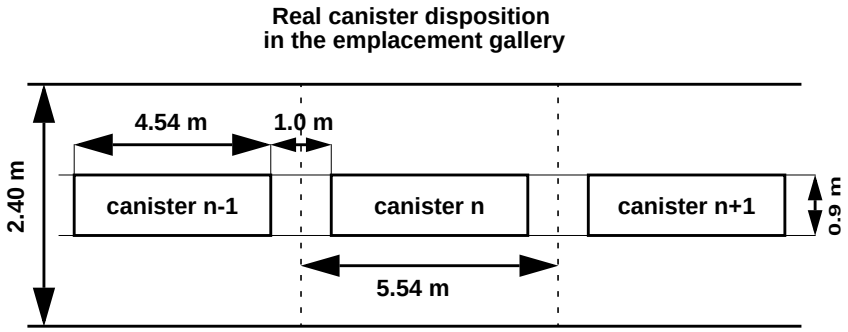

Fig. A1.1: Canister disposition in the emplacement galleries

For the transport calculations we have used cylindrical coordinates. If the z-axis coincides with the gallery axis, the concentrations will be independent of the azimuth. The transport can be considered as one-dimensional.

For the purpose of near-field modelling the geometrical model shown in Figure 1.2 has been used. Each canister is greater (*equivalent length*) than the real one (5.54 m instead of 4.54 m) to compensate for the 1D approach. Canisters are arranged end-to-end, forming an equivalent canister of infinite length. By doing so, the area available for the transport of radionuclides is conservatively increased.

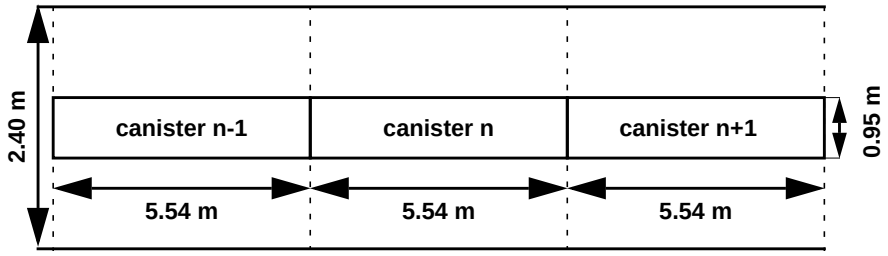

Fig. A1.2: Model used in the calculations of the near-field transport

A1.2.1.2 Radionuclide release

As seen from the aspect of release mechanisms, the activity content of a fuel assembly can be divided into six groups. The major part of the activity is bound to the UO_2 **fuel matrix**. Some of the noble gases and other volatile elements have migrated to the **grain**

boundaries of the fuel matrix and into the **gap** between the fuel pellets and the cladding tube. The zircaloy **cladding** of the fuel rod and the **structural parts** of the fuel assembly contain some activation products. On the surfaces of the fuel assembly a thin layer of **corrosion products** ("crud") exists that contains activation products. The radionuclides in each of these groups are released at different rates. For the intercomparison, only two groups - the fuel matrix and an instant release fraction (gap) - are assumed.

After canister failure the interior of the canister becomes water-saturated, and the radionuclides are mobilised. In the model, a hypothetical "volume of dissolution" V_{dis} [L^3] is assumed into which radionuclides are released from the waste forms. The inventory M^i [M] of the i-th radionuclide with decay constant λ^i [1/T], mobilised in the volume of water surrounding the waste, is calculated using the following equation:

$$\begin{aligned} \frac{\partial}{\partial t} M^i(t) \;=\; & -\lambda^i M^i \;+\; \sum_j \lambda^j k_{ij} \frac{A_i}{A_j} M^j \\ & + S^i(t) \;-\; 2\pi r_{in} h D_b \varepsilon_b \frac{\partial}{\partial r} C^i(t) \Big|_{r \,=\, r_{in}}, \end{aligned} \qquad (46)$$

where r [L] is the radial distance, r_{in} [L] denotes the initial radius of the bentonite, D_b [L^2/T] the pore diffusion coefficient, ε_b the bentonite porosity and h [L] the *equivalent length* corresponding to one canister (see Figure 1.2). The index j denotes the parent nuclides of the i-th radionuclide; k_{ij} is the fraction of the radionuclide j that will produce radionuclide i, A_i and A_j (g/mol) are respectively the mass numbers of radionuclides i and j. The term $S^i(t)$ [M/T] determines the release from the different components of the waste.

A1.2.1.3 Precipitation and dissolution

The radionuclide concentration in the water surrounding the waste forms is

$$C^i(t)\Big|_{r \,=\, r_m} \;=\; \min\left(\frac{M^i}{V_{\text{dis}}},\; \frac{M^i}{M^e} C^e{}_{\max} \right), \qquad (47)$$

where

V_{dis} volume of water surrounding the waste [L^3]

M^i mass of radionuclide i in the "volume of dissolution" [M]

M^e mass of element e in the "volume of dissolution" [M]

C^e_{max} saturation concentration for element e [M/L^3]. Radionuclide i is an isotope of element e.

A1.2.1.4 Transport through the bentonite

The mobilised radionuclides are assumed to be transported through the bentonite only by diffusion because the hydraulic conductivity is extremely low (K = 10^{-14} - 10^{-13} m/s) and thus will restrict the groundwater flow. Nevertheless, the RIP program used by EN-RESA has the possibility to consider the radionuclide transport by diffusion and advection.

For the purpose of the transport calculation the geometrical model shown in Figure 1.2 has been used. Canisters are arranged end-to-end, forming an equivalent canister with infinite length. Under such conditions solute transport will occur only by one-dimensional radial diffusion from the canister to the granite, and concentrations will not be z dependent (gallery axis). Then the governing equation for the transport through the bentonite is given by

$$\varepsilon_b R^i \frac{\partial}{\partial t} C^i = De^i \left[\frac{1}{r} \frac{\partial}{\partial r} \left(r \frac{\partial C^i}{\partial r} \right) \right] - \lambda^i \varepsilon_b R^i C^i + \sum_j \lambda^i \varepsilon_b k_{ij} R^j \frac{A_i}{A_j} C^j \quad , \quad (48)$$

where:

C^i concentration of radionuclide i in the pore-water [M/L^3]

C^j concentration of radionuclide j (parent of i) in the pore water [M/L^3]

ε_b porosity of the buffer material [-]

R^i retardation coefficient of radionuclide i [-]

R^j retardation coefficient of radionuclide j [-]

λ^i decay constant of radionuclide i [T^{-1}]

λ^j decay constant of radionuclide j [T^{-1}]

k_{ij} fraction of the radionuclide j desintegrations that will produce radionuclide i

A_i mass number of radionuclide i (g/mol)

A_j mass number of radionuclide j (g/mol)

De^i effective diffusion coefficient of radionuclide i in the porous media [L^2/T] with

$$De^i = Dw^i \frac{\delta_b}{\tau^2} \varepsilon_b = D_b^i \varepsilon_b \ , \qquad (49)$$

where

Dw^i diffusion coefficient of radionuclide i in free water [L^2/T]

δ_b / τ^2 geometry factor.

The retardation coefficient R^i is described as follows:

$$R^i = 1 + \frac{1 - \varepsilon_b}{\varepsilon_b} \rho_b K_d \ , \qquad (50)$$

with the density of the bentonite ρ_b [M/L^3] and the element-specific distribution coefficient K_d [L^3/M].

A1.2.1.5 Radioactive decay

Evaluation of all the stages above is made by taking into account both the decay chains and the radioactive decay (or ingrowth) in the near-field, and allows prediction of the release of any radionuclide into the far-field to be assessed as a function of time.

A1.2.1.6 Bentonite-host rock interface

At the outer boundary a “mixing tank” condition is applied in which the concentration gradient is set such that the diffusive flux across the boundary is equal to the advective transport rate from the excavation-disturbed zone into the geosphere. Accordingly, the outer boundary condition is given by

$$2\pi r_{\text{out}} h D_b \varepsilon_b \frac{\partial}{\partial r} C^i(t)\Big|_{r = r_{\text{out}}} = q_{\text{EDZ}} C_{\text{EDZ}} \ , \qquad (51)$$

where h [L] is the “equivalent length” of one canister, q_{EDZ} [L^3/T] the groundwater flow through the excavation-disturbed zone, and C_{EDZ} [M/L^3] the concentration in the EDZ.

A1.2.2 Code description

The former models are implemented in computer codes. In this way, the test cases have been performed by ENRESA with the computer code RIP, and by GRS with the computer code GRAPOS, respectively.

A1.2.2.1 RIP

Within RIP, the bentonite buffer is divided into an *arbitrary* number of cells (or layers) as illustrated in Figure 1.3. As can be seen from the figure, in this particular case, the boundaries of the cells are actually concentric cylinders.

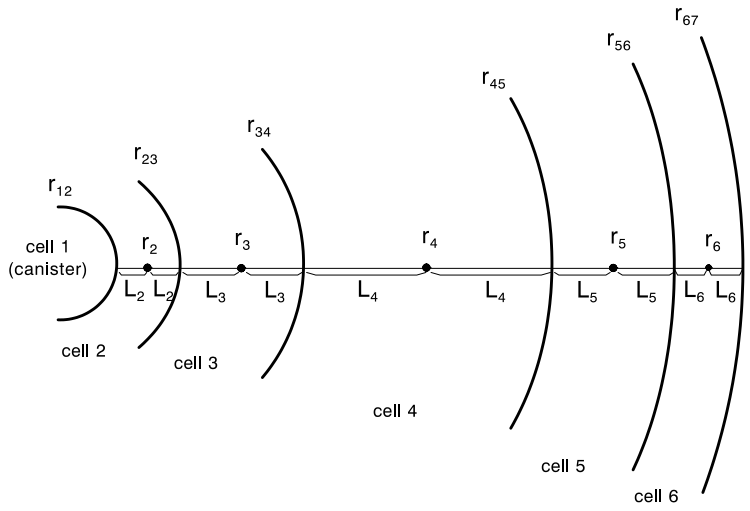

Fig. A1.3: Schematic representation of the cells in the near-field

The basic mass balance equation for radionuclide i in cell **n** is:

$$\frac{dm_{in}}{dt} = S_{in} - m_{in}\lambda_i + m_{jn}\lambda_i k_{ij}\frac{A_i}{A_j} + \sum_{c=1}^{NCn} f_{cin} \quad , \qquad (52)$$

where

m_{in} mass of species i in cell n [M]

S_{in} rate of direct input of species i to cell n from a waste package [M/T]

λ_i decay rate for species i [1/T]

λ_j decay rate for species j [1/T]

m_{jn} mass of species j (parent of radionuclide i) in cell n [M]

k_{ij} stoichiometric ratio of mass of species i produced per mass of species j decayed

A_i mass number of radionuclide i (g/mol)

A_j mass number of radionuclide j (g/mol)

NCn number of mass transfer connections to cell n

f_{cin} influx rate of species i into cell n through connection c [M/T].

The first term in the equation represents the rate of direct input from waste packages to the cell; the second term represents the radioactive decay; the third term represents ingrowth; and the fourth term represents mass transfer into or out of the cell. The system of equations described above is coupled in two ways:

- by ingrowth terms
- by mass-transfer terms.

Within RIP this system of equations is solved using a fully implicit (backward difference) finite approximation.

The rate of input from waste packages (S_{in}) is non-zero only for cell 1 (see Figure 1.3) the cell which actually represents the canister. It is computed by the RIP waste package component model as a function of canister failure-time and alteration and dissolution rate. Decay rates and stoichiometric ratios are input parameters.

The mass transfer terms (f_{cin}) represent the mass flux associated with mass transfer connections. A mass transfer connection is defined by a pair of cells (or pathways), a medium in each cell (in this case water), and a connection type (advective or diffusive). Each cell is involved in at least one mass transfer connection.

The flux f_{cin} for diffusive mass transfer connections involving a single fluid, assuming no contribution from suspended particulate matter, is given as follows:

$$f_{\mathrm{cin}} = D_{ci}(-c_{in} + c_{im}) \ , \qquad (53)$$

where

D_{ci} diffusive conductance for species i in connection c [L^3/T]
c_{in} the dissolved concentration of species i within cell n for connection c [M/L^3]
c_{im} the dissolved concentration of species i within cell m for connection c [M/L^3].

The diffusive conductance terms for this system are computed as follows:

$$D_{ci} = \frac{S_c}{\frac{L_{cn}}{De_{in}} + \frac{L_{cm}}{De_{im}}} , \qquad (54)$$

where

S_c the area of diffusive connection c [L^2]
L_{cn} diffusive length for connection c in cell n [L]
L_{cm} diffusive length for connection c in cell m [L]
De_{in} effective diffusion coefficient for species i in cell n [L^2/T]
De_{im} effective diffusion coefficient for species i in cell m [L^2/T].

The diffusive lengths and areas are determined by the geometry of the cells. Appropriate definition of these geometric terms facilitates the representation of the cylindrical nature of the diffusive process.

The flux f_{cin} for advective mass-transfer connections involving a single fluid, assuming no contribution from suspended particulate matter, is as follows:

$f_{cin} = - c_{in}\, q_c$ if advection is from n to m
$f_{cim} = c_{im}\, q_c$ if advection is from m to n

where c_{in} and c_{im} are described above, and q_c is the rate of advection for connection c [L^3/T].

In this particular case (see Figure 1.3), the near-field has been divided into six cells of different thicknesses (smaller near the boundaries). Cell 1 is diffusively connected to cell 2; cell 2 is diffusively connected to cell 1 and cell 3 and so on. Note that cell 6 is diffusively connected to cell 5, but advectively connected with the EDZ.

A1.2.2.2 GRAPOS

Within GRAPOS, the model geometry is divided into N+1 different sections, as illustrated in Figure 1.4.

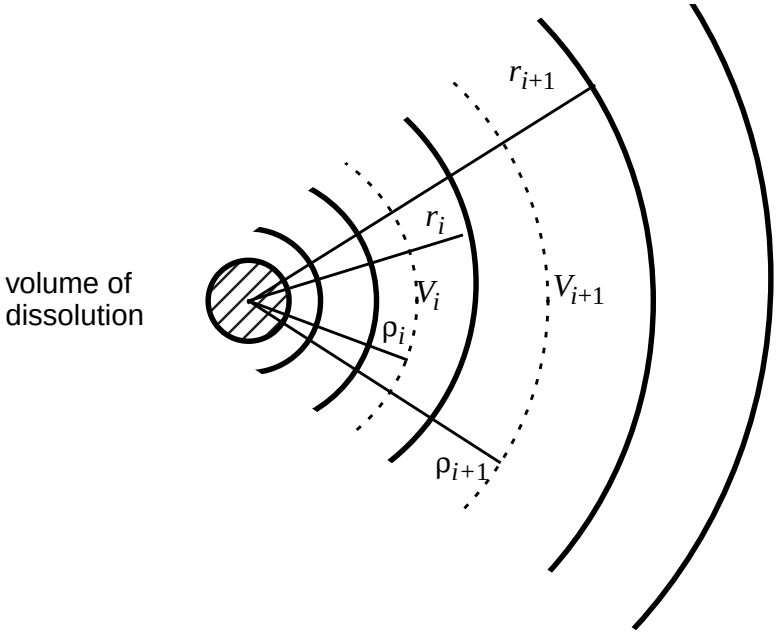

Fig. A1.4: Schematic representation of the discretization

The bentonite buffer and the EDZ are discretized by N tori V_i (i = 2,..,N+1) with inner radius r_{i-1} and outer radius r_i. The radii r_i are given by

$$r_i = r_{i-1}\left(\frac{r_N}{r_0}\right)^{1/N} \qquad (55)$$

which results in logarithmically increasing widths of the tori. The “volume of dissolution” is represented by V_0. For each element V_i an inner node ρ_i is defined for which the concentration c_i is calculated. The nodes ρ_i are located inside the cell V_i accordingly:

$$\rho_i = r_i \frac{\ln(A)}{1 - A}, \qquad A = \left(\frac{r_N}{r_0}\right)^{1/N} . \tag{56}$$

The diffusive fluxes across the boundaries of an inner torus V_i is approximated by the following Finite Difference scheme:

$$De^i r \frac{\partial}{\partial r}\left(r \frac{\partial C}{\partial r}\right) = De^i \frac{1}{\rho_i (r_i - r_{i-1})} \cdot \left(r_i \frac{c_{i+1} - c_i}{\rho_{i+1} - \rho_i} - r_{i-1} \frac{c_i - c_{i-1}}{\rho_i - \rho_{i-1}}\right) . \tag{57}$$

The release rates from the waste packages S_{in} represents the source term for cell V_0. The concentration C_R at the boundary r_0 of cell V_0 is determined by the source term from the waste packages, but limited by the element-specific solubilities. For calculation of the diffusive flux into the bentonite according to the above approximation an inner concentration C_0 for the ”volume of dissolution” is introduced where $C_0 = C_R - 2C_1$.

At the bentonite–EDZ interface the diffusive flux is assumed to be equal to the advective flux through the EDZ. This condition is approximatly fulfilled within the GRAPOS code according to

$$2\pi r_{\text{out}} h De^i \frac{c_{N+1} - c_N}{\rho_{N+1} - \rho_N} = q_{\text{EDZ}} c_{\text{EDZ}} , \tag{58}$$

where the concentration c_{EDZ} within the EDZ is given by $(c_N + c_{N+1})/2$.

For the time scheme a fully implicit difference approximation is used. Radioactive decay and ingrowth are calculated analytically.

A1.3 Case Specification

For the intercomparison of the RIP and GRAPOS codes different test cases have been performed, as defined in a common case specification for ENRESA and GRS

A1.3.1 Base Case (BC)

In the repository concept to be modelled, carbon steel canisters are emplaced horizontally in cylindrical receptacles constructed inside horizontal drifts 500 m long and 2.4 m in diameter. The canisters of 4.54 m length and 0.90 m diameter are separated by 1 m from each other and surrounded by precompacted bentonite blocks.

The following hypotheses have been considered:

- The canister disappears instantaneously at time 0 years.
- After failure, canister and cladding provide no physical resistance to water or solute transport.
- No corrosion products originate (neither sorption nor pressure effects are considered).
- Although canisters are 4.54 m in length, the transport model considers fictitious canisters of 5.54 m in length arranged end-to-end with respect to one another.
- No credit is given to advection through the bentonite.
- Transport in bentonite is represented as one-dimensional radial diffusion from canister to granite. This means that the concentrations are independent of the gallery axis.
- Advection of radionuclides occurs uniformly from the bentonite/disturbed-rock zone (EDZ) interface into the granitic formation.
- number of canisters: 1
- volume of water within the canister: 1 m^3
- pore diffusion coefficient: $2 \cdot 10^{-10}$ m^2/s
- bentonite porosity: 40%
- bentonite bulk density: 2667 kg/m^3
- flow per canister through the EDZ: 0.15 l/year

- constant fuel matrix alteration rate with total fuel matrix dissolution time of 10^4 years.

NUCLIDES:

The following six representative radionuclides have been selected for the analysis:

- I-129, a nuclide with unlimited solubility and no retardation in the bentonite
- Cs-135, a nuclide with unlimited solubility, which is retarded in the bentonite
- Se-79, a nuclide with limited solubility and low retardation in the bentonite
- Pu-239, U-235 to analyse the effect of decay chains
- U-236 in order to consider the coupling of the two uranium nuclides due to element-specific solubility limits.

Tabelle A.1: Nuclide-specific data

Radionuclide	Inventory [Bq/canister]	Half-life [y]
I-129	$2.582 \cdot 10^9$	$1.57 \cdot 10^7$
Se-79	$3.399 \cdot 10^{10}$	$6.50 \cdot 10^4$
Cs-135	$3.769 \cdot 10^{10}$	$3.00 \cdot 10^6$
U-236	$2.284 \cdot 10^{10}$	$2.34 \cdot 10^7$
Pu-239	$2.400 \cdot 10^{13}$	$2.41 \cdot 10^4$
U-235	$1.522 \cdot 10^9$	$7.04 \cdot 10^8$

Tabelle A1.2: Element-specific data

Elements	Instant release fraction [%]	Solubility limits [mol/l]	Sorption coefficients [m^3/kg]
I	10	unlimited	0.00
Se	5	10^{-6}	0.01
Cs	10	unlimited	0.10
Pu	0	10^{-8}	1.00
U	0	10^{-6}	1.00

OUTPUTS:

The outputs to be compared are the release rates from the bentonite at the following times: 10, 50, 100, 1000, 10^4, $5 \cdot 10^4$, 10^5, $5 \cdot 10^5$ and 10^6 years.

A1.3.2 Parameter variations

In addition to the base case, a set of parameter variations has been considered in order to show the influence of individual assumptions and effects. The data, which are not explicitly listed in the following table, are given according to the base case:

Tabelle A1.3: Definition of the parameter variations

Test cases	Description
BC_D5	(5 times increased diffusion coefficient) pore diffusion coefficient: $1 \cdot 10^{-9}$ m^2/s
BC_F10	(10 times increased flow through EDZ) flow per canister through the EDZ: 1.5 l/year
BC_MD100	(100 times increased matrix dissolution time) total fuel matrix dissolution time: 10^6 years
BC_GBB	(geometry of German bentonite barrier) bentonite inner diameter: 0.53 m bentonite outer diameter: 1.2 m length corresponding to one canister: 4.70 m volume of water within the canister: 0.3 m^3
BC_NS	(no solubility limits): unlimited solubility limits

A1.3.2.1 Code specification

A1.3.2.2 RIP

The RIP version 5.18 computer programme has been used by ENRESA to calculate radionuclide transport in the near-field. Although this is a probabilistic calculation programme, the input data for this comparison exercise are the constant values assigned to the parameters in 3.1.

For the calculations, the near-field has been divided into six cells of different thicknesses (as was done in the integrated performance assessment within the SPA Project). However, a higher discretization of the bentonite (with 10 and 15cells) has been done, in order to determine the sensitivity of the results.

The time-step is an important factor to be taken into account in performing the calculations. The shorter the time-step, the more accurate the results, but the more the time required to carry out the calculations. Consequently, this time-step must be selected such that the accuracy of the results is adequate and the calculation time is reasonable. In this exercise, three runs of RIP have been carried out for each case. The transport calculations were performed using time steps of 1 year for the first 100 years, 10 years for the modelling time up to one-hundred-thousand years, and 100 years for the calculations up to 1 million years.

A1.3.2.3 GRAPOS

The GRAPOS version 1.01 has been used by GRS to calculate the radionuclide transport in the near-field. The code GRAPOS is implemented as a near-field module within the integrated performance assessment code EMOS.

For the calculations, the bentonite buffer has been divided into 15 different parts. The time-steps are controlled automatically using a time step strategy which starts with small time-steps (0.1 year) and increases successively the time-steps after the mobilisation of the instant release fraction at 1‰ until a maximum time-step of 100 years is reached.

A1.4 Analysis of results

Radionuclide transport through the near-field was analysed using the models and data described above. For each instant *i* and each radionuclide *j* the release rate (Bq/y) from the bentonite into the geosphere is determined.

A1.4.1 Base Case

The time evolution of the radionuclide release rates from the bentonite for the base case is shown in Figure 1.5. In this figure the results from RIP (for a bentonite discretization into 5 cells) are represented by empty symbols at different points of time, while the results obtained with GRAPOS are represented by curves.

Table 1.4 summarise the maximum release rates at the bentonite-host rock interface for the considered radionuclides obtained with both codes.

If we evaluate the results we can conclude that:

- There is a good general agreement for all radionuclides for the entire time period. In particular, the maximum release rate and time of occurrence are very coincident.
- Some differences appear at early times. The values obtained with RIP are higher than the ones obtained with GRAPOS.

Two new calculations of the base case, using ten and fifteen cells in the bentonite buffer, respectively, have been performed with the RIP programme to check the influence of space discretization. The results for the finer discretization (15 cells) are presented in Figure 1.5 by solid symbols. The finer discretization of the bentonite gives a better agreement

between the results from RIP and the results from GRAPOS. Starting from this data, the variations of the base case have been performed considering that the bentonite buffer is divided in both codes into fifteen cells.

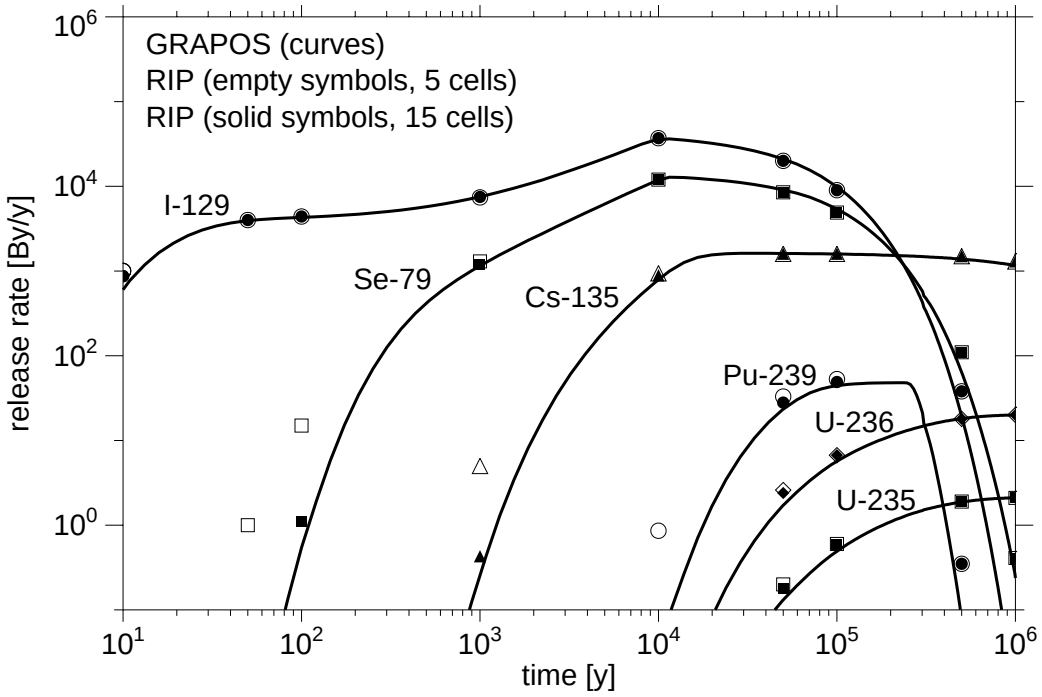

Fig. A1.5: Comparison between time evolution of release rates from the bentonite obtained with RIP (symbols) and GRAPOS (lines)

Table A1.4: Maximum release rates in Bq/y at the bentonite-host-rock interface

BC	I-129	Se-79	Cs-135	U-236	Pu-239	U-235
RIP	$3.8 \cdot 10^4$	$1.3 \cdot 10^4$	$1.6 \cdot 10^3$	$2.0 \cdot 10^1$	$5.7 \cdot 10^1$	$2.1 \cdot 10^0$
GRAPOS	$3.6 \cdot 10^4$	$1.3 \cdot 10^4$	$1.6 \cdot 10^3$	$2.0 \cdot 10^1$	$4.8 \cdot 10^1$	$2.1 \cdot 10^0$

Figure 1.5 shows the following migration behaviour of the nuclides:

- The differences between the release rates of the respective radionuclides depend on the different inventories, solubility limits, and sorption constants.
- An increase of the release rates after the time of matrix dissolution of 10^4 years is caused by sorption and precipitation.

- The arrival times of the first branch of the release rates from the bentonite depend on the K_d-value and are reduced for lower K_d-values.
- Iodine has unlimited solubility and is not sorbed in the bentonite. Therefore, the instant release fraction results in a peak of release rates almost immediately after canister failure. A steady state is never attained since the concentration at the source is not maintained.
- Selenium is slightly sorbed onto the bentonite. The rapid decline of the release rates after 10^4 years occurs because the supply of Se-79 remaining in the bentonite buffer and volume of dissolution has been depleted by radioactive decay.
- Compared with I-129, Cs-135 is also a long-lived nuclide and released by gap and matrix release processes but is more strongly sorbed than I-129. The peak of the release rate curve suffers some delay and reaches a steady-state value.
- The release rates of plutonium decrease drastically after several 10^5 years since the Pu inventory in the system is depleted because of radioactive decay.
- Uranium is strongly sorbed. This causes considerable delay in the attainment of a steady-state release level. Both isotopes have very long half-lives and are limited by their common solubility limits. Furthermore,
  - U-235 is not much affected by the decay of its parent as the contribution of the decay of Pu-239 to the maximum release rate value is less than 20%.
  - U-236 is the dominant uranium isotope.

A1.4.2 Case BC_D5

When the diffusion coefficient is increased by a factor of 5 ($D=10^{-9}$ m^2/s) both codes give similar results as in the base case. Table 1.5 presents the maximum release rates at the bentonite-host-rock interface for the considered radionuclides obtained with both codes. The time evolution of the radionuclide release rates from the bentonite is shown in Figure 1.6. The results with RIP are represented by symbols at different points of time, while the results obtained with GRAPOS are represented by curves.

It can be seen that there are only slight differences between the maximum release rates obtained with both codes. We found a maximum difference of 4% for the maximum release rates of iodine, cesium and plutonium.

Table A1.5: Maximum release rates in Bq/y at the bentonite-host-rock interface

BC_D5	I-129	Se-79	Cs-135	U-236	Pu-239	U-235
RIP	$3.8 \cdot 10^4$	$1.3 \cdot 10^4$	$1.7 \cdot 10^3$	$2.1 \cdot 10^1$	$3.2 \cdot 10^2$	$2.1 \cdot 10^0$
GRAPOS	$3.6 \cdot 10^4$	$1.3 \cdot 10^4$	$1.6 \cdot 10^3$	$2.1 \cdot 10^1$	$3.1 \cdot 10^2$	$2.1 \cdot 10^0$

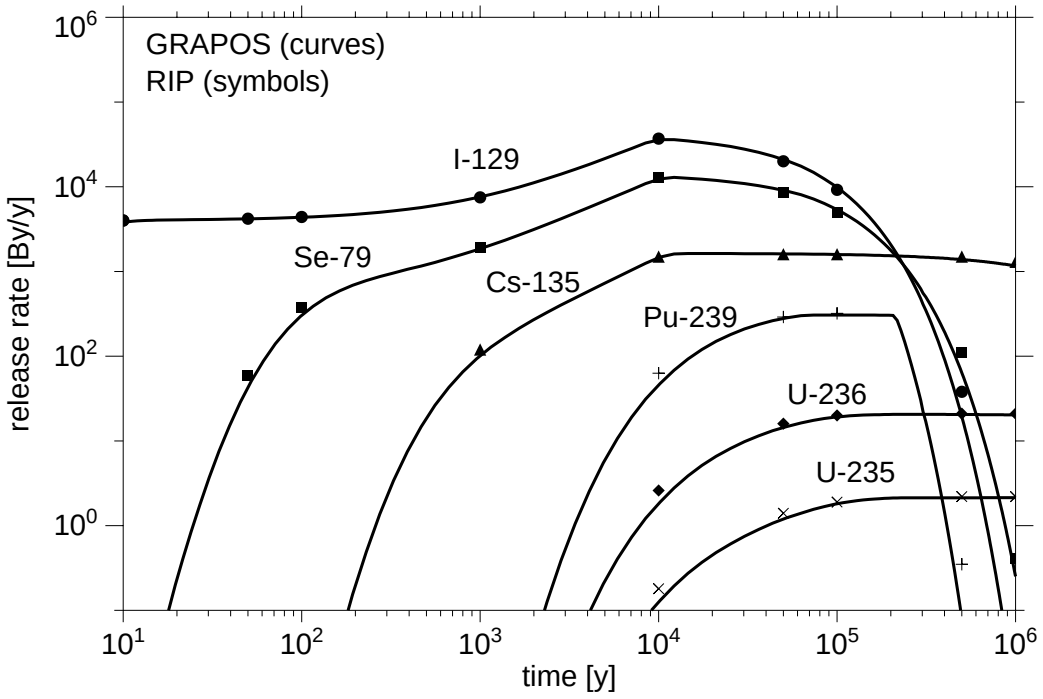

Fig. A1.6: Time evolution of release rates from the bentonite for case BC_D5

If we compare these results with those for the base case (BC) we can conclude that:

- The values of release rates are higher for times below 1000 years.
- The peak values for Se, Cs, and I are similar and occur at the same time (10^4 years).
- The peak value for the release rate of Pu-239 is one order of magnitude higher, but occurs at the same time.
- The maximum values for the uranium isotopes are identical, but appear earlier ($5 \cdot 10^5$ years instead of 10^6 years for the BC).

A1.4.3 Case BC_F10

If we increase the flow per canister through EDZ by a factor of 10 (q_{EDZ}=1.5 l/y) both codes give similar results. Table 1.6 presents the maximum release rates at the bentonite-host-rock interface for the considered radionuclides obtained with both codes. The time evolution of the radionuclide release rates from the bentonite is shown in Figure 1.7.

Table A1.6: Maximum release rates in Bq/y at the bentonite-host-rock interface

BC_F10	I-129	Se-79	Cs-135	U-236	Pu-239	U-235
RIP	$1.9 \cdot 10^5$	$1.3 \cdot 10^5$	$1.6 \cdot 10^4$	$2.0 \cdot 10^2$	$5.6 \cdot 10^2$	$2.1 \cdot 10^1$
GRAPOS	$1.9 \cdot 10^5$	$1.2 \cdot 10^5$	$1.6 \cdot 10^4$	$2.0 \cdot 10^2$	$4.8 \cdot 10^2$	$2.1 \cdot 10^1$

There are only slight differences between the maximum release rates obtained with both codes. These differences are similar to the BC (the maximum difference in the peak values for Plutonium is 14%).

.

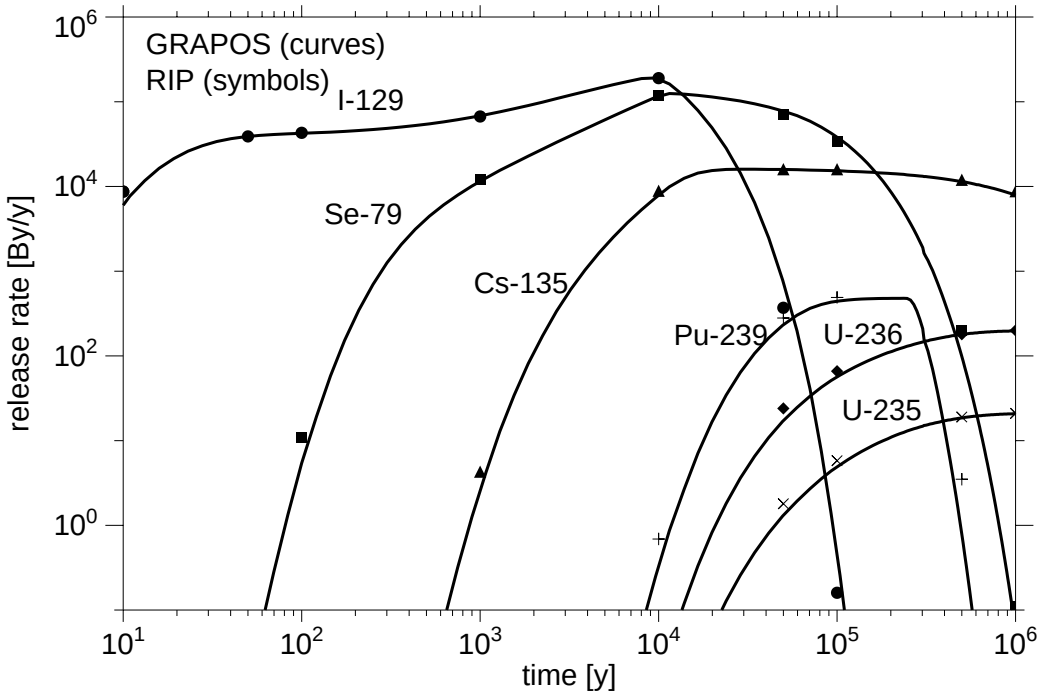

Fig. A1.7: Time evolution of release rates from the bentonite for case BC_F10

If we compare these results with those for the base case (BC) we can conclude that:

- There is an increase in the release rates. The release values are strongly influenced by the flow through the EDZ.
- The peak values appear at the same time as in the BC.
- The release rates from the bentonite for I-129 increase by a factor of 5.
- The release rates of the other radionuclides from the bentonite increase by a factor of 10.

A1.4.4 Case BC_MD100

In the same way as in the BC, an increase of the total fuel mass dissolution time by a factor of 100 gives similar results with both codes. Table 1.7 presents the maximum release rates at the bentonite-host-rock interface for the considered radionuclides. The time evolution of the radionuclide release rates from the bentonite is shown in Figure 1.8.

Table A1.7: Maximum release rates in Bq/y at the bentonite-host-rock interface

BC_MD100	I-129	Se-79	Cs-135	U-236	Pu-239	U-235
RIP	$4.1 \cdot 10^{3}$	$8.3 \cdot 10^{2}$	$1.3 \cdot 10^{3}$	$2.0 \cdot 10^{1}$	$5.7 \cdot 10^{1}$	$2.1 \cdot 10^{0}$
GRAPOS	$4.0 \cdot 10^{3}$	$8.6 \cdot 10^{2}$	$1.2 \cdot 10^{3}$	$2.0 \cdot 10^{1}$	$4.8 \cdot 10^{2}$	$2.1 \cdot 10^{0}$

There are small differences between the maximum release rates obtained with both codes. The maximum difference in the peak values for plutonium is 16%.

If we compare these results with those of the base case (BC) we can conclude that:

- There is a flat behaviour in the time evolution of the release rate at the bentonite-EDZ interface for I-129 and Se-79.
- The peak value for I-129 decreases by one order of magnitude and appears earlier.
- The peak value for Se-79 decreases by a factor of 15 and appears later than in the BC.

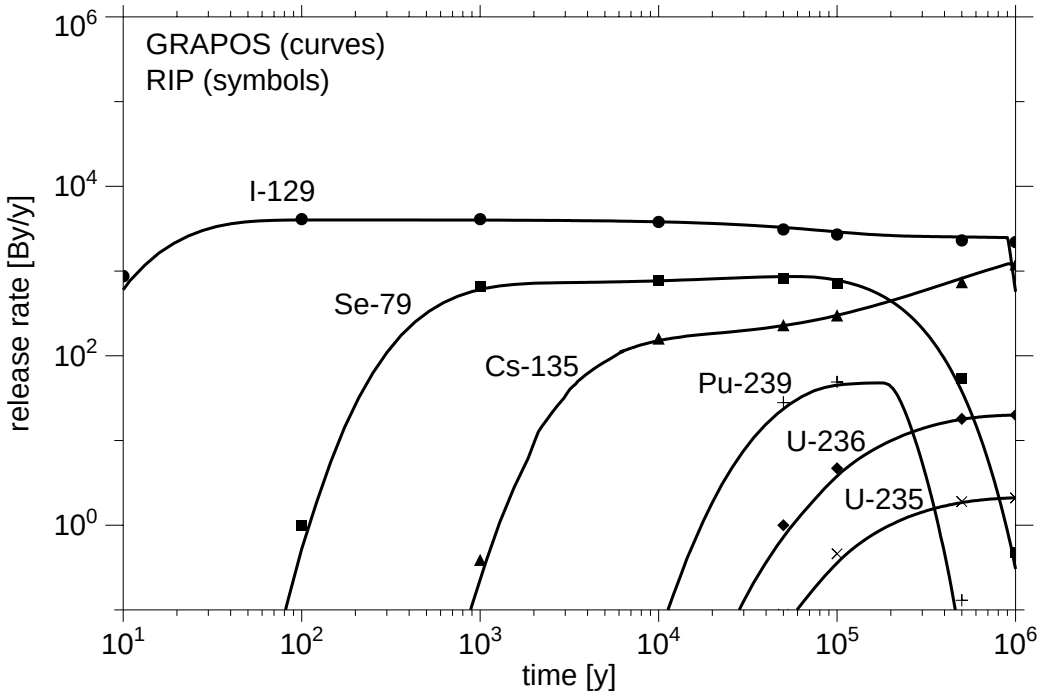

Fig. A1.8: Time evolution of release rates from the bentonite for case BC_MD100

- It seems that Cs-135 has not reached the peak value within 10^6 years but the value observed for this time is close to the peak value observed in the BC.
- There are differences in the behaviour neither of plutonium nor of uranium.

A1.4.5 Case BC_GBB

The consideration of a different geometry for the bentonite barrier gives similiar results with both codes. Table 1.8 presents the maximum release rates at the bentonite-host-rock interface for the considered radionuclides obtained with both codes. The time evolution of the radionuclide release rates from the bentonite is shown in Figure 1.9.

There are only differences for U-235 (4%) between the maximum release rates obtained from the two codes.

Table A1.8: Maximum release rates in Bq/y at the bentonite-host-rock interface

BC_GBB	I-129	Se-79	Cs-135	U-236	Pu-239	U-235
RIP	$1.3 \cdot 10^5$	$3.0 \cdot 10^4$	$8.2 \cdot 10^3$	$2.1 \cdot 10^1$	$3.2 \cdot 10^2$	$2.2 \cdot 10^0$
GRAPOS	$1.3 \cdot 10^5$	$3.0 \cdot 10^4$	$8.2 \cdot 10^3$	$2.1 \cdot 10^1$	$3.2 \cdot 10^2$	$2.1 \cdot 10^0$

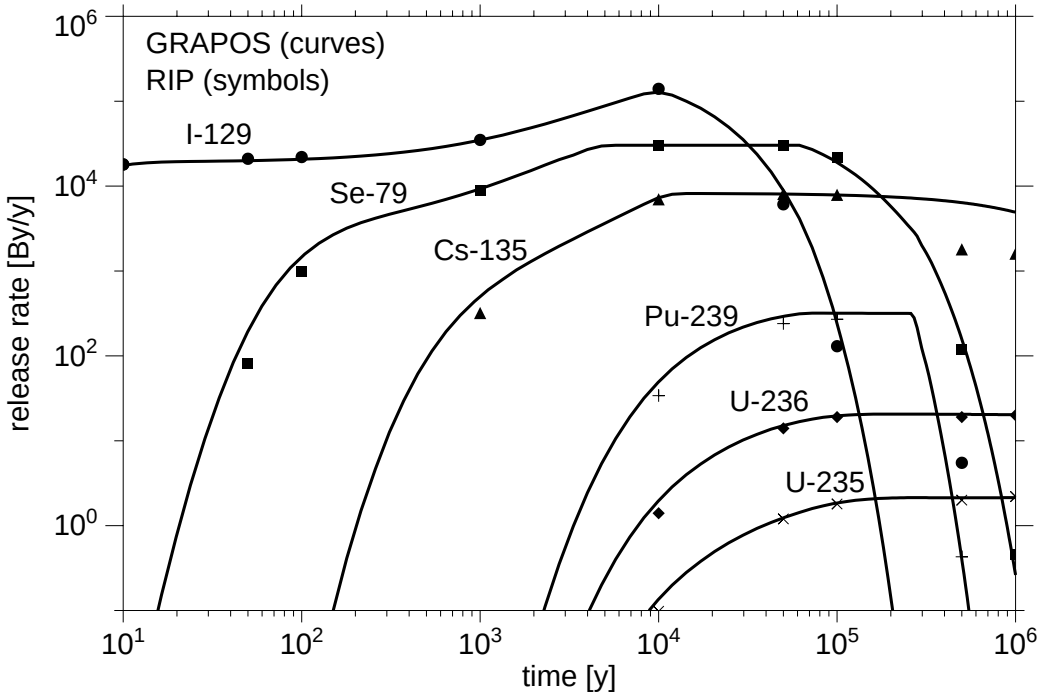

Fig. A1.9: Time evolution of release rates from the bentonite for case BC_GBB

If we compare these results with those for the base case (BC) we can conclude as follows in the case of a reduction in the thickness of the bentonite buffer (77% of mass reduction):

- There is a general increase in release rates at the outer boundary of the bentonite.
- The peak values of the release rates increase for all radionuclides except the uranium isotopes. The maximum release rate of
  - I-129 increases by a factor of 3.
  - Se-79 increases by a factor of 2.3.
  - Cs-135 increases by a factor of 5.
  - Pu-239 increases by a factor of 6.

A1.4.6 Case BC_NS

If there is no solubility limit assumed for all the radionuclides the results obtained with both codes are similar. Table 1.9 presents the maximum release rates at the bentonite-host rock-interface for the considered radionuclides obtained with both codes. The time evolution of the radionuclide release rates from the bentonite is shown in Figure 1.10.

Table A1.9: Maximum release rates in Bq/y at the bentonite-host-rock interface

BC_NS	I-129	Se-79	Cs-135	U-236	Pu-239	U-235
RIP	$3.8 \cdot 10^{4}$	$1.3 \cdot 10^{4}$	$1.7 \cdot 10^{3}$	$1.0 \cdot 10^{2}$	$1.4 \cdot 10^{4}$	$1.0 \cdot 10^{1}$
GRAPOS	$3.6 \cdot 10^{4}$	$1.3 \cdot 10^{4}$	$1.6 \cdot 10^{3}$	$9.8 \cdot 10^{1}$	$1.3 \cdot 10^{4}$	$1.0 \cdot 10^{1}$

There are only slight differences in the maximum release rates obtained with both codes. If we compare these results with those of the base case (BC) we can conclude that:

- I-129 and Cs-135 show the same behaviour (both radionuclides have no solubility limits in the BC).
- For the GRAPOS code the release rates obtained for selenium are slightly higher for times up to 100 years. This effect is not observed using the RIP code. For times longer than 100 years the results obtained with both codes are identical and equal to the BC results.
- Pu-239 shows much higher values than in the BC. The maximum release rate is elevated by a factor of 260 and appears earlier ($5 \cdot 10^{4}$ years instead of 10^{5} years in the BC).
- Uranium isotopes have also higher values than in the BC. The maximum release rates appear earlier ($5 \cdot 10^{5}$ years instead of 10^{6} years) with values increased by a factor of five.

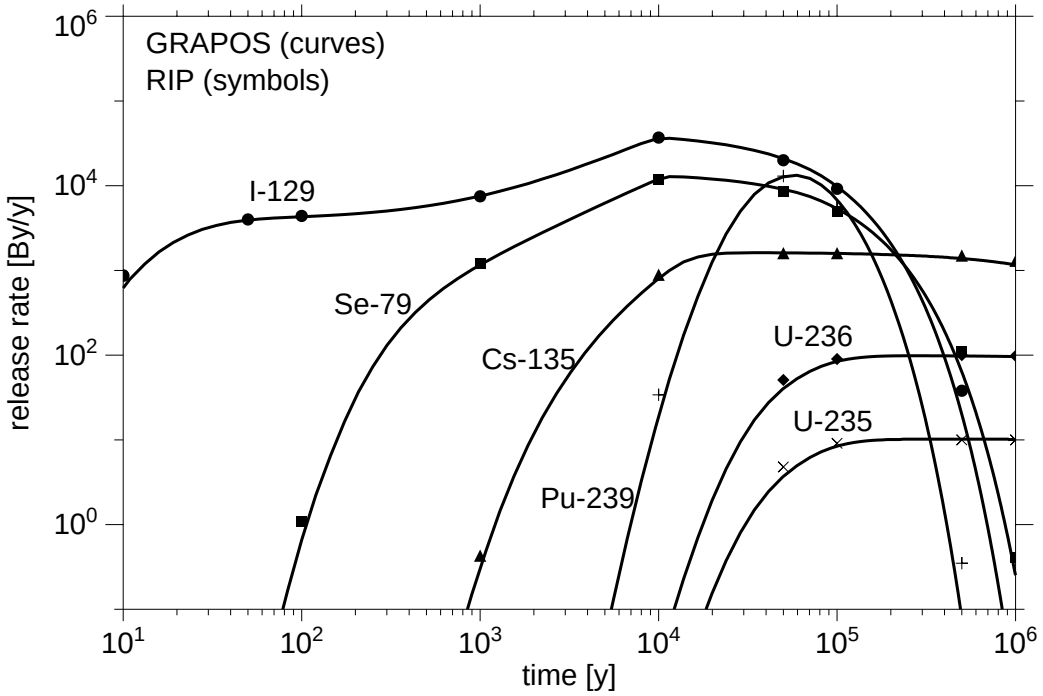

Fig. A1.10: Time evolution of release rates from the bentonite for case BC_NS

A1.5 Overall conclusion

A code intercomparison of the numerical models used for ENRESA and GRS for the radionuclide mobilisation from the waste packages and transport through the bentonite barrier has been made.

A base case has been defined including geometry, parameter and nuclide-specific data (six representative radionuclides were chosen). Several variations of the base case were made to cover the parameter variability expected in a performance assessment.

The results of the comparison of the near-field releases between the RIP and GRAPOS codes allow us to conclude that:

- There is a good agreement between the release rates from the bentonite obtained with both codes, not only in the maximum values and time of occurrence but also in the shapes of the curves.
- The values obtained with RIP are slightly higher than those obtained with GRAPOS.
- With respect to RIP, the results for times up to 1000 years are sensitive to the spatial discretization of the bentonite zone. The calculations with RIP have been done considering discretizations of bentonite into 5, 10 and 15 cells. However, with a higher discretization more precise results have only been obtained for earlier times. Therefore, from a practical point of view, a discretization of the bentonite in 5 cells would be sufficient.

A2 Far-field code verification

A2.1 Comparison of the migration codes FTRANS and CHETMAD

Contribution for the EU-project “Spent fuel Performance Assessment (SPA)” from

Ludger Lührmann
Gesellschaft für Anlagen- und Reaktorsicherheit (GRS) mbH
Henrik Nordman
VTT ENERGY

A2.1.1 Introduction

The modelling of the radionuclide transport through the geosphere, as it is performed by the SPA participants VTT and GRS, is based on the migration pathway concept. For the code comparison the following phenomena are involved:

- advection
- dispersion
- matrix diffusion
- linear sorption within the matrix
- radioactive decay.

The mathematical description of the transport of a single radionuclide i is given by the equation for the advection and dispersion in the fracture:

$$\frac{\partial C_f^i}{\partial t} = -v_f \frac{\partial C_f^i}{\partial z} + D \frac{\partial^2 C_f^i}{\partial z^2} + \frac{1}{b} n_p D_p \left. \frac{\partial C_p^i}{\partial y} \right|_{|y| = b} - \lambda^i C_f^i \,, \qquad (59)$$

and the equation for the diffusion and retardation in the matrix:

$$\frac{\partial}{\partial t} R_p^i C_p^i = D_p \frac{\partial^2 C_p^i}{\partial y^2}\bigg|_{|y| \le y_p} - \lambda^i R_p^i C_P^i \,, \qquad (60)$$

with

C_f^i	concentration of radionuclide *i* in the water-conducting zones [Bq/m^3]
C_p^i	concentration of radionuclide *i* in the stagnant matrix water [Bq/m^3]
v_f	pore velocity of the groundwater [m/y]
W	total width of flow channels per rock area [m/m^2]
D	dispersion coefficient [m^2/y]
b	half aperture of flow channels [m]
y_p	penetration depth of matrix diffusion [m]
n_p	matrix porosity
D_p	pore matrix diffusion coefficient [m^2/y]
λ^i	radioactive decay constant of radionuclide *i* [1/y].

The retardation parameters are defined by

$$R_p^i = 1 + \frac{1 - n_p}{n_p} \rho K_d^i \,, \qquad (61)$$

with the element-specific distribution coefficient K_d^i and the bulk density ρ. The computer codes FTRANS and CHETMAD, which are used by VTT and GRS for the far-field calculations, respectively, are available for the numerical solution of equations (60) and (61). The code FTRANS is based on the Finite Element method, whereas the code CHETMAD is based on the Finite Difference method.

A2.1.2 Definition of the test cases

For the code comparison of FTRANS and CHETMAD the following three test cases are defined:

- BC: base case
- BC-nd: base case, no dispersion
- BC-ul: base case, unlimited matrix diffusion, no dispersion.

For the base case the following transport and sorption parameters are used:

Flow path

- pathway length L = 200 m
- pore velocity v_f = 4 m/y
- volume aperture of fractures $2b$ = 1 mm
- total width of flow channels per rock area W = $5 \cdot 10^{-3}$ m/m^2
- Peclet number Pe = 10

➡ transport resistance (WL / Darcy-velocity) = $5 \cdot 10^4$ y/m

Rock matrix

- porosity n_p = 0.05
- pore diffusivity D_p = $3.0 \cdot 10^{-11}$ m^2/s
- penetration depth of matrix diffusion y_p = 5 cm
- bulk density ρ = 2700 kg/m^3

Nuclides

	half life [y]	K_d in rock matrix [m^3/kg]
C-14	$5.7 \cdot 10^3$	$1.0 \cdot 10^{-5}$
I-129	$1.6 \cdot 10^7$	$1.0 \cdot 10^{-5}$
Cs-135	$2.3 \cdot 10^6$	$4.2 \cdot 10^{-2}$
U-238	$4.5 \cdot 10^9$	$5.0 \cdot 10^{-2}$
Pu-240	$6.5 \cdot 10^3$	$5.0 \cdot 10^{-1}$

The release rates from the near-field calculations in the RS scenario of TILA-96 [40] are used as input pulses (see Figure 2.1). Release starts at 10,000 years and ends at one million years which represents also the cut-off time of our calculations. A zero-concentration boundary condition is applied at the outflow boundary.

A2.1.3 Results

For the code comparison the following discretization in space is used: Both migration codes for the calculation of the matrix diffusion use 11 elements for the test cases BC and BC-nd, and 22 elements in the BC-ul cases. The next element deeper in the matrix was always 50% thicker than the previous one. For the BC-ul case a 5 m thick rock matrix is assumed. For FTRANS the 200 m long flow path is divided into 20 parts in the BC and BC-nd cases and into 30 parts in the BC-ul case. The next element along the flow path is always 2% longer than the previous one. For the CHETMAD calculations an equidistant discretization of 21 and 34 elements is used, respectively.

The maximum release rates and their arrival times are given in the Tables 2.1 - 2.3. The Figures 2.2 - 2.4 show the calculated release rates for the different test cases. A sufficiently good agreement between the results of the two migration codes is achieved. But, it has to be mentioned that the results are sensitive to the discretization applied. The different maximum release rate for Cs-135 in the BC-ul case is due to numerical dispersion in the CHETMAD calculation and disappears immediately when using a slightly finer discretization in space. The releases of Pu-240 are negligible in all cases and are not listed in the tables.

Table A2.1: Maximum release from the geosphere for case BC

	BC			
	FTRANS		CHETMAD	
	Time [y]	Maximum [Bq/y]	Time [y]	Maximum [Bq/y]
C-14	$1.1 \cdot 10^{4}$	$1.2 \cdot 10^{6}$	$1.1 \cdot 10^{4}$	$1.3 \cdot 10^{6}$
I-129	$1.1 \cdot 10^{4}$	$1.4 \cdot 10^{5}$	$1.1 \cdot 10^{4}$	$1.4 \cdot 10^{5}$
Cs-135	$5.3 \cdot 10^{5}$	$1.9 \cdot 10^{4}$	$4.9 \cdot 10^{5}$	$2.3 \cdot 10^{4}$
U-238	$1.0 \cdot 10^{6}$	2.7	$1.0 \cdot 10^{6}$	2.8

Table A2.2: Maximum release from the geosphere for case BC-nd

	BC-nd			
	FTRANS		CHETMAD	
	Time [y]	Maximum [Bq/y]	Time [y]	Maximum [Bq/y]
C-14	$1.1 \cdot 10^{4}$	$1.3 \cdot 10^{6}$	$1.1 \cdot 10^{4}$	$1.4 \cdot 10^{6}$
I-129	$1.1 \cdot 10^{4}$	$1.5 \cdot 10^{5}$	$1.1 \cdot 10^{4}$	$1.5 \cdot 10^{5}$
Cs-135	$6.4 \cdot 10^{5}$	$3.1 \cdot 10^{4}$	$6.0 \cdot 10^{5}$	$3.5 \cdot 10^{4}$
U-238	$1.0 \cdot 10^{6}$	3.0	$1.0 \cdot 10^{6}$	3.0

Table A2.3: Maximum release from the geosphere for case BC-ul

	BC-ul			
	FTRANS		CHETMAD	
	Time [y]	Maximum [Bq/y]	Time [y]	Maximum [Bq/y]
C-14	$1.7 \cdot 10^{4}$	$3.4 \cdot 10^{4}$	$1.7 \cdot 10^{4}$	$3.7 \cdot 10^{4}$
I-129	$2.4 \cdot 10^{4}$	$1.2 \cdot 10^{4}$	$2.4 \cdot 10^{4}$	$1.2 \cdot 10^{5}$
Cs-135	--	--	$1 \cdot 10^{6}$	1.9
U-238	--	--	--	--

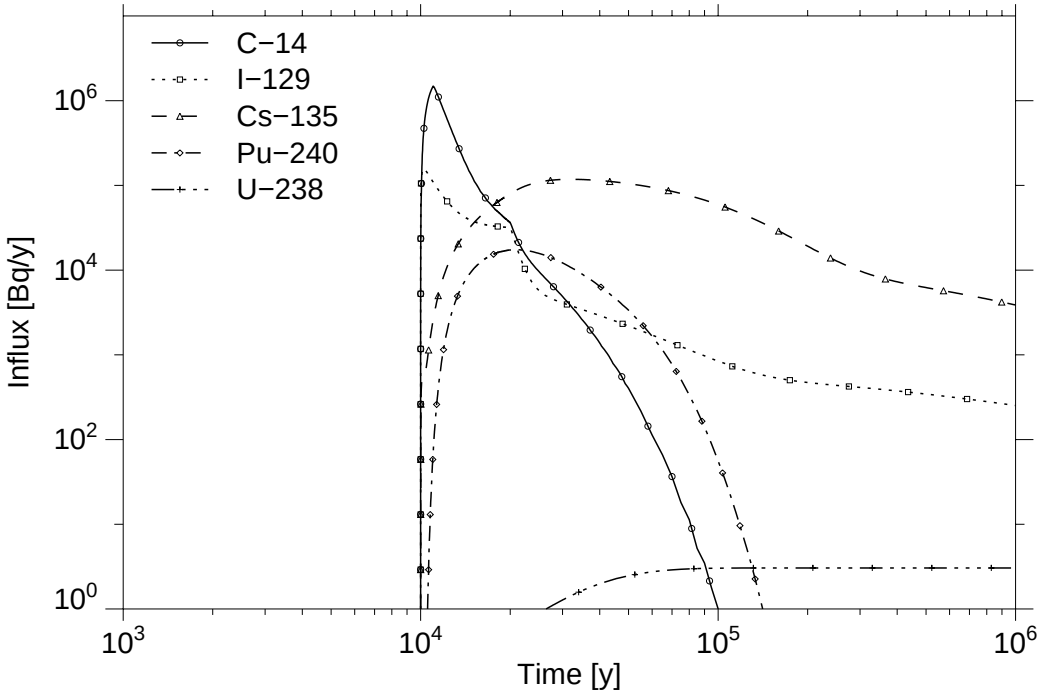

Fig. A2.1: Release rates from the near-field calculations of TILA-96 applied as influx for the test cases

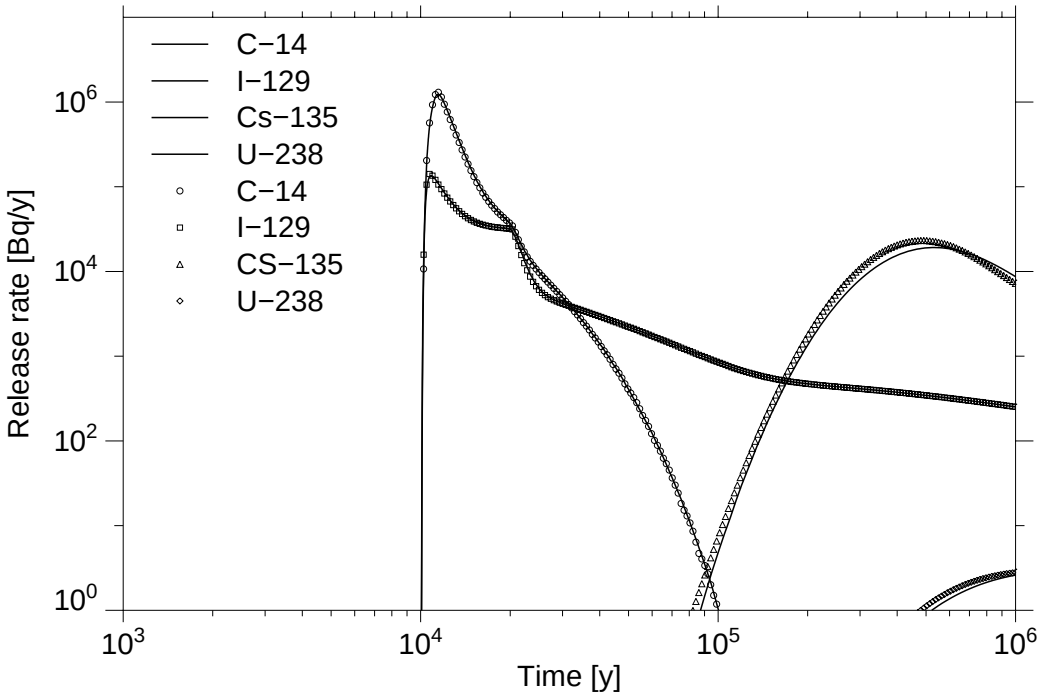

Fig. A2.2: Release rates for the base case BC calculated by FTRANS (lines) and CHETMAD (symbols)

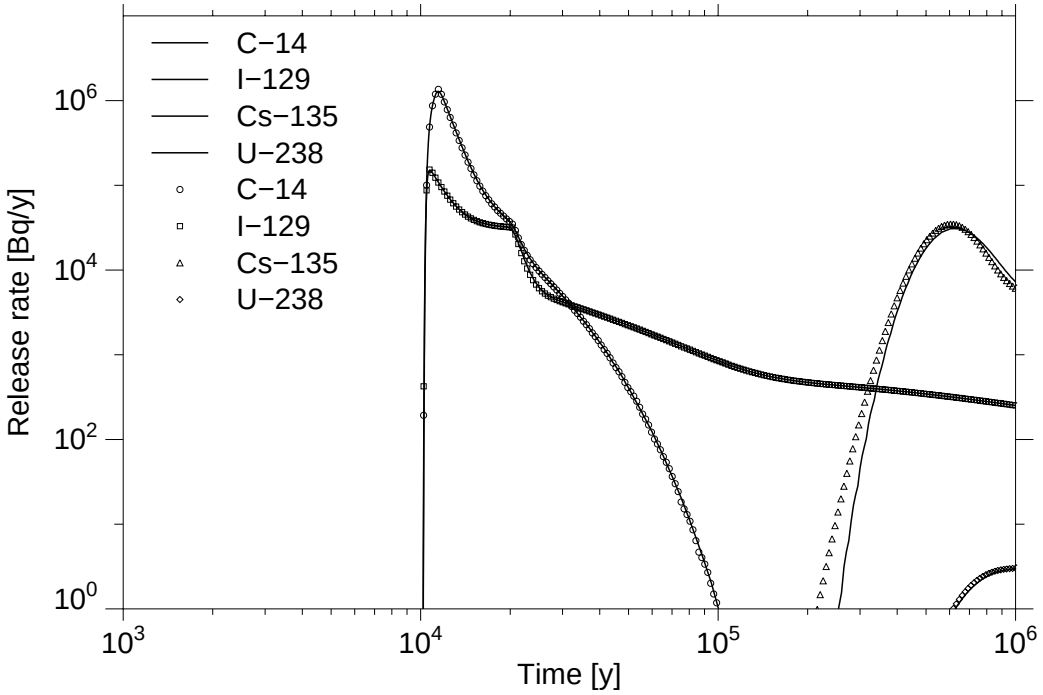

Fig. A2.3: Release rates for the test case BC-nd calculated by FTRANS (lines) and CHETMAD (symbols)

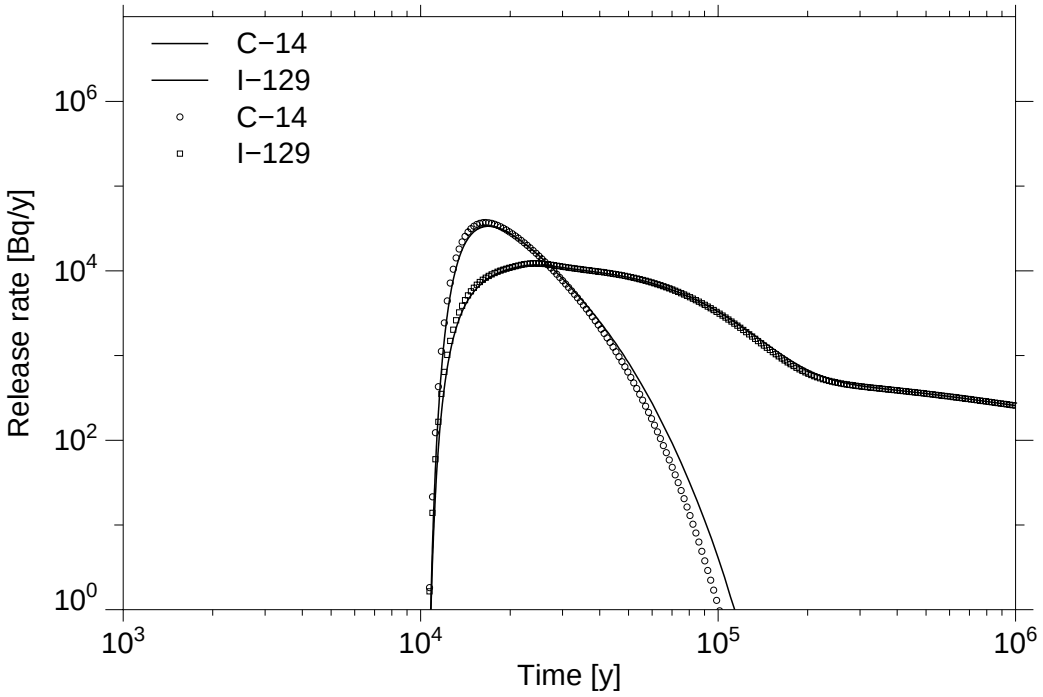

Fig. A2.4: Release rates for the test case BC-ul calculated by FTRANS (lines) and CHETMAD (symbols)

A2.2 Effective surface sorption approximation

A2.2.1 Mathematical description

If the diffusion into a limited, altered zone of the rock matrix is sufficiently fast, the assumption of equal concentrations within the fracture and the limited, adjacent zone, i.e. $C_f^i = C_p^i$, could be a good approximation. Therewith, the transport equations (59) and (60) can be simplified to [15, 20]

$$\frac{\partial}{\partial t} R_f^i C_f^i = - v_f \frac{\partial C_f^i}{\partial z} + D \frac{\partial^2 C_f^i}{\partial z^2} - \lambda^i C_f^i \,, \qquad (62)$$

with the effective surface retardation factor R_f^i:

$$R_f^i = 1 + \frac{(1 - n_p)\rho K_d^i}{b} \delta \,, \qquad (63)$$

where δ denotes the depth of the altered zone. If the diffusion into the matrix is not confined to the altered zone, but also occurs in the adjacent rock matrix, the transport of a radionuclide *i* can be described by the following equations:

$$\begin{aligned} \frac{\partial}{\partial t} R_f^i C_f^i &= - v_f \frac{\partial C_f^i}{\partial z} + D \frac{\partial^2 C_f^i}{\partial z^2} + \frac{1}{b} \frac{n_p}{n_f} D_p \frac{\partial C_p^i}{\partial y}\bigg|_{|y| = b + \delta} - \lambda^i C_f^i \\ \frac{\partial}{\partial t} R_p^i C_p^i &= D_p \frac{\partial^2 C_p^i}{\partial y^2}\bigg|_{|y| \le y_p} - \lambda^i R_p^i C_P^i \,, \end{aligned} \qquad (64)$$

where the porosity $n_f = b / (b + \delta)$ describes the volume fraction of the fracture and altered zone which is available for advective flow.

The effective diffusivity within the rock matrix is commonly assumed to be significantly reduced some centimetres beyond the fracture. Therefore, for modelling the matrix diffusion the matrix is often divided in two parts with different properties concerning the diffusivity and the porosity. The procedure described above is sometimes a useful approximation for the calculation of the diffusive flux within the different regions of the rock matrix. This is demonstrated in the next section.

A2.2.2 Test case description

In the safety analysis TILA-96 [40] the following two matrix regions with different porosities and effective diffusion coefficients have been assumed:

	Distance from the fracture 0 - 1cm	Distance from the fracture > 1cm
Non-anions	$n_p = 0.5\%$	$n_p = 0.1\%$
	$D_e = 10^{-13}$ m^2/s	$D_e = 10^{-14}$ m^2/s
Anions	$n_p = 0.1\%$	$n_p = 0.02\%$
	$D_e = 10^{-14}$ m^2/s	$D_e = 10^{-15}$ m^2/s

In order to investigate how far the effective surface sorption approximation could describe the diffusive flux and retardation within the first region of the rock matrix, far-field calculations using the geosphere data from the reference scenario of TILA-96, have been performed. The effective surface sorption approximation leads to the following input data for the calculations with CHETMAD:

Flow path

- pathway length L = 600 m
- pore velocity v_f = 60 m/y
- volume aperture of fractures $2b$ = 0.5 mm
- depth for effective surface sorption δ = 1 cm
- total width of flow channels per rock area $W = 1 \cdot 10^{-3}$ m/m^2

- Peclet number $Pe = \infty$

➡ transport resistance = $2 \cdot 10^4$ y/m

Rock matrix

- porosity $n_f = b / (b + \delta) \approx 2.5\,\%$
- porosity n_p = 0.5 % (non-anions), 0.1 % (anions)
- effective diffusivity D_e = $1.0 \cdot 10^{-14}$ m^2/s (non-anions), =$1.0 \cdot 10^{-15}$ m^2/s (anions)
- penetration depth of matrix diffusion y_p = 5 m (unlimited matrix diffusion)
- bulk density ρ = 2700 kg/m^3

Nuclides

	half live [y]	K_d in rock matrix [m^3/kg]
C-14	$5.7 \cdot 10^3$	$1.0 \cdot 10^{-4}$
I-129	$1.6 \cdot 10^7$	$2.0 \cdot 10^{-5}$
Cs-135	$2.3 \cdot 10^6$	$5.0 \cdot 10^{-2}$
U-238	$4.5 \cdot 10^9$	$1.0 \cdot 10^{-1}$
Pu-240	$6.5 \cdot 10^3$	$5.0 \cdot 10^{-1}$

Input pulses

- RS scenario of TILA-96

A2.2.3 Results

For the calculations with the code CHETMAD the 600 m long flow path is divided into 34 equidistant elements. For the diffusion equation 22 elements are used. The next element deeper in the matrix is always 50 % thicker than the previous. At the outflow boundary a zero-concentration boundary condition is used.

The maximum release rates and their arrival times are given in Table 2.4. The calculated release rates as a function of time are shown in Figure 2.5. The release of Pu-240 is negligible and is not listed. The release rates obtained from the effective surface sorption approximation are in satisfactory agreement with the results from the TILA-96 analysis.

Table A2.4: Maximum release rates from the geosphere for the test case TILA-96

Nuclide	TILA-96		CHETMAD	
	Time [y]	Maximum [Bq/y]	Time [y]	Maximum [Bq/y]
C-14	$1.1 \cdot 10^4$	$1.2 \cdot 10^6$	$1.1 \cdot 10^4$	$1.4 \cdot 10^6$
I-129	$1.1 \cdot 10^4$	$1.1 \cdot 10^5$	$1.0 \cdot 10^4$	$1.4 \cdot 10^5$
Cs-135	$1.5 \cdot 10^5$	$3.7 \cdot 10^4$	$1.4 \cdot 10^5$	$4.3 \cdot 10^4$
U-238	$1.0 \cdot 10^6$	2.4	$1.0 \cdot 10^6$	2.4

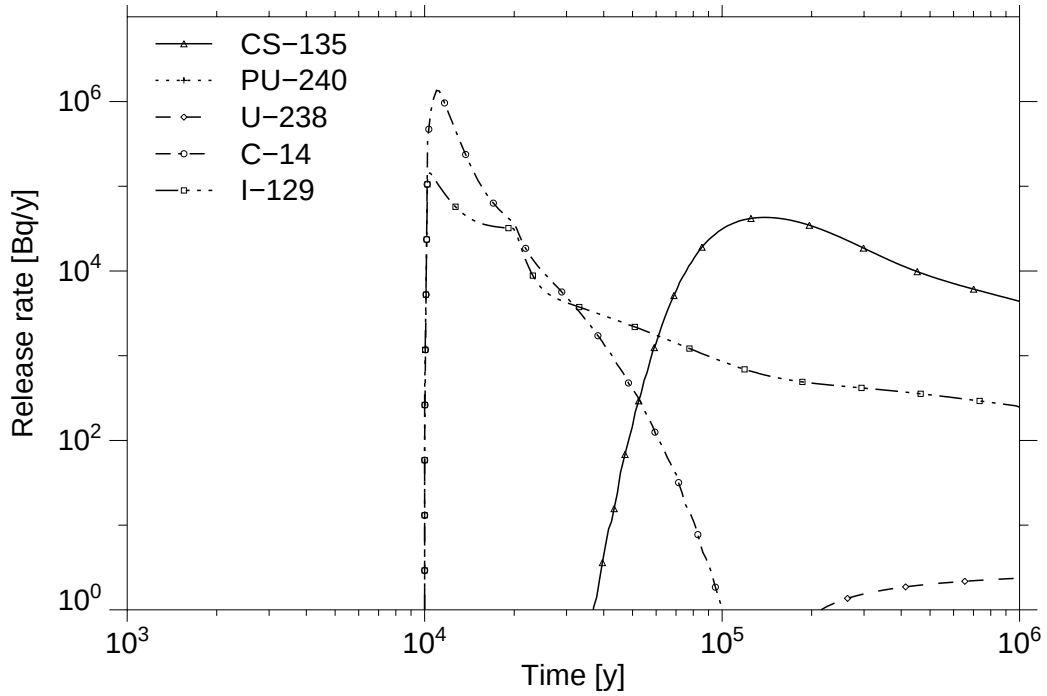

Fig. A2.5: Release rates from the geosphere into the biosphere in the reference scenario of TILA-96 applying an effective surface sorption approximation

A2.3 INTRACOIN test cases of level 3

A2.3.1 Test case description

The INTRACOIN test cases of Level 3, Variations 1 - 9 [19], are calculated for an additional verification of the computer code CHETMAD. The test cases describe the transport of the single nuclide Np-237 through a fractured medium where the fractures run between cubic rock blocks. The migration is assumed to take place from a waste canister to a nearby fracture zone. The test cases are described in detail in [19]. In the variations 1 - 9 the following effects are included:

- advection
- longitudinal dispersion
- diffusion into the matrix accompanied by sorption on interior surfaces
- sorption on the fracture walls
- solubility limited source term
- radioactive decay.

In the central case (CC) advection, dispersion, sorption on fracture surfaces, and radioactive decay are taken into account. Based on the central case the variations are created by either adding or taking away some of the physical effects as summarized in Table 2.5. The term sorption refers to sorption on the fracture walls.

A2.3.2 Results

The results for maximum discharge rates are listed in Table 2.5. The discharge rates as a function of time are given in Figure 2.6. The results from CHETMAD agree in a satisfactory way with the results from the numerical codes used at INTRACOIN level 3 [19]. The differences obtained for the maximum discharge rates are in a range of only few percent.

Table A2.5: Description of the variations and the maximum discharge rates obtained from the calculations by the code CHETMAD

Variation	Description	CHETMAD	
		T_{max}	C_{max}
CC		$4.4 \cdot 10^{5}$	$1.99 \cdot 10^{-6}$
1	no dispersion, no sorption	$5.2 \cdot 10^{1}$	$1.50 \cdot 10^{-5}$
2	no dispersion, no sorption, matrix diffusion	$7.3 \cdot 10^{7}$	$1.29 \cdot 10^{-29}$
3	no dispersion	$8.3 \cdot 10^{5}$	$1.14 \cdot 10^{-5}$
4	no dispersion, matrix diffusion	$7.4 \cdot 10^{7}$	$9.46 \cdot 10^{-30}$
5	no sorption	$2.0 \cdot 10^{2}$	$1.50 \cdot 10^{-5}$
6	no sorption, solubility limited source term	$2.0 \cdot 10^{2}$	$1.70 \cdot 10^{-7}$
7	solubility limited source term	$4.2 \cdot 10^{6}$	$1.39 \cdot 10^{-7}$
8	matrix diffusion	$9.3 \cdot 10^{6}$	$2.75 \cdot 10^{-13}$
9	matrix diffusion, solubility limited source term	$1.17 \cdot 10^{7}$	$1.27 \cdot 10^{-13}$

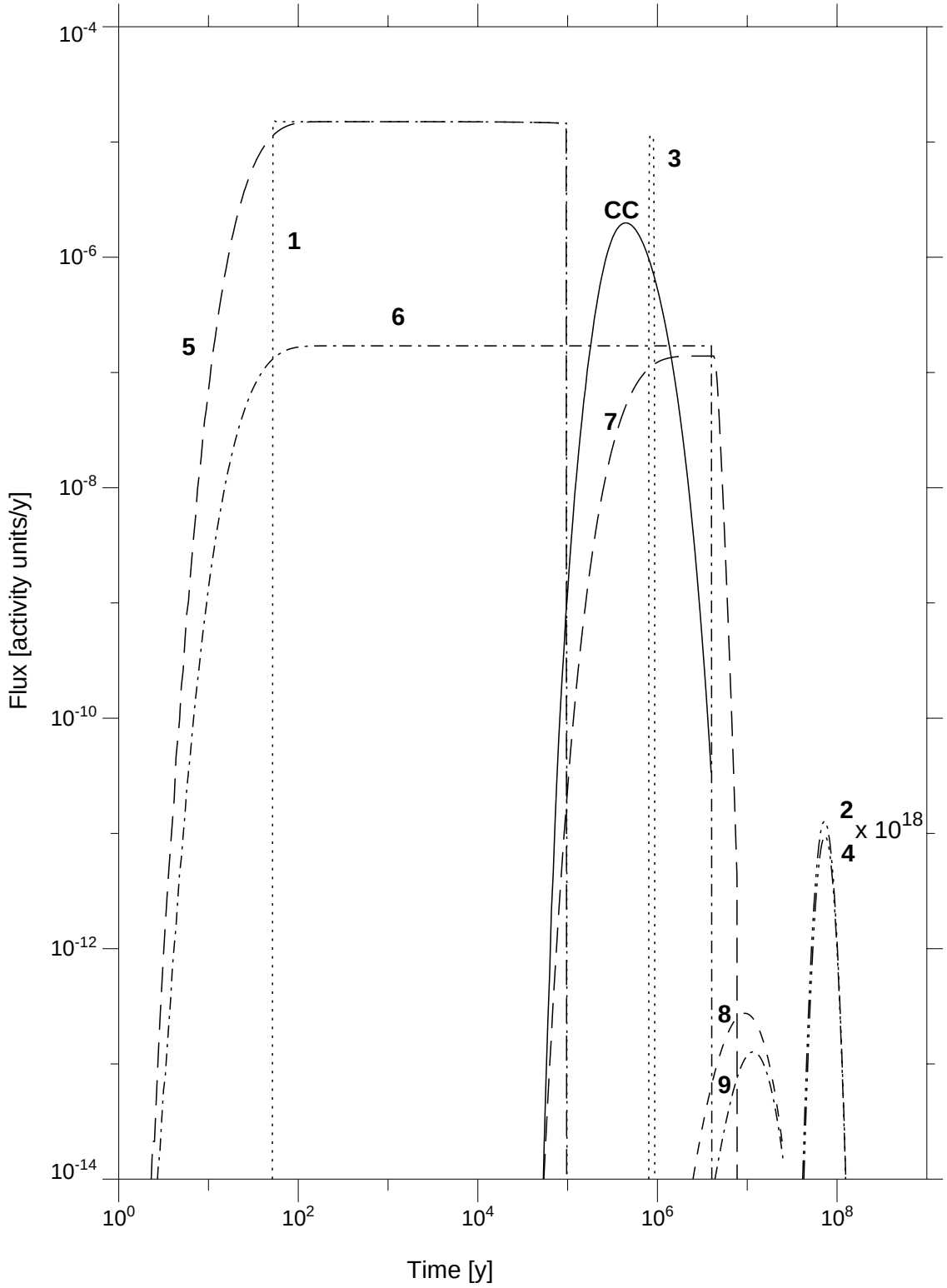

Fig. A2.6: Discharge rates calculated with CHETMAD as a function of time for the test cases of INTRACOIN Level 3: central case (CC) and variations 1 - 9

Figures

Appendix

Tables

Gesellschaft für Anlagen- und Reaktorsicherheit (GRS) mbH

Schwertnergasse 1
50667 Köln
Telefon +49 221 2068-0
Telefax +49 221 2068-888

Forschungsinstitute
85748 Garching b. München
Telefon +49 89 32004-0
Telefax +49 89 32004-300

Kurfürstendamm 200
10719 Berlin
Telefon +49 30 88589-0
Telefax +49 30 88589-111

Theodor-Heuss-Straße 4
38122 Braunschweig
Telefon +49 531 8012-0
Telefax +49 531 8012-200

www.grs.de

ISBN 3-931995-16-X